Interacting white dwarfs in binaries and triples

Abinaya Swaruba Rajamuthukumar

München 2025

Interacting white dwarfs in binaries and triples

Abinaya Swaruba Rajamuthukumar

Dissertation
der Fakultät für Physik
der Ludwig-Maximilians-Universität
München

vorgelegt von
Abinaya Swaruba Rajamuthukumar
aus Tenkasi, Indien

München, den 12.03.2025

Erstgutachter: Prof. Dr. Selma E. de Mink
Zweitgutachter: Prof. Dr. Achim Weiß
Tag der mündlichen Prüfung: 08.05.2025

Contents

List of Figures

List of Tables

Zusammenfassung

Weiße Zwerge stellen das häufigste Endstadium der Sternentwicklung dar und spielen eine entscheidende Rolle in verschiedenen astrophysikalischen Phänomenen, wie thermonuklearen Explosionen, Verschmelzungen kompakter Doppelsterne und die Entstehung von Gravitationswellen. Während die Entwicklung Weißer Zwerge in Doppelsternsystemen bereits umfassend untersucht wurde, bleiben viele offene Fragen, insbesondere in Bezug auf die Wechselwirkungen, die zu thermonuklearen Ereignissen wie Typ-Ia-Supernovae führen. Darüber hinaus ist die Rolle hierarchischer Dreifachsysteme bei der Bildung und den Wechselwirkungen Weißer Zwerge weniger gut verstanden. In dieser Dissertation untersuche ich, wie sowohl Doppelstern- als auch Dreifachsternsysteme die Population Weißer Zwerge formen und ihre Wechselwirkungen beeinflussen.

Zunächst führe ich eine Populationssynthese-Studie hierarchischer Dreifachsysteme mit dem Multiple Stellar Evolution (`MSE`)-Code durch. Dabei konzentriere ich mich auf den Einfluss der Sternentwicklung, der Wechselwirkungen in Doppelsternsystemen und dynamischer Effekte auf die Bildung Weißer Zwerge. Diese Studie berücksichtigt sowohl den einzel- als auch den doppelt-degenerierten Entstehungskanal und analysiert Dreifachsysteme über den gesamten Parameterraum hinweg, einschließlich solcher mit engen inneren Doppelsternen. Zudem untersuche ich die Auswirkungen oft vernachlässigter oder unsicherer physikalischer Prozesse, wie Vorbeiflüge anderer Sterne und Unsicherheiten in der Entwicklung in einer gemeinsamen Sternhülle. Durch den Vergleich der Ergebnisse aus Dreifach- und Doppelsternkanälen bewerte ich die Bedeutung von Dreifachsystemen bei der Entstehung von Typ-Ia-Supernovae.

Anschließend verwende ich den `MESA`-Sternentwicklungs-Code, um Heliumstern + Weißer-Zwerg-Systeme im Detail zu modellieren. Diese Simulationen stellen die aktuellste Untersuchung einzel-degenerierter Supernova-Progenitoren dar und erforschen ein breites Spektrum an heißen Subzwerg + Weißer-Zwerg-Konfigurationen sowie deren mögliche Entwicklungspfade, darunter die Bildung von binären Systemen zweier Weißer Zwerge, Heliumnovae und thermonukleare Explosionen. Zusätzlich berechne ich die Fluchtgeschwindigkeiten überlebender Donorrsterne in Systemen, in denen eine Explosion stattfindet.

Schließlich untersuche ich binäre Systeme zweier Weißer Zwerge, die aus Dreifachsystemen entstehen und mit der Laser Interferometer Space Antenna (LISA) detektiert werden können. Durch die Kombination von `MSE` mit einem Milchstraßen-ähnlichen Galaxienmodell aus den kosmologischen Simulationen (`TNG50`) konstruiere ich eine synthetische galaktische Population weißer Zwerge und vergleiche den Beitrag aus Dreifachsystemen mit dem

aus isolierten Doppelsternen. Während frühere Studien sich hauptsächlich auf die isolierte Entwicklung von Doppelsternen konzentrierten, präsentiert diese Arbeit die erste detaillierte Untersuchung der Rolle der Dreifachstern-Evolution bei der Bildung binärer Systeme zweier Weißer Zwerge, die mit LISA detektiert werden können. Ich prognostiziere sowohl die Gesamtzahl binärer Systeme aus dem Dreifachkanal, die als diffuses astrophysikalisches Rauschen messbar sein werden, als auch die Anzahl der individuell auflösbaren Systeme.

Diese Dissertation hebt die zentrale Bedeutung von Doppelstern- und hierarchischen Dreifachstern-Systemen für die Entstehung und Entwicklung Weißer Zwerge sowie deren Einfluss auf die beobachtbare Population kompakter Objekte hervor. Die Ergebnisse haben weitreichende Implikationen für die Gravitationswellenastronomie, wechselwirkende Weiße Zwerge und unser allgemeines Verständnis der Evolution von Doppel- und Mehrfachsternsystemen.

Abstract

White dwarfs are the most common endpoints of stellar evolution and play a crucial role in various astrophysical phenomena, such as thermonuclear explosions, compact binary mergers, and gravitational wave sources. While the evolution of white dwarfs in binary systems has been extensively studied, many open questions remain, particularly regarding the interactions that lead to thermonuclear events such as Type Ia supernovae. Moreover, the role of hierarchical triples in shaping white dwarf formation and interactions is less well understood. In this thesis, I investigate how both binary and triple-star dynamics shape the white dwarf population and influence their interactions.

First, I conduct a population synthesis study of hierarchical triples using the Multiple Stellar Evolution (`MSE`) code, focusing on the impact of stellar evolution, binary interactions, and dynamical effects on white dwarf formation. This study simultaneously considers both the single and double degenerate channels and accounts for triples across the entire parameter space, including those with tight inner binaries. Additionally, I investigate the effects of typically overlooked or uncertain physics, such as fly-bys and common envelope prescription parameters. By comparing the outcomes of triple and binary evolution channels, I assess the significance of triples in producing Type Ia supernovae.

Next, I use the `MESA` stellar evolution code to model He star + white dwarf systems in detail. These simulations represent the most up-to-date study of single degenerate progenitors, exploring an extensive grid of hot subdwarf + white dwarf configurations and their possible evolutionary outcomes, including double white dwarf formation, helium novae, and thermonuclear explosions. Additionally, I calculate the runaway velocities of surviving donor stars in systems where an explosion occurs.

Finally, I examine the contribution of white dwarfs from the triple channel to the Galactic population of double white dwarfs detectable by the Laser Interferometer Space Antenna (LISA). By combining `MSE` with a Milky Way-like galaxy model from cosmological simulations (`TNG50`), I construct a synthetic Galactic white dwarf population and compare the contribution from triple systems to that of isolated binaries. While previous studies have primarily focused on binary formation and evolution in isolation, this work presents the first detailed investigation into the role of triple stellar evolution in shaping the LISA double white dwarf population. I predict both the total number of double white dwarfs from the triple channel contributing to LISA's astrophysical noise and the number of individually resolvable double white dwarfs.

This thesis emphasizes the critical role of binary and hierarchical triple systems in the

formation and evolution of white dwarfs, as well as their influence on shaping the observable population of compact objects. The findings have significant implications for gravitational wave astronomy, interacting white dwarf binaries, progenitors of Type Ia supernovae, and our broader understanding of binary and multiple-star evolution.

Chapter 1

Introduction

> *"Stars are phoenixes, rising from their own ashes."*
>
> – Neils Bohr

White dwarfs are the end products of low-to intermediate-mass stars, that is stars with masses less than about 8 times the mass of the Sun. They form after these stars exhaust their nuclear fuel and shed their outer layers in a planetary nebula, leaving behind a hot, dense core. This core is primarily composed of carbon and oxygen, though in some cases it can be made of oxygen and neon, or even just helium. The white dwarf, held up by electron degeneracy pressure from the Pauli exclusion principle, stays stable and inert in isolation without binary interactions. Despite being only roughly the size of Earth, white dwarfs have masses comparable to the Sun. This results in extreme densities, where a teaspoon of white dwarf material would weigh several tons on Earth. White dwarfs start extremely hot, with surface temperatures exceeding 100,000 K, but cool over billions of years, eventually becoming some of the oldest objects in the universe.

While white dwarfs are interesting due to their high density, extreme temperatures, and long cooling timescales, they are even more intriguing in binary and multiple-star systems. In these systems, white dwarfs interact with companion stars, often through the accretion of material, but also through physical collisions or mergers. These interactions often involve the accretion of material but can also include physical collisions or mergers, leading to a range of astrophysical phenomena such as cataclysmic variables (Warner, 1995), AM CVn systems (Solheim, 2010), novae (Bode & Evans, 2008), and thermonuclear runaways that may trigger a Type Ia supernova (Hoyle & Fowler, 1960). In addition, white dwarfs in close binaries are significant as sources of gravitational waves. As these systems evolve, the white dwarf and its companion lose energy through gravitational radiation, causing them to spiral inward. This process not only plays a crucial role in the eventual fate of the system but also provides an opportunity to test general relativity in extreme gravitational fields.

Studying white dwarfs in multiple-star systems is essential for understanding their formation, evolution, dynamics, and ultimate fate in interacting binaries. These systems play a crucial role in both electromagnetic and gravitational-wave astronomy, serving as progenitors of SNe Ia and key sources of gravitational waves. In the following sections, I describe the key processes that shape the formation and evolution of white dwarfs in binary and triple systems. I also discuss white dwarfs as progenitors of SNe Ia and gravitational-wave sources.

1.1 Key evolutionary processes of white dwarfs in binaries

A significant fraction of white dwarfs form in binary systems, with approximately 10% found in double white dwarf pairs with short orbital periods (Maoz et al., 2018). The formation and subsequent evolution of these white dwarfs are heavily influenced by a variety of binary interactions. In this section, I describe key interactions such as stable mass transfer, common-envelope evolution, tidal interactions, and gravitational-wave interactions, all of which play crucial roles in shaping the mass, orbital configurations, and ultimately the fate of white dwarfs in binary systems.

In a binary system, each star has a Roche lobe, a teardrop-shaped equipotential surface within which material remains gravitationally bound to the star. If a star expands beyond its Roche lobe, matter flows toward the companion through the inner Lagrangian point. The stability of mass transfer depends on the donor star's response to mass loss and the accretor's ability to accept material without overflowing its Roche lobe (Paczyński, 1971; Ritter, 1988). Stable Roche-lobe overflow allows for gradual mass exchange, often leading to the formation of an accretion disk. This process is fundamental in forming interacting binaries, including cataclysmic variables, AM CVn systems, and certain X-ray binaries. However, if the mass transfer becomes unstable, it may trigger a common-envelope phase, leading to rapid orbital decay (Paczynski, 1976; Hjellming & Webbink, 1987).

When mass transfer occurs on a timescale shorter than the thermal adjustment timescale of the accretor, the system enters a common envelope phase. The donor's outer layers engulf both stars, resulting in rapid orbital decay due to frictional forces within the envelope (Iben & Livio, 1993; Ivanova et al., 2013). The fate of the system depends on whether enough orbital energy is deposited into the envelope to unbind it. If envelope ejection occurs, the binary system emerges with a much smaller orbital separation, leading to a compact binary system. This is a critical process in the formation of short-period white dwarf binaries and progenitors of gravitational wave sources (Webbink, 1984). In cases where the envelope is not ejected, the stars may merge, potentially forming a single massive object or an unstable remnant that continues to evolve (Ivanova et al., 2013).

As the binary evolves, tidal forces start playing an increasingly important role. These forces arise from the differential gravitational attraction between the two stars, causing each star to deform slightly and dissipate energy in the form of heat, known as tidal dissipation. Tidal forces act to synchronize the stars' rotational motion with their orbital motion, a process called tidal locking (Hut, 1981). Over time, the stars adjust their spins so that they rotate at the same rate as they orbit each other, similar to the way the Moon always shows

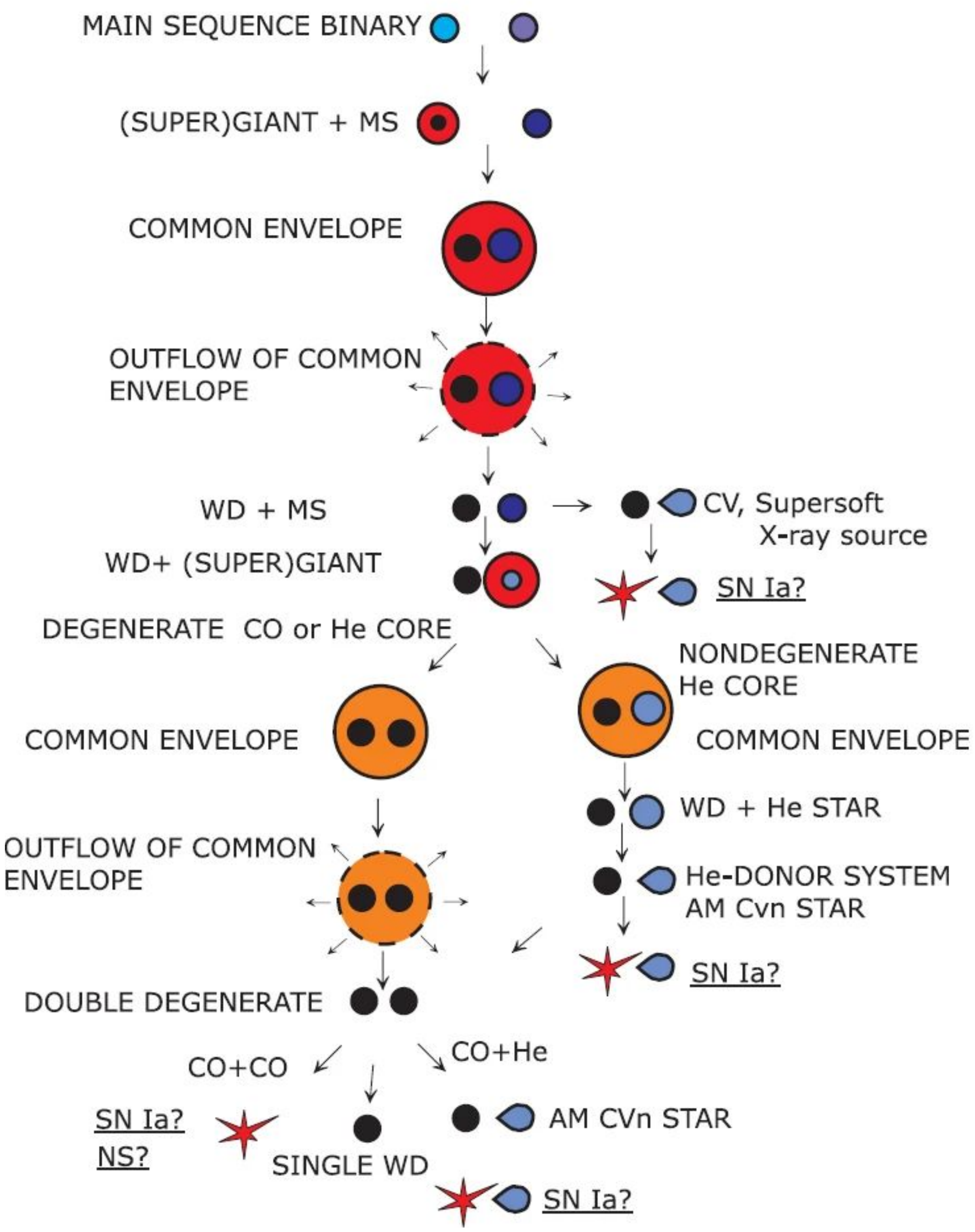

Figure 1.1: Formation of white dwarfs in binaries and their descendants. MS: Main Sequence, WD: White dwarf, NS: Neutron star, SN Ia: Type Ia supernova, CV: Cataclysmic Variable, AM CVn: AM Canum Venaticorum star, CO: Carbon-Oxygen, He: Helium. Adapted from Postnov & Yungelson (2014).

the same face to Earth. In addition to synchronization, tidal forces also help to circularize the orbit. If the binary system's orbit is initially elliptical, tidal forces gradually transform the orbit into a more circular one over time. This circularization process is faster in short-period binaries, where the stars are closer together, and tidal interactions are stronger (Zahn, 1977).

In compact binaries such as double white dwarf systems, gravitational-wave emission becomes the dominant mechanism driving orbital decay. As the stars orbit each other, they lose energy in the form of gravitational radiation, causing their orbits to shrink. This process accelerates as the binary system tightens, eventually leading to coalescence (Peters, 1964). The inspiral of such systems serves as a primary source of gravitational waves detectable by future observatories like LISA. Their eventual mergers could lead to dramatic astrophysical events, including SNe Ia.

Fig. 1.1 illustrates how binary interactions directly impact the formation and long-term evolution of white dwarfs in binary systems. These interactions regulate the mass transfer rate and drive orbital decay, leading to gravitational-wave emission as the system tightens. Understanding these processes is crucial for interpreting both electromagnetic and gravitational-wave observations, offering valuable insights into the fate of these binaries.

1.2 Key evolutionary processes of white dwarfs in triples

Observations suggest that approximately 10% of solar-mass stars are in triples, which are direct progenitors of white dwarfs (Moe & Di Stefano, 2017). Understanding their evolution is crucial, as their complex gravitational interactions can lead to various outcomes, including mass transfer, common envelope, mergers, and physical collisions.

A fundamental dynamical mechanism governing the evolution of triple star systems is the von Zeipel-Lidov-Kozai (ZLK) effect, which plays a crucial role in driving oscillations in both inclination and eccentricity (von Zeipel, 1909; Kozai, 1962; Lidov, 1962). These oscillations result from the gravitational interaction between the inner binary and the third, more distant star in the system. When the initial mutual inclination between the inner binary and the outer orbit is sufficiently large, the inner binary undergoes high-amplitude eccentricity oscillations. As the eccentricity oscillates, it significantly influences the orbital parameters of the inner binary, including its mutual inclination.

Due to dynamical stability constraints, inner binaries in triple systems must remain relatively compact to avoid disruption by the tertiary companion. As a result, triple systems tend to host tighter inner binaries compared to isolated binary systems, increasing their susceptibility to gravitational interactions and orbital perturbations (Tokovinin, 2008). This compact configuration amplifies gravitational interactions, heightening the likelihood of dynamical effects. The combination of ZLK oscillations and the compact nature of these binaries further intensifies the potential for extreme orbital changes, making them more susceptible to interactions induced by the third star.

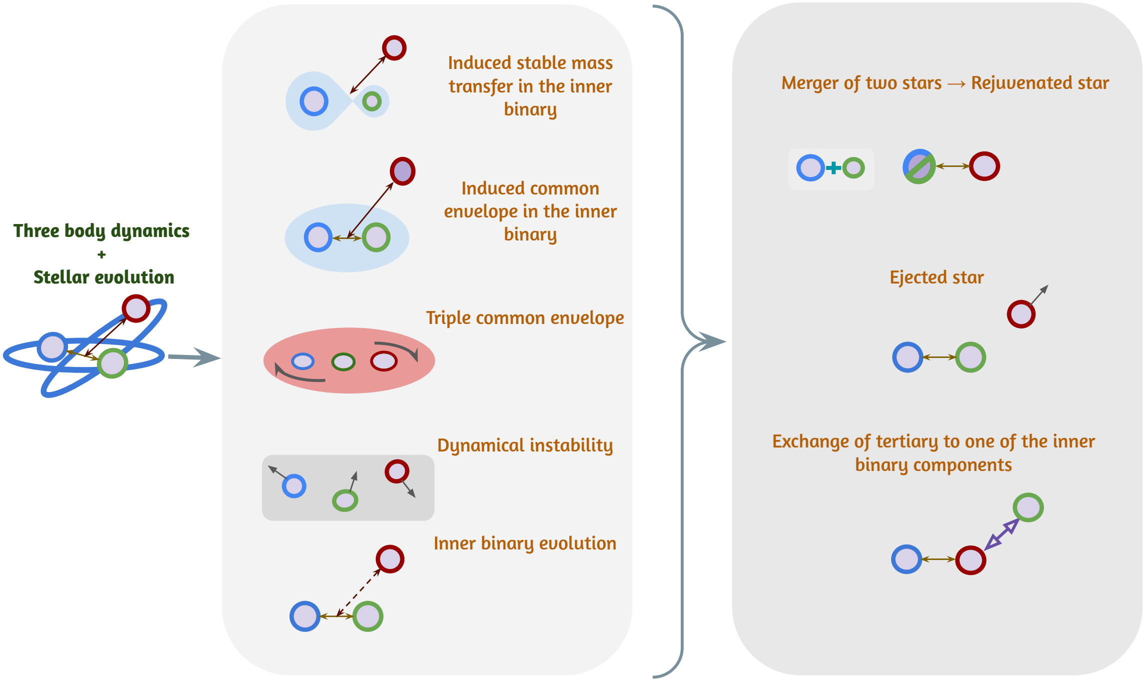

Figure 1.2: A schematic diagram illustrating the key processes that drive the evolutionary phases of a triple system, ultimately leading to a SNe Ia or the emission of gravitational waves.

A critical consequence in compact inner binaries is the enhancement of short-range forces such as tidal forces. Tidal forces work to reduce orbital eccentricity and gradually shrink the inner binary's orbit. When ZLK-driven eccentricity oscillations are present, tides can accelerate orbital decay, further tightening the orbit and enhancing the likelihood of mass transfer or merger events (Kiseleva et al., 1998a; Eggleton & Kiseleva-Eggleton, 2001a; Fabrycky & Tremaine, 2007). Additionally, gravitational perturbations from the third star introduce further modifications to the inner binary's evolution, adding another layer of complexity to the system's long-term dynamics.

The perturbations from the third star can induce Roche-lobe overflow, triggering common envelope evolution. Eccentricity-driven orbital shrinkage may cause a star to fill its Roche lobe, leading to mass transfer that can form cataclysmic variables, low-mass X-ray binaries, or ultra-compact binaries (Tokovinin, 2016). In some cases, this mass transfer can become unstable, leading to common-envelope evolution that accelerates orbital decay and results in either a merger or envelope ejection, altering the system's outcome. These induced mass transfer episodes either do not occur or occur at different times compared to those in isolated binaries, ultimately influencing the system's fate.

As the inner binary's eccentricity increases, periastron passages bring the stars closer together, accelerating orbital decay. In compact object binaries, gravitational-wave emission becomes the dominant mechanism in the final evolutionary stages (Peters, 1964). ZLK-induced eccentricity oscillations significantly enhance gravitational-wave emission, reducing the merger timescale by orders of magnitude compared to circularized binaries (Wen, 2003; Antonini et al., 2014). This effect is especially strong in systems with compact objects like white dwarfs, where extreme eccentricities drive rapid inspirals and potential electromagnetic counterparts. A merger could trigger a highly energetic explosion, such as a SNe Ia, or physical collisions in highly eccentric systems may directly detonate a white dwarf, producing luminous transients, possibly SNe Ia.

In triple star systems, an intriguing evolutionary phase is triple common envelope (TCE) evolution, where the outer star engulfs both inner binary components within a shared envelope. Although not fully understood, TCE has been proposed as a formation channel for tight hierarchical triples, binary white dwarfs, or prompt stellar mergers due to extreme orbital decay (Comerford & Izzard, 2020; Glanz & Perets, 2021). The expulsion of the envelope can lead to the formation of compact hierarchical triples, ejection of one of the stars, exchange interactions or mergers from extreme orbital shrinkage. Understanding TCE events is crucial for predicting compact object populations observed in gravitational wave detections.

Dynamical instabilities in triple systems can significantly alter evolutionary paths, inducing chaotic orbital behavior that leads to extreme eccentricity excursions, direct stellar collisions, or ejections of one component (Perets & Kratter, 2012). These processes contribute to the formation of compact binaries, some of which are key progenitors of gravitational-wave events. When perturbations from the outer star destabilize the inner binary, chaotic interactions can lead to direct collisions, highly eccentric mergers, or star ejections, all of which are critical in shaping compact object binaries and contributing to gravitational-wave signals.

Fig. 1.2 illustrates the key processes in the evolution of triple star systems. ZLK oscillations, combined with tidal effects, mass transfer, common envelope evolution, and dynamical instabilities, drive the system toward mergers, physical collisions, or the formation of compact binaries and potential SNe Ia progenitors. Understanding these processes is essential for interpreting both electromagnetic and gravitational-wave signals, providing key insights into the ultimate fate of these binaries.

1.3 Progenitors of SNe Ia and gravitational wave sources

SNe Ia are thought to result from thermonuclear explosions in white dwarfs. Two commonly suggested binary progenitor channels (Fig. 1.3) for SNe Ia explosions include the double degenerate (DD) channel, where both components of the binary system are white dwarfs (Webbink, 1984; Iben & Tutukov, 1984), and the single degenerate (SD) channel, in which an accreting Chandrasekhar-mass white dwarf may explode via delayed detonation,

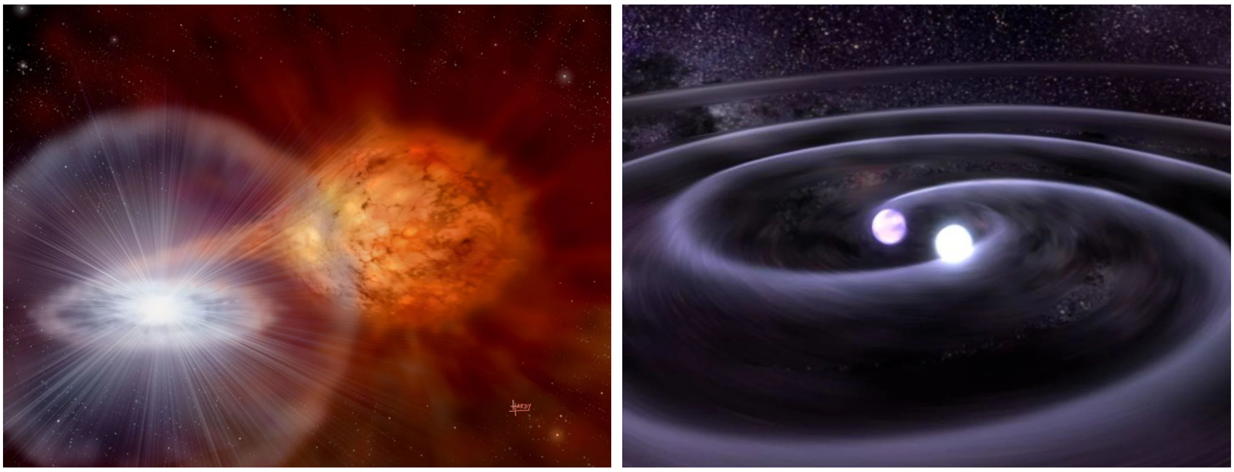

Figure 1.3: Artist's representation of the two main progenitor channels. On the left is the single degenerate scenario, where a white dwarf accretes H/He-rich material from a non-degenerate companion star. On the right is the double degenerate channel, where a white dwarf binary loses angular momentum through gravitational radiation and eventually merges. Image credits: Tod Strohmayer (GSFC)/Dana Berry (CXC), David A. Hardy & PPARC.

or an accreting sub-Chandrasekhar-mass white dwarf may explode via double detonation (Whelan & Iben, 1973). However, there are three key challenges in understanding SNe Ia: (1) discrepancies between theoretical predictions and observed rates, (2) uncertainty regarding the progenitor systems, and (3) a lack of understanding of the explosion mechanisms.

A substantial amount of work has been done to understand the progenitors through binary evolution (Nomoto, 1980, 1982a; Yoon & Langer, 2004a; Neunteufel et al., 2016, 2017, 2019; Boos et al., 2021). However, the consensus is that the rates from binary channels are too low to explain the observed frequency of SNe Ia (Ruiter et al., 2011; Claeys et al., 2014). Binary population synthesis models (Claeys et al., 2014) account for only a fraction of the observed rates (Maoz et al., 2012). This motivates the exploration of additional progenitor channels. Chapter 2 discusses the formation pathways and supernova Ia rates from triple star systems. The SD rates discussed in Chapter 2 require a very narrow parameter space for the explosion of the white dwarf as a SNe Ia. Building on this, Chapter 3 further explores one of the SD channels, the He-donor channel, as a potential progenitor for double-detonation supernova. We detail how mass transfer rate influences the fate of He-star and white dwarf binary.

SNe Ia require that the exploding white dwarfs have a mass of at least $0.9\,\mathrm{M}_{\odot}$. However, more massive white dwarfs tend to be fainter and harder to observe. The mass distribution in the galaxy peaks near the galactic center, which hosts a higher concentration of white dwarfs. As a result, these more massive white dwarfs, which could serve as progenitors for SNe Ia, are more challenging to detect through electromagnetic observations. However, LISA (Laser Interferometer Space Antenna) is expected to detect approximately $\mathcal{O}(10^6)$ Galactic double white dwarfs as part of a stochastic, unresolved gravitational-wave background, with a high enough signal-to-noise ratio to be above instrumental noise but not high enough to be individually resolvable. Additionally, it is anticipated that LISA will individually resolve around 10^3 to 10^4 of the "high signal-to-noise ratio" double white dwarfs, providing valuable insights into these systems (Korol et al., 2017; Lamberts et al., 2019; Wilhelm et al., 2021; Thiele et al., 2023; Li et al., 2023; Tang et al., 2024). However, as discussed in the previous section, triple systems are particularly efficient at forming short-period binaries. In this context, Chapter 4 focuses on how triples contribute to the formation of double white dwarf binaries, which can be detected by LISA.

1.4 Content of this thesis

Having introduced various aspects of interacting white dwarfs, I delve into some interesting aspects of white dwarfs in multiple star systems in this thesis. Each of the next three chapters presents one of my studies.

In Chapter 2, I conduct a population synthesis study of triple-star systems to understand their significance as progenitors of SNe Ia. I estimate the SNe Ia rate by studying interactions in higher-order multiple-star systems, such as triple systems. I used the evolutionary population synthesis code Multiple Stellar Evolution (`MSE`) to study stellar evolution, binary interactions, and gravitational dynamics of triple-star systems.

In Chapter 3, I focus on detailed modeling of He star + white dwarf systems using the `MESA` code, open-source 1D stellar evolution code. I simulated a range of hot subdwarf + white dwarf configurations and explored their outcomes, including supernovae, helium novae, and double white dwarfs. I also calculate the runaway velocities of surviving donor stars in systems that explode.

In Chapter 4, I examine the contribution of LISA-detected double white dwarfs from the triple channel. I combine `MSE` (population synthesis) with a Milky Way-like galaxy model from cosmological simulations (`TNG50`) to construct the Galactic LISA double white dwarf population from the triple channel and compare it with the contribution from the isolated binary channel. We predict a total number of double white dwarfs from the triple channel that will be observed as astrophysical noise, and we also predict the number of individually resolvable double white dwarfs from the triple channel.

In Chapter 5, I conclude the thesis by summarizing the major findings and providing an outlook for future research.

Chapter 2

Triple evolutionary pathways for type Ia supernovae

The contents of this chapter have been published in the Astrophysical Journal, 950, 9, 2023 as Rajamuthukumar et al. (2023)

2.1 Introduction

SNe Ia are standard candles that play a key role in distance measurements on cosmological scales. As such, they play an important role in our understanding of the structure and expansion rate of the Universe. SNe Ia are important for our comprehension of the chemical evolution of galaxies and of iron-group element nucleosynthesis. The origin of SNe Ia is thought to be thermonuclear explosions in white dwarfs, though our understanding of their progenitors and explosion mechanisms is not very clear (Wang & Han, 2012; Maoz et al., 2014; Livio & Mazzali, 2018; Ruiter, 2020).

Nevertheless, there are two commonly suggested binary progenitor channels (Ruiter, 2020) to produce SNe Ia explosions, which include the double degenerate (DD) channel (in which both the components of the binary system are white dwarfs, Webbink 1984, Iben & Tutukov 1984) and the single degenerate (SD) channel (in which an accreting Chandrasekhar mass white dwarf may explode via delayed detonation, or an accreting sub-Chandrasekhar mass white dwarf may explode via double detonation, Whelan & Iben 1973). Although substantial amount of work (Nomoto, 1980, 1982b,a; Yoon & Langer, 2004a,b; Neunteufel et al., 2016, 2017, 2019; Bauer et al., 2021) has been done to understand the progenitors through binary evolution, the general consensus is that the rates from the binary channels are too low to explain the observations (Ruiter et al., 2011; Claeys et al., 2014). The observed time integrated rate from Maoz et al. (2012) is $(1.3 \pm 0.2) \times 10^{-3}\,\mathrm{M}_{\odot}{}^{-1}$. Claeys et al. (2014) studied the formation channels for SNe Ia through binary population synthesis and estimated the time integrated overall SN rate to be $4.5 \times 10^{-4}\,\mathrm{M}_{\odot}{}^{-1}$, which could explain only a fraction of the observed rates from Maoz et al. (2012). This motivates the study of other progenitor channels.

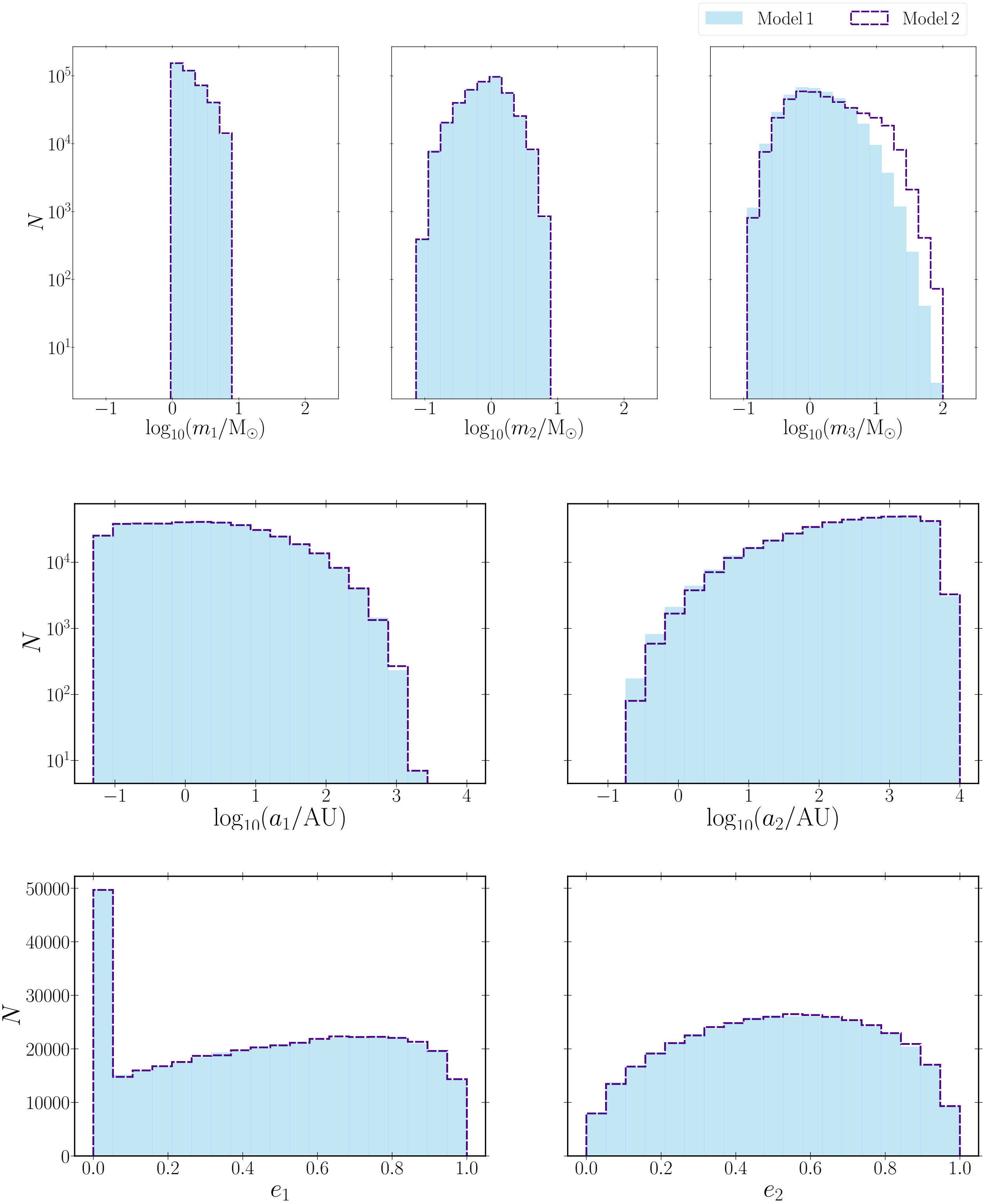

Figure 2.1: Initial parameter distributions of the constructed initial populations with two q_{out} models : the decaying exponential model (model 1, blue filled column) and the Moe & Di Stefano (2017) q distribution (model 2, dashed indigo line). The top panels show the mass distributions of the primary, secondary, and tertiary star. The middle panels represent the semimajor axis distributions for the inner and outer orbits. The bottom panels show the eccentricity distributions for the inner and outer orbit.

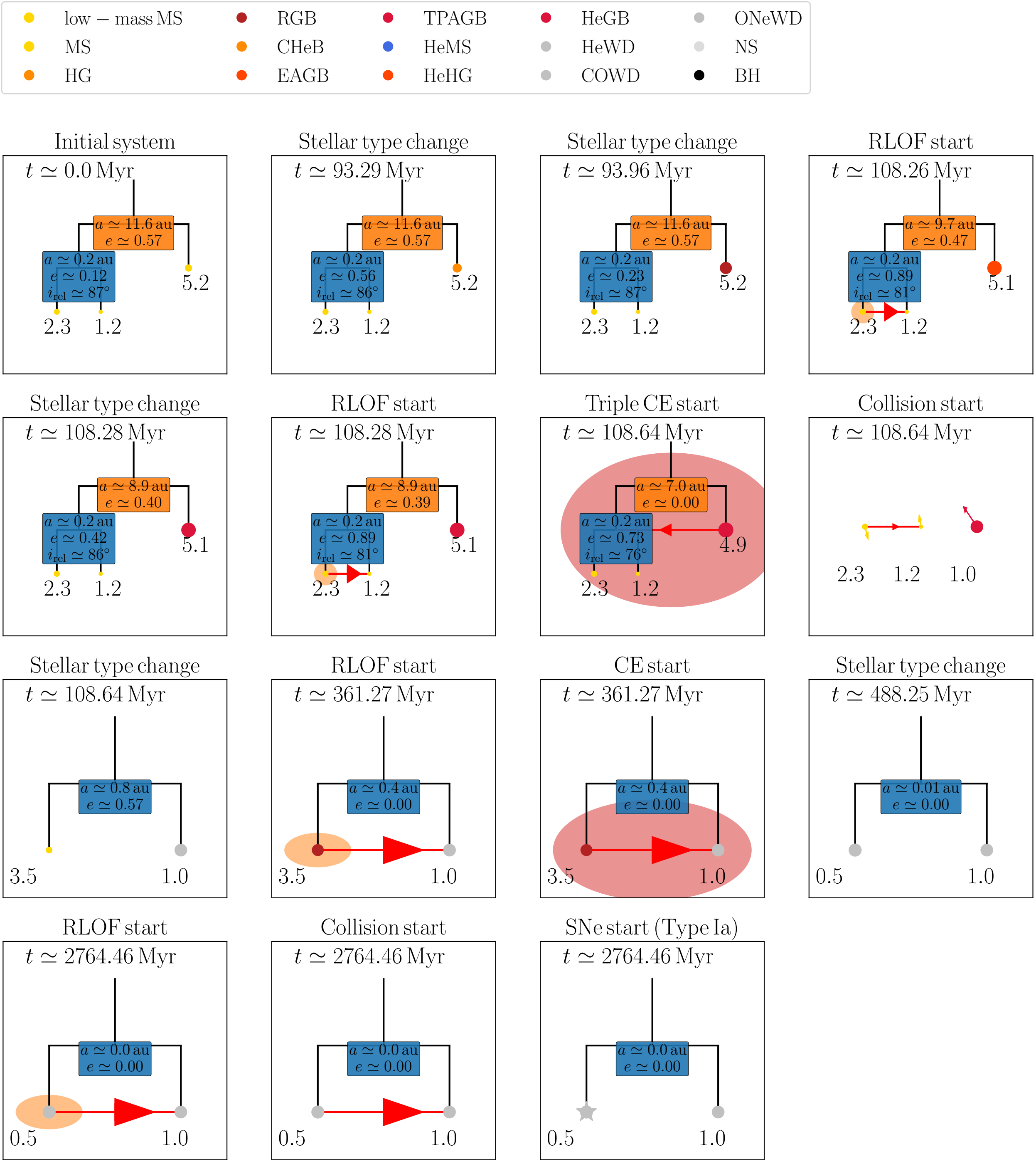

Figure 2.2: Example of a system undergoing triple common envelope (TCE). A triple system with a massive tertiary evolves first to transfer mass on top of the inner binary, to form a TCE. The inner binary merges to form a rejuvenated star at the end of TCE, which then interacts with the tertiary star to explode as SNe Ia. Refer to Appendix A.1 for more details on the mobile diagrams presented in this paper.

A formation channel for SNe Ia that has not been studied as extensively as the binary channel is the triple channel which involves hierarchical triple-star systems containing white dwarfs. This channel is particularly interesting because of its contribution to producing and disrupting close binaries. For an isolated binary, it is difficult to produce close binaries and mergers within a Hubble time. However, in a triple system, if the initial mutual inclination is sufficiently large, the inner binary can undergo high-amplitude eccentricity oscillations. This in turn also leads to changes in the mutual inclination of the system. These oscillations are known as von Zeipel Lidov Kozai (ZLK) oscillations (von Zeipel 1910; Kozai 1962; Lidov 1962, see Naoz 2016 for a review). ZLK oscillations, combined with tidal effects, can shrink the inner binary which results in the formation of close binaries (Mazeh & Shaham, 1979; Eggleton & Kiseleva-Eggleton, 2001a; Eggleton & Kisseleva-Eggleton, 2006; Fabrycky & Tremaine, 2007), cause earlier CE evolution (Hamers & Thompson, 2019; Toonen et al., 2020), accelerate mergers (Blaes et al., 2002; Thompson, 2011; Toonen et al., 2018), and induce dynamical instability which in turn results in a merger of two white dwarfs, and a SNe Ia explosion. From studies by Moe & Di Stefano (2017) and Raghavan et al. (2010), I know that about 10% of solar mass stars are found to be in triples with possible SNe Ia progenitors.

Previous studies of triple-star systems considered SNe Ia rates from head-on collisions arising from dynamical interactions (Katz & Dong, 2012), contributions from white dwarf mergers taking into account stellar evolution and dynamics (Hamers et al., 2013), isolated triples with a circular approximation for mass transfer (Toonen et al., 2018), the postulated progenitor triples from Gaia DR2 database (Hallakoun & Maoz, 2019), and ultra-wide white dwarf triples affected by fly-bys (Hamers & Thompson, 2019; Michaely, 2021). These studies considered dynamical interactions and/or stellar evolution and binary interactions such as tidal effects. However, their focus was on the DD formation pathway; there are no studies on the contribution of single degenerate channels (in which an accreting Chandrasekhar mass white dwarf may explode via delayed detonation, or an accreting sub-Chandrasekhar mass white dwarf may explode via double detonation, Whelan & Iben 1973) in triple systems, and in particular also self-consistently taking into account stellar and binary evolution (especially mass transfer in eccentric orbits), as well as gravitational dynamics.

In this paper, I present a comprehensive study of candidates for thermonuclear explosions originating from triple-star systems through both the single and DD channels. I note that not all thermonuclear SNe will result in SNe Ia, but may form related transients such as SNe Iax instead. For the purposes of this study, I use SN Ia as a catch-all form for transients resulting from the thermonuclear detonation of a white dwarf. In addition, in our simulations, I take into account the possibility for the tertiary star to transfer mass onto to the inner binary system which in turn can produce a triple common envelope (TCE). The paper begins with the methodology in Section 2, followed by the different formation channels for SNe Ia in Section 3. In Section 4, I present our statistical results. I discuss and conclude the results in Sections 5 and 6, respectively.

2.2 Methodology

2.2.1 Population sysnthesis

MSE

In this work, I use the evolutionary population synthesis code MSE (Multiple Stellar Evolution; Hamers et al. 2021, version-v0.87). The advantage of this code is that it incorporates prescriptions for stellar evolution, binary interactions (tides, mass transfer, etc.), dynamical perturbations from higher-order multiple systems, and fly-bys. MSE is a publicly available C/C++ code with a Python interface. It can evolve any number of stars as long as the system is originally hierarchical (later potential dynamical instabilities are modelled self-consistently through N-body methods). In order to tackle the complicated long-term dynamical evolution of multiple-star systems, MSE uses a hybrid approach which switches between the secular approximation (Hamers & Portegies Zwart, 2016; Hamers, 2018, 2020) and N-body integration (Rantala et al., 2020) during run time. Throughout the dynamical evolution, post-Newtonian (PN) terms are taken into account up to and including 2.5 PN order.

Single star evolution in MSE is based on the SSE algorithms (Hurley et al., 2000) based on stellar evolutionary tracks by Pols et al. (1998). The code uses modified BSE prescriptions (Hurley et al., 2002) for binary interactions. Tidal evolution is modelled following the equilibrium tide model (Eggleton et al., 1998). Here the tides are applied to star-star and star-composite systems. The code takes into account eccentric mass transfer, adopting the model of Hamers & Dosopoulou (2019). When mass transfer is deemed unstable, CE is modelled using the energy conservation mechanism, i.e, the α-λ CE prescription (Paczynski, 1976). The outer companion, when massive enough, can transfer mass onto the inner binary components, and the subsequent evolution is modelled following approximate prescriptions (Hamers et al., 2022).

In MSE, the effects of passing stars (fly-bys) are taken into account as appropriate for low-density ($n_\star = 0.1\,\mathrm{pc}^{-3}$) environments. An exploration of the impact on triples of encounters in high-density environments such as globular clusters, although interesting, is beyond the scope of this paper. The perturber mass is sampled either from Kroupa (2001) and encounters are sampled assumed an encounter sphere of radius $R_\mathrm{enc} = 10^5$ au with velocities sampled from Maxwellian distribution of dispersion $\sigma_\star = 30\,\mathrm{kms}^{-1}$. These fly-bys become significant when the semimajor axis of the orbit exceeds approximately 10^3 au.

SNe Ia prescription

The initial version of MSE (Hamers et al., 2021) uses BSE (Hurley et al., 2002) prescriptions for SNe Ia explosions. Within these prescriptions, an accreting CO white dwarf has accumulated 0.15 $\mathrm{M}_\odot$ of of helium, the white dwarf explodes in a SNe Ia. This assumption, however, has been shown to be incomplete since its first implementation. The amount of material required to initiate a helium detonation, and subsequent ignition of the CO-core has been shown to depend on other parameters of the progenitor binary, most notably the mass of the accretor, the mass transfer rate and, to some extent, assumptions on rotation, angular momentum transport and viscose heating (Yoon & Langer, 2004b,a, 2005; Woosley & Kasen, 2011; Piersanti et al., 2014; Neunteufel et al., 2017). Further, as summarized particularly by Piersanti et al. (2014), depending on the mass transfer rate, outcomes of He-accretion onto CO-white dwarfs range from possible double detonation ($\dot{M} \lesssim 7 \cdot 10^{-8}\,\mathrm{M_\odot/yr}$) via massive He-novae of decreasing intensity $\dot{M} \gtrsim 7 \cdot 10^{-8}\,\mathrm{M_\odot/yr}$), (see Kato & Hachisu, 2004) to steady burning and re ignition as a He-red giant ($\dot{M} \gtrsim 1 \cdot 10^{-6}\,\mathrm{M_\odot/yr}$) in a space of about two orders of magnitude. As further shown by Neunteufel et al. (2016), a system may move between these different mass transfer regimes, with systems, e.g., first undergoing weak helium flashes to then finally terminate in a SN.

In order to take these different possibilities into account, this study employs a refined prescription, considering the mass of the accretor as well as the rate of mass accretion, for deciding on the final outcome of helium accretion Neunteufel et al. (2016). This prescription combines the accretion-rate-dependent accretion efficiencies (η) presented by Kato & Hachisu (2004) at values of mass transfer rates with the occurrence of detonation at low mass transfer rates as presented by Woosley & Kasen (2011). The resulting prescription can be written

$$\eta = \begin{cases} 1, & \text{if } 0 < [\dot{M}] < \dot{M}_{\mathrm{WK,max}} \ , \\ 0, & \text{if } \dot{M}_{\mathrm{WK,max}} < \dot{M} < \dot{M}_{\mathrm{KH,min}} \ , \\ \eta_{\mathrm{KH}}(M_{\mathrm{WD}}, \dot{M}), & \text{if } \dot{M}_{\mathrm{KH,min}} < \dot{M} \ , \\ 1, & \text{if } \dot{M}_{\mathrm{KH,max}} < \dot{M} \end{cases} \tag{2.1}$$

with $\dot{M}_{\mathrm{WK,max}}$ and $\dot{M}_{\mathrm{KH,min}}$ the upper and lower limits of accretion rates studied by Woosley & Kasen (2011) and Kato & Hachisu (2004) respectively. I note that, while Neunteufel et al. (2016) used a time-averaged mass transfer rate in order to exclude ignitions resulting from spurious variations in the mass transfer rate, as are prone to happen in detailed stellar evolution, this approach is unnecessary in the context of population synthesis.

With regards to the DD SNe Ia, a new prescription combining results from varies previous hydrodynamics simulation studies has been incorporated into MSE. Collisions in MSE can happen either via a circular merger, usually following CE evolution, or eccentric collision driven by secular evolution. I assume the outcome will be SNe Ia when there is a circular merger of a He white dwarf and CO white dwarf (irrespective of their masses). I also assume that the coalescence of two CO white dwarfs in which one of them is more massive than 0.9 $\mathrm{M_\odot}$ results in a SNe Ia explosion (Pakmor et al., 2010, 2013). In the event of an eccentric collision, the collision of two CO white dwarfs, two ONe white dwarfs, or a CO white dwarf and an ONe white dwarf is assumed to lead to SNe Ia.

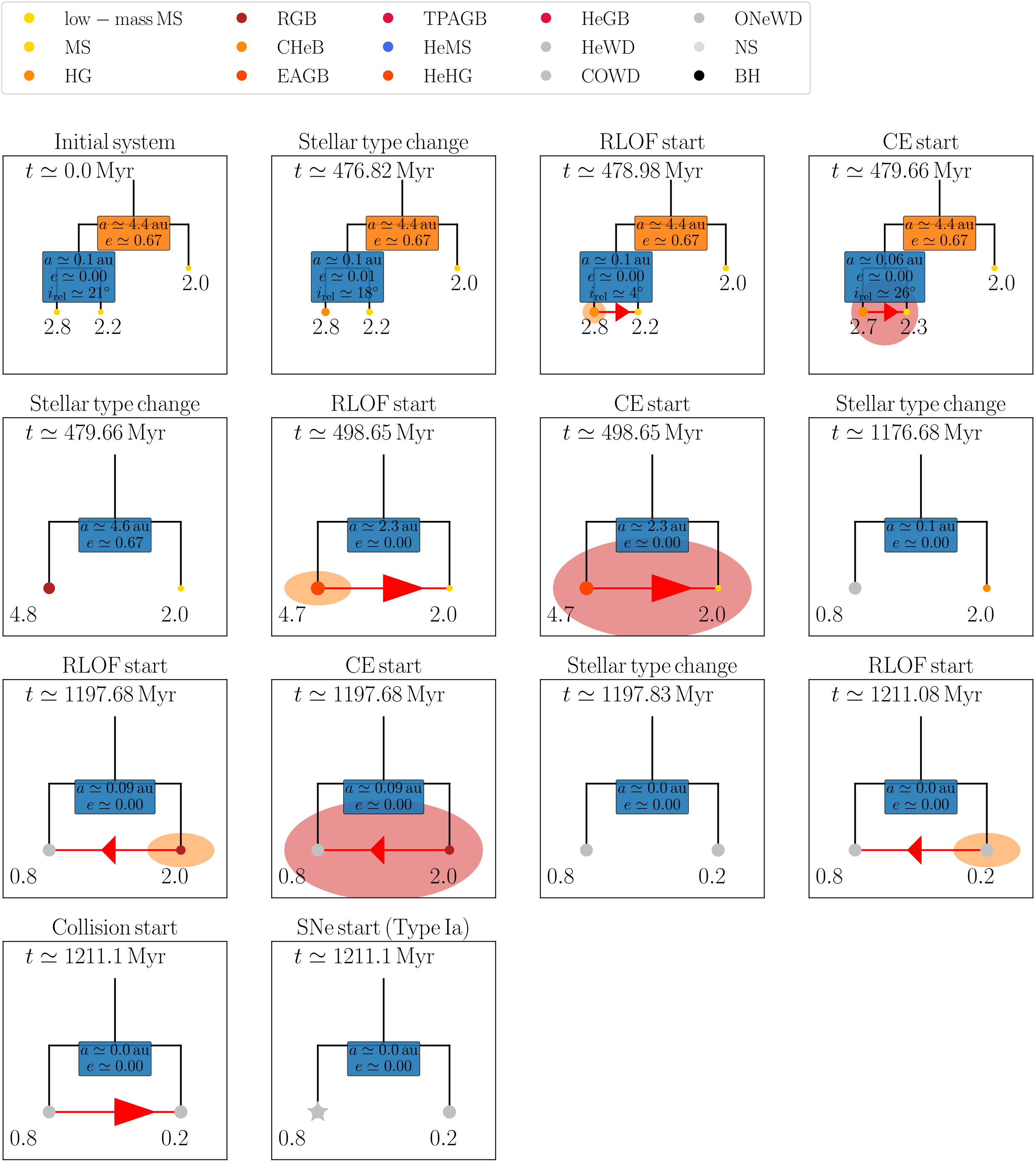

Figure 2.3: Example of a SNe Ia from the binary system that is formed as a result of double merger. A triple system in which the inner binary components merges to form a new massive star which then interacts with the tertiary star to produce SNe Ia explosion.

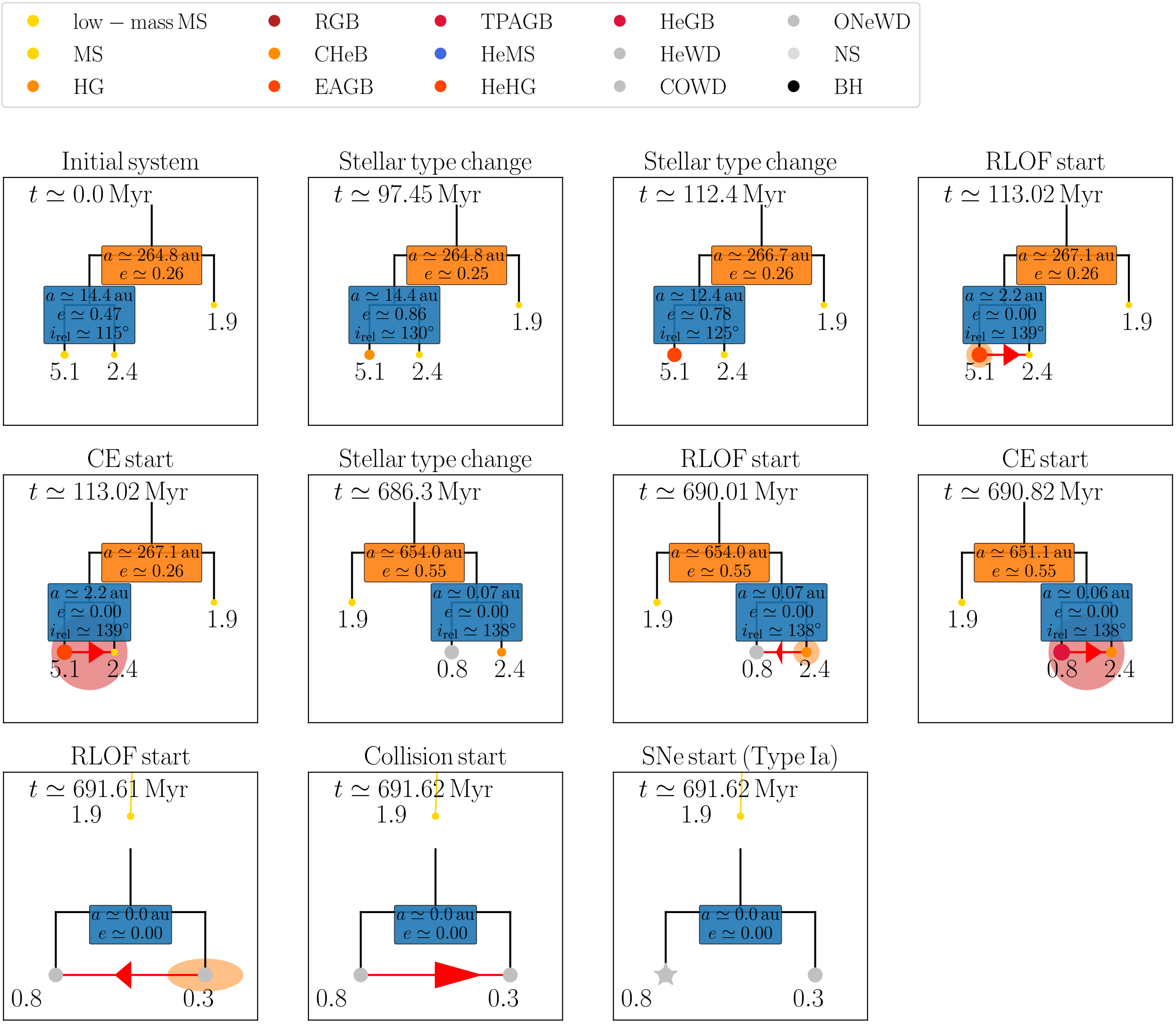

Figure 2.4: Example of an triple evolution channel in which the tertiary is unbound at the time of SNe Ia explosion. A triple system in which the primary star of the inner binary fills its Roche lobe and undergoes a first CE phase at around 113 Myr. At the end of CE, the primary evolves into a white dwarf which then accretes mass from the secondary star forming a second CE. At the end of the second CE, the tertiary star has become unbound due to rapid mass loss in the inner orbit the secondary also evolves into a white dwarf which then collides with the other white dwarf to explode as SNe Ia.

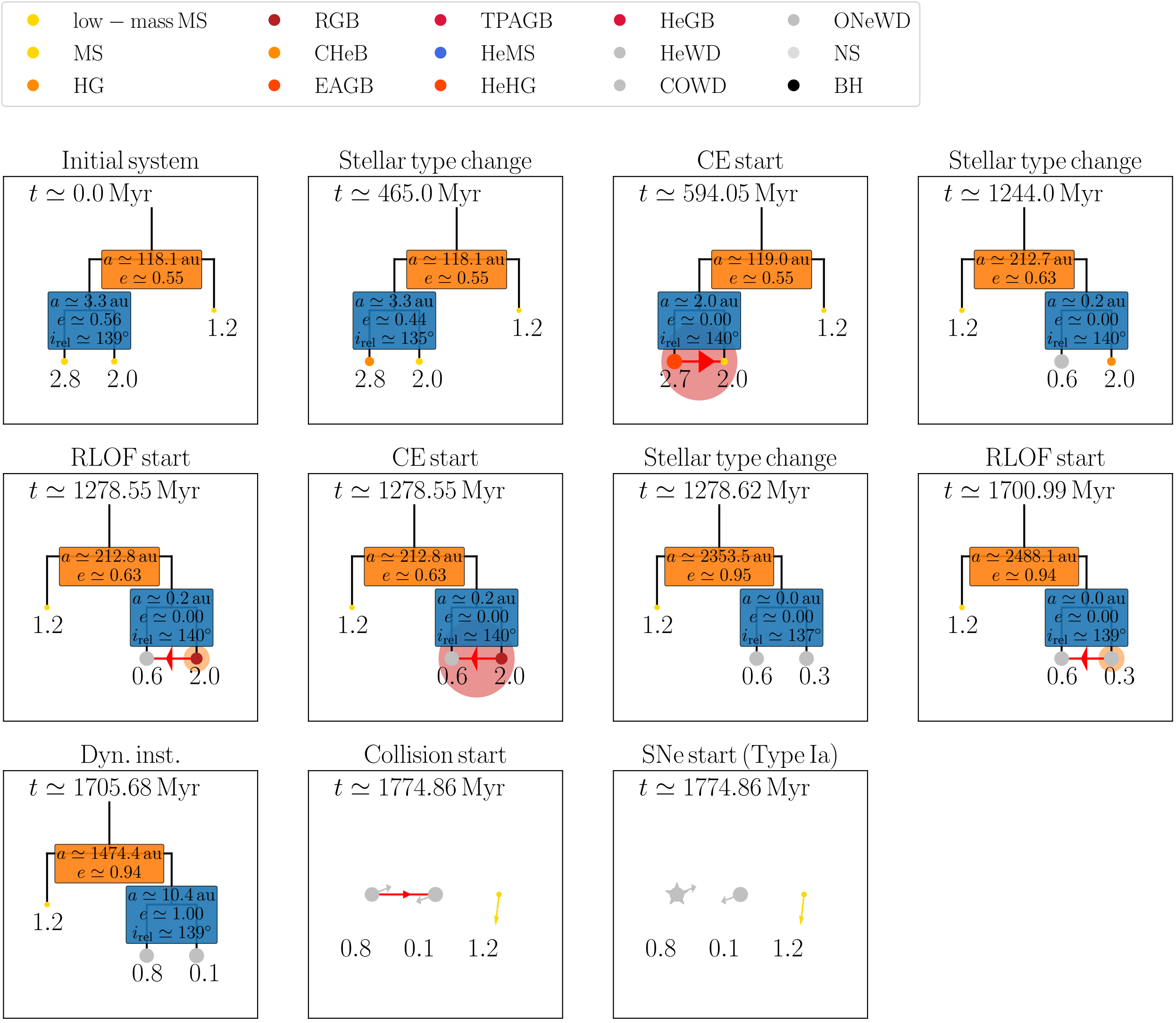

Figure 2.5: Example of an eccentric collision. The isolated binary channel usually predicts that the binary gets circularized ($e \approx 0$) after a CE episode. Here, the figure shows that the inner binary can still achieve high eccentricities from dynamical perturbations, which then can lead to a SNe Ia explosion via collision.

2.2.2 Initial distributions

I adopt a population synthesis method, in which the initial conditions for a large number of triple-star systems are generated based on a Monte Carlo approach. Here, I describe the assumptions made in this procedure. The primary mass of the inner binary m_1 (i.e., the mass of the initially most massive star in the inner binary system), is set between 1 $M_\odot$ and 6.5 $M_\odot$ to ensure the formation of at least one CO white dwarf within a Hubble time in

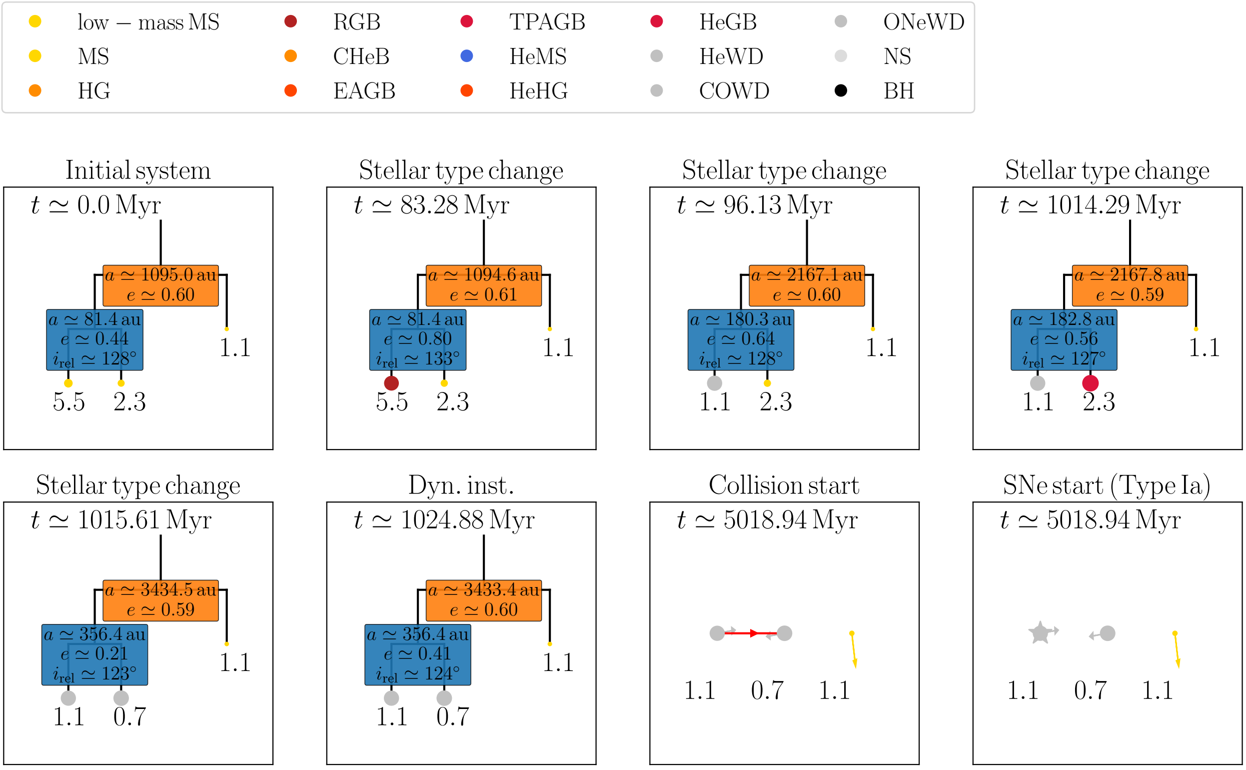

Figure 2.6: Example of a SNe Ia driven by dynamical instability, without any CE evolution phases. A triple system undergoes eccentricity oscillations in the inner binary, and then the inner binary white dwarfs collide due to dynamical instability, producing a SNe Ia explosion. This channel is particularly interesting in the sense that it does not involve any CE phase.

isolation, and it follows Kroupa (2001). The distribution of the secondary mass is modeled after the observational fit functions of Moe & Di Stefano (2017). The initial orbital period and eccentricity distributions (for both inner and outer orbits) are also drawn from the observational fit functions of Moe & Di Stefano (2017). The orbital periods are sampled in the range $0.2 < \log(P/\text{days}) < 8$. Eccentricities of both orbits are sampled between 0 and 1. The initial mutual inclinations are uniformly distributed in $\cos(i)$. The longitudes of the ascending node and arguments of periapsis are sampled from uniform distributions. These assumptions correspond to isotropic orientations of the inner and outer orbits. The systems that does not satisfy the stability criteria of Mardling & Aarseth (2001) are rejected. I also eliminate systems with stars that are filling their Roche lobes at the start of the evolution at periapsis, using the fit of Eggleton (1983), and using the mass-radius relation $R \propto M^{0.7}$ to estimate the initial stellar main-sequence radii[1].

The mass-ratio distribution involving the tertiary (outer) star in triple systems, specif-

---

[1] This more approximate method of determining the main-sequence radii is only adopted for sampling purposes.

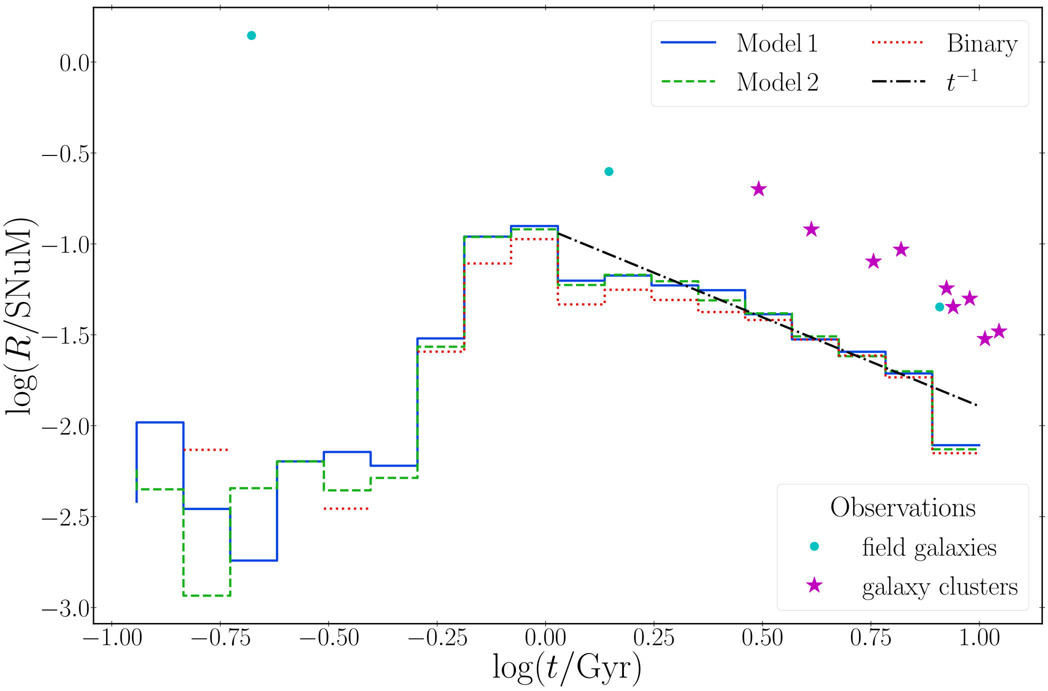

Figure 2.7: Delay time distribution (DTD) from all DD SNe Ia in our simulations. The solid blue line (Decaying exponential q_{out} model) and dashed green line (Extrapolating q from Moe & Di Stefano (2017) q_{out} model) correspond to the DTD from triple population synthesis. The dotted red line represents the DTD from isolated binary population synthesis. Also, the black dashed dot line shows that the later parts of the DTD is found to follow a power law shape ($\propto t^{-1}$). In addition, observational SNe Ia rates from field galaxies (Refer to Table 2 from Maoz & Graur (2017)) and galaxy clusters (Refer to Table 3 from Maoz & Graur (2017)) are shown by cyan and magenta points, respectively.

Models	q_{out}	α_{CE}	Fly-bys	Metallicity
Model 1	$\exp(-q_{\mathrm{out}}\lambda)$; $\lambda = 1.05$	1	Included	0.02
Model 2	Extrapolating Moe & Di Stefano 2017	1	Included	0.02
Model 3	$\exp(-q_{\mathrm{out}}\lambda)$; $\lambda = 1.05$	10	Included	0.02
Model 4	$\exp(-q_{\mathrm{out}}\lambda)$; $\lambda = 1.05$	0.1	Included	0.02
Model 5	$\exp(-q_{\mathrm{out}}\lambda)$; $\lambda = 1.05$	1	Ignored	0.02
Model 6	$\exp(-q_{\mathrm{out}}\lambda)$; $\lambda = 1.05$	1	Included	0.001

Table 2.1: Overview of the different models, stating the assumptions for the distribution of the mass ratio between the outer star and the inner binary $q_{\mathrm{out}} \equiv m_3/(m_1+m_2)$, the choice for the CE paramater α_{ce}, whether or not fly-bys are accounted for, and the metallicity

ically, the outer mass ratio $q_{\rm out} \equiv m_3/(m_1+m_2)$, is not very well constrained. From the Multiple Star Catalogue (MSC; Tokovinin 2018), there are about seven per cent of systems in which the tertiary star is more massive than the total mass of the inner binary. These systems are potentially interesting because they favor channels which involve triple mass transfer, i.e., when the tertiary star fills its Roche lobe around the inner binary (Glanz & Perets, 2021; Hamers et al., 2022). In order to allow for the possibility of systems with a massive tertiary star, I have constructed two different models for the initial outer mass ratio distribution. For the first model (hereafter Model 1), I fit a decaying exponential function to the data from the MSC and find the best fitted parameters. The second model (hereafter Model 2) is an extrapolation of the mass ratio distribution of Moe & Di Stefano (2017). The first mass ratio model is of the form

$$\frac{{\rm d}N}{{\rm d}q_{\rm out}} \propto \exp(-q_{\rm out}\lambda), \tag{2.2}$$

where $\lambda = 1.05$. The decaying exponential model best fits the current observations. However, the MSC has substantial observational biases for triple (and higher-order) systems and I especially expect strong observational biases against triples with high-mass tertiaries and low mass inner binaries (high mass-ratio systems). Thus, I take into account both models in our work, as a means to explore the current uncertainties in the outer mass ration distribution.

In addition to considering two models for the assumed distribution of $q_{\rm out}$, I vary physical model parameters in our simulations to investigate the impact of physical uncertainties, as well as effects that are often ignored in the literature. I inspect the effects of fly-bys and various CE parameters in our work. I also study the SNe Ia rate from stars with sub-solar metallicity.

2.2.3 Construction of the initial population

Our population pool includes 4×10^5 triple systems for both Models 1 and 2. Triple systems which include all the varying model parameters such as CE, flybys and metallicity constitute 4×10^5 systems. In total, our triple population sample size sums up to be 1.2×10^6. In addition, in order to investigate the effect of the tertiary star, I re-run our main models without the tertiary star (only inner binary systems). The size of the inner binary population is 8×10^5. I also study the contribution from isolated binaries, for which I construct a binary population of size 1×10^5. As explained later in Section 4.4, the latter isolated binary population is significantly different from the triple population with the tertiary star removed. In total, our population pool consists of 2.1×10^6 systems. The constructed population is evolved for a period of 10 Gyr with an imposed maximum wall time of 5 hours.

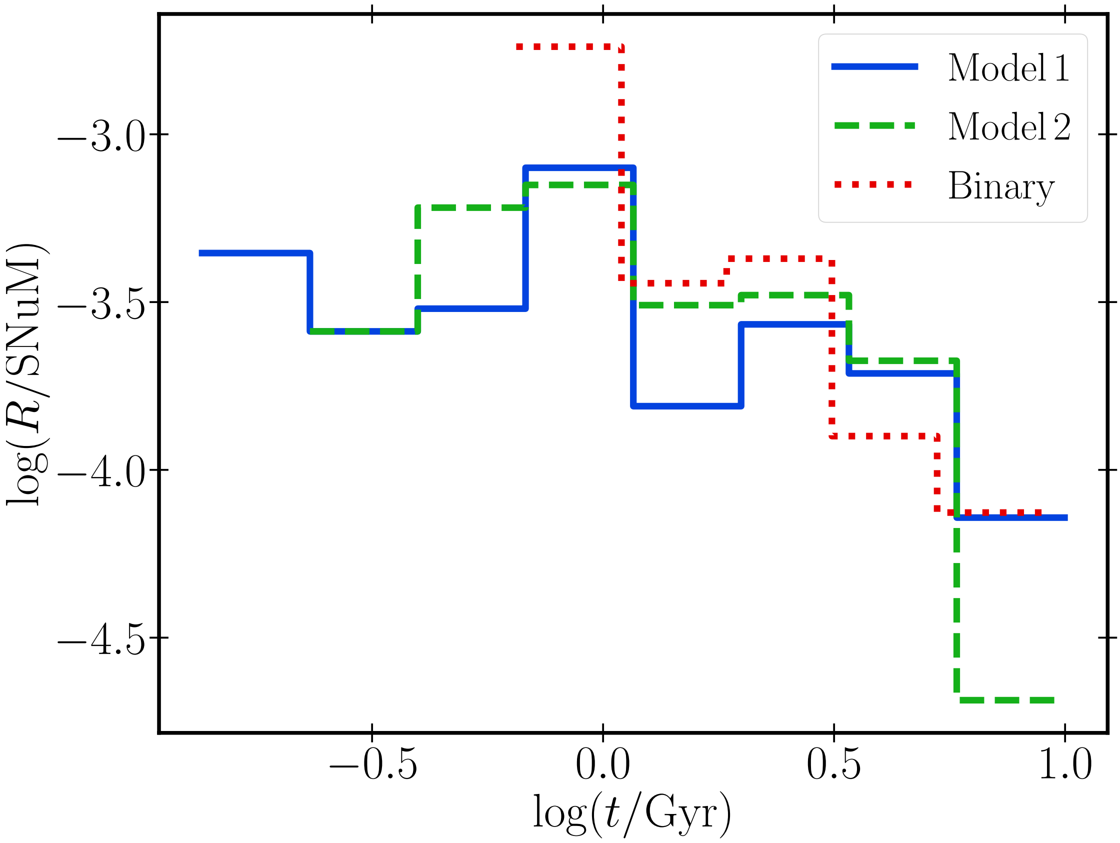

Figure 2.8: DTD from SD SNe Ia. The solid blue line (q_{out} model - Decaying exponential q_{out} model) and dashed green line (q_{out} model - Extrapolating q from Moe & Di Stefano (2017)) correspond to the DTD from our simulated triples. The dotted red line represents the DTD from our simulated isolated binaries.

2.3 Evolutionary Pathways

In this section, I summarize evolutionary pathways for forming SNe Ia in triple systems as found in our population synthesis calculations. I restrict our explanation to formation channels that demand a tertiary to form SNe Ia. In order to select the systems that have a effect from the tertiary, I compare SNe Ia from triple population synthesis with those from inner binary (without tertiary) population synthesis. I provide 5 unique formation channels for producing SNe Ia only from triple systems. Table 2.2 quantifies the contribution from these evolutionary pathways. The presented evolutionary pathways are unique to triples and not mutually exclusive. The evolutionary pathways in which the tertiary does not contribute in producing SNe Ia explosion is similar to binary evolution channels and not being presented here.

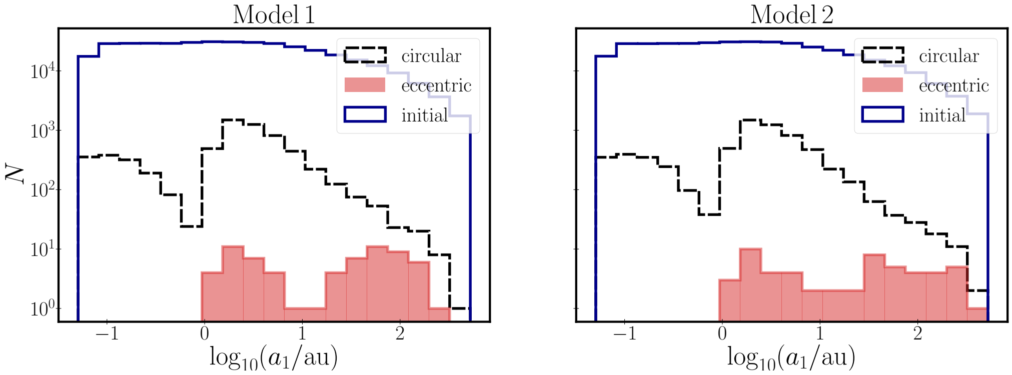

Figure 2.9: Distribution of the initial inner semimajor axes of all triple systems (blue solid lines),that explode as SNe Ia via circular mergers (black dashed lines) and eccentric collision (red filled columns). The two models represent the results from the two q_{out} models: Model 1 - Decaying Exponential fit to q_{out} observations, Model 2 - Extrapolating Moe & Di Stefano (2017) q distribution.

2.3.1 Triple common envelope

From our results, TCE is an important channel for producing SNe Ia from triple-star systems, responsible for $4-13\%$ of all SNe Ias by triples in our set of models. Fig. 2.2 shows a mobile diagram (see Appendix A.1 for an explanation of the mobile diagrams presented here) of a triple system undergoing TCE, causing a merger of the inner binary, which then leads to a SNe Ia later.

If the tertiary star is relatively close and more massive than the total mass of the inner binary, it can start transferring mass on to the inner binary, forming a TCE around the inner binary. At the end of TCE, if dynamical instability is triggered, one of the inner binary components can get exchanged with the tertiary, forming an exchange triple. Other possibilities include TCE evolution followed by a merger of the inner binary, or a merger of an inner binary component with the tertiary. TCE evolution can disrupt the triple system by unbinding the tertiary or inner binary component, resulting in a binary system with the remaining components. If the CE is assumed to be more efficient ($\alpha_{\mathrm{CE}} = 10$), it induces more inner binary mergers and thereby fewer TCE episodes.

2.3.2 Double mergers

I identify two different cases of scenarios leading to SNe Ia and involving double mergers. In the first case, there is an early mass-transfer episode during the main sequence, which merges the inner binary components to a rejuvenated main-sequence star. This results in a new binary, with one the component being the original tertiary star, and the other as the merger remnant of the inner binary. These two stars then evolve, and this later leads to a SNe Ia explosion. In the second case, the tertiary star, as a result of secular eccentricity excitation coupled with tides, shrinks the inner binary which leads to an early CE phase

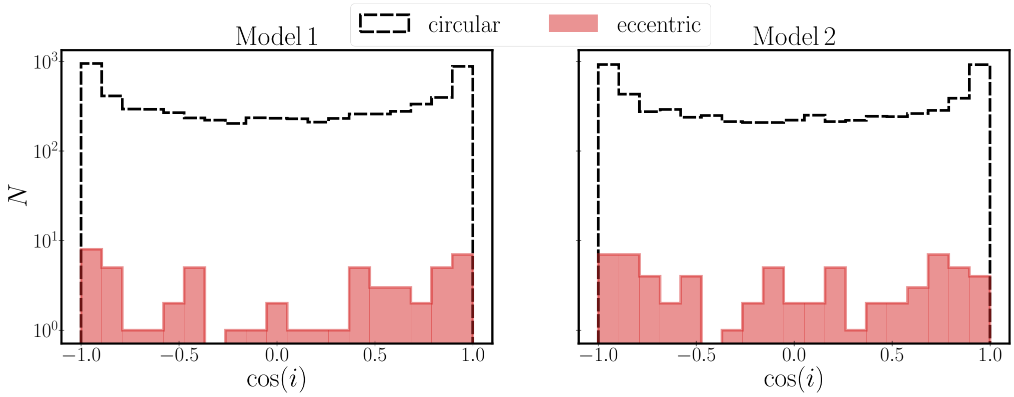

Figure 2.10: Distribution of the mutual inclinations of triple systems that explode as SNe Ia via circular mergers (black dashed lines) and eccentric collisions (red filled columns). The two models represent the results from the two q_{out} models: Model 1 - Decaying Exponential fit to q_{out} observations, Model 2 - Extrapolating Moe & Di Stefano (2017) q distribution.

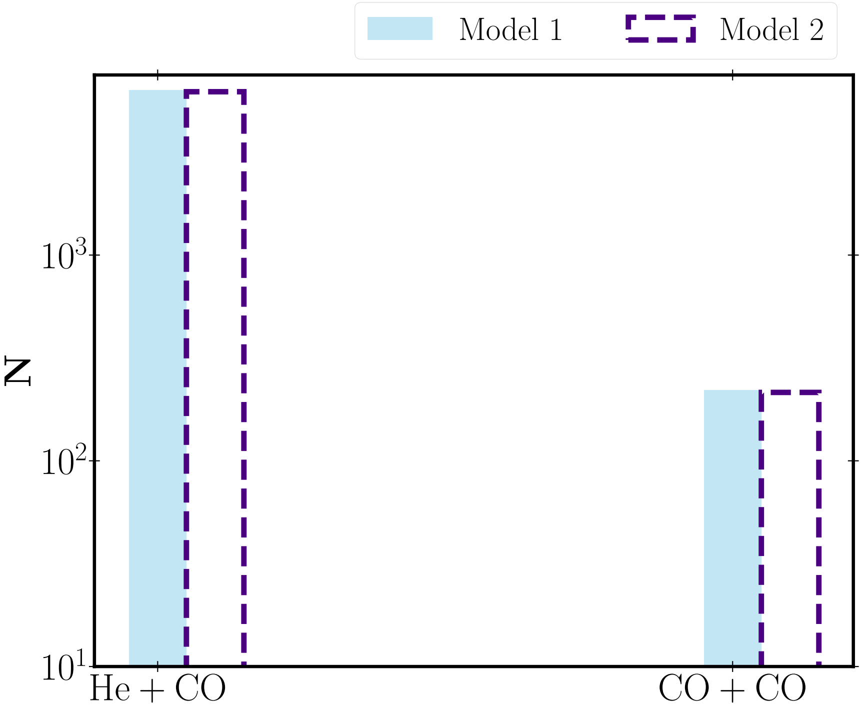

Figure 2.11: Combinations of mergers/collisions of He+CO white dwarfs and CO+CO white dwarfs contributing to DD SNe Ia.

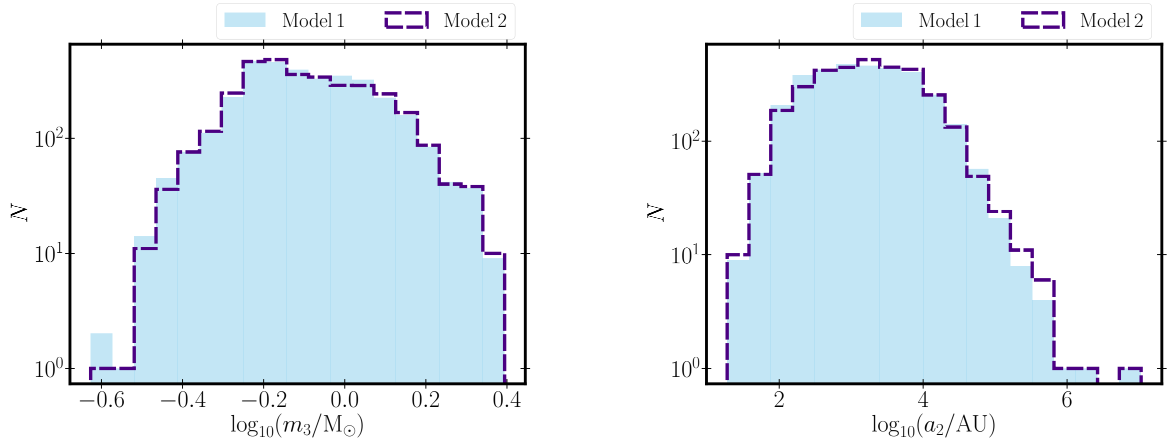

Figure 2.12: Distribution of third star properties. Left panel: Distribution of the tertiary star mass when the inner binary explodes as SNe Ia, in those cases when the tertiary is still bound at the time of the explosion. Right panel: Outer semimajor axis distribution for systems in which the inner binary explodes as SNe Ia.

that subsequently merges the inner binary. This forms a new binary with the merger remnant and original tertiary star, and produces a SNe Ia event later. Fig. 2.3 shows a triple-star system in which the inner binary merges through a CE phase to produce a new star, which then further undergoes two more CE phases and then collide with the tertiary star to produce SNe Ia.

2.3.3 Unbound tertiary

In the course of the evolution, the tertiary star can get unbound due to different reasons. For example, Fig. 2.4 shows a triple channel in which the tertiary gets unbound when the inner binary undergoes a CE phase. CE in inner binary and TCE are responsible for unbinding the tertiary star in about 67 per cent and 7 per cent of SNe Ia events through this channel, respectively. When the tertiary star is massive enough, it can collapse into a neutron star resulting in a type II supernovae. In about 22 per cent of the Unbound tertiary channel, the mass loss and/or natal kick during this type II supernovae can unbind the tertiary star, while the inner binary later produces a SNe Ia event. The tertiary star can also become unbound when there is a CE episode in the inner binary, which is associated with rapid mass loss in the inner binary. Fly-bys unbind the tertiary star when the semimajor axis is of the order of 10^3 au or wider. When the triple system becomes dynamically unstable, one of the stars can get ejected out of the system. Fly-bys and dynamical unstability contribute 2 per cent each to this channel.

2.3.4 Eccentric collision

The formation of close binaries in the isolated binary channel is mainly explained by CE phases. These systems are nearly always circularized at the end of the CE phase. But in the case of triple star systems, there is a possibility that, even after the CE phase, the tertiary can induce eccentricities in the close inner binary through secular evolution. I see that about 1 per cent of systems that form SNe Ia, experience eccentric collisions. There is also another possibility of forming a SNe Ia only through the dynamical channel. In these type of systems, the eccentricity of the inner binary oscillate due to the perturbations from the tertiary star and after an elapse of time, the secular approximation breaks down (Antonini et al., 2014; Antognini et al., 2014; Luo et al., 2016), the inner binary components collide at extremely-high eccentricity, leading to a SNe Ia explosion. Fig. 2.5 shows an example of a system achieving such high eccentricities ($e \approx 1$), then causing a collision and hence a SNe Ia explosion.

2.3.5 SNe Ia driven by dynamical instability

In an isolated binary channel, the formation of SNe Ia cannot be explained without undergoing a CE phase. In our simulations, in addition to mergers during CE, there is also the possibility of physical collisions driven by (chaotic) few-body dynamics, following the onset of dynamical instability. For example, Fig. 2.6 shows a pure dynamical channel to produce SNe Ia. During the course of the evolution, if the inner binary becomes dynamically unstable following Mardling & Aarseth (2001), there can be a head-on collision between the binary components which leads to a SNe Ia explosion.

2.4 Statistical Results

I present the delay time distribution and detailed statistical analysis of the contribution from different progenitors in this section. Table 2.3 gives the overview of the time-integrated rate from triple (various models) and binary channels. Table 2.4 summarizes the contributions of different progenitors to SNe Ia events.

2.4.1 Delay time distribution and SNe Ia rate

I assume a starburst at time $t = 0$; the SNe Ia rate during a particular time interval ΔT is then calculated using

$$R = \frac{N}{M_\star \Delta T}, \tag{2.3}$$

where N is the total number of SNe Ia explosions during ΔT and $M_\star$ is the total mass of the synthesized stellar population. I assume that the synthesized stellar population only constitutes of single, binary and triple stars. And, any contribution from higher order systems is neglected. I use the primary mass dependent multiplicity fraction from Moe &

Models	TCE (%)	Double mergers (%)	Unbound Tertiary (%)	Eccentric collision (%)	Dynamical Instability (%)
Model 1	12.0 ± 0.5	21.4 ± 0.5	28.1 ± 0.7	0.8 ± 0.1	1.1 ± 0.1
Model 2	12.6 ± 0.5	20.1 ± 0.5	29.9 ± 0.8	1.1 ± 0.1	1.0 ± 0.1
Model 3	3.8 ± 0.6	20.1 ± 1.0	31.2 ± 1.9	4.0 ± 0.6	2.3 ± 0.5
Model 4	12.6 ± 1.8	60.0 ± 3.4	14.3 ± 1.9	2.3 ± 0.7	2.1 ± 0.7
Model 5	11.8 ± 0.9	20.1 ± 1.0	26.5 ± 1.4	0.4 ± 0.1	0.7 ± 0.2
Model 6	11.7 ± 0.9	21.0 ± 1.0	27.8 ± 1.5	0.9 ± 0.2	1.1 ± 0.3

Table 2.2: Relative contribution of the formation channels for SNe Ia in triples. The channels listed in the table are the ones in which the tertiary plays a role in producing SNe Ia events. Note that they are not mutually exclusive. Error bars indicate statistical (Poisson) uncertainties.

Di Stefano (2017) (Refer to Table 13 from Moe & Di Stefano 2017) from when calculating the total stellar mass.

Firstly, the total number of systems to be sampled are calculated using the following expression

$$N_{\rm tot} = N_{\rm triple} + N_{\rm binary} + N_{\rm single} = \frac{N_{\rm calc}}{F_{\rm calc}} + \sum_{m \in m_{\rm bins}} N_{{\rm triple},\, m} \frac{\alpha_{{\rm binary},\, m}}{\alpha_{{\rm triple},\, m}} + \sum_{m \in m_{\rm bins}} N_{{\rm triple},\, m} \frac{\alpha_{{\rm single},\, m}}{\alpha_{{\rm triple},\, m}}, \tag{2.4}$$

where $F_{\rm calc}$ is the numerically calculated fraction of triple stars in which the primary mass of the inner binary is in the mass range 1-6.5 $M_\odot$ and $N_{\rm calc}$ is number of triple stars originally sampled (in our case, 4×10^5 for each $q_{\rm out}$ model). $N_{{\rm triple},\, m}$ is the number of triple stars in the particular mass bin with $\alpha_{{\rm single},\, m}$, $\alpha_{{\rm binary},\, m}$, and $\alpha_{{\rm triple},\, m}$ being the single, binary, and triple fractions in the respective mass bins which I adopt from Moe & Di Stefano (2017). A stellar population is constructed with the calculated number of single, binary and triple stars in each mass bin. The single star population is created by assuming the IMF from the Kroupa (2001) between 0.08 $M_\odot$ and 100 $M_\odot$. The primary mass of the binary population is constructed similarly to the single star population. The separations are calculated as a function of primary mass following Moe & Di Stefano (2017). The secondary mass and eccentricities are sampled following the primary mass and period-dependent distribution functions from Moe & Di Stefano (2017). The triple population is constructed similarly as described in Section 2.2.3, except that now the primary masses of the inner binary are sampled in the mass range 0.08-100 $M_\odot$, to cover the entire mass range. Finally, $M_\star$ is calculated by adding all the stellar masses.

The delay time distribution (DTD) for the DD and SD pathways are shown in Fig. 2.7 and Fig. 2.8, respectively. The later part of the DD DTD is found to follow a power law shape, $\propto t^{-1}$. The delay time distribution is calculated in the units of SNuM (number of SNe Ia per 10^{10} $M_\odot$ per century).

The time integrated SNe Ia rate $N_{\rm total}/M_\star$ for Model 1 and Model 2 are calculated as

Models	Channel	SNe Rate ($10^{-4}\mathrm{M}_{\odot}{}^{-1}$)
Model 1	Triple	3.60 ± 0.04
	Inner Binary	2.90 ± 0.04
Model 2	Triple	3.50 ± 0.04
	Inner Binary	2.90 ± 0.04
Model 3	Triple	2.40 ± 0.07
Model 4	Triple	0.90 ± 0.04
Model 5	Triple	3.70 ± 0.09
Model 6	Triple	3.60 ± 0.09
Isolated Binary		3.2 ± 0.1
Observed rate		13.0 ± 1.5

Table 2.3: SNe rate from different channels (triple, inner-binaries of triples with the tertiary removed, and isolated binaries) and models.

$(3.60 \pm 0.04) \times 10^{-4}$ $\mathrm{M}_{\odot}^{-1}$ and $(3.50 \pm 0.04) \times 10^{-4}$ $\mathrm{M}_{\odot}^{-1}$, respectively.

2.4.2 Circular and eccentric mergers

In the isolated binary evolution channels, most SNe Ia explosions result from the formation of close white dwarf binaries following CE evolution. However, in triple-star systems, in addition to CE evolution, the tertiary star can also aid the formation of SNe Ia. Fig. 2.9 represents the initial semimajor axis distribution of systems that explode as SNe Ia. From the semimajor axis distribution, it is evident that that the systems with wide semimajor axes undergo collisions triggered by high eccentricity oscillations in the inner binary due to the tertiary star. This is because the triples with wide inner binaries have shorter secular time-scales (all else being the same), whereas the short-range precession time-scales in the inner binaries are longer. Both these effects contribute to a larger probability for exciting high eccentricities in the inner binary. The ZLK mechanism produces high amplitude eccentric oscillations in systems with high intial mutual inclinations. Furthermore, from Fig. 2.10, I can see that the systems with high initial mutual inclinations are more likely to undergo eccentric collisions than circular mergers. There is a strong decrease in the number of systems undergoing circular mergers for higher inclinations near 90 degrees (note that Fig. 10 uses a log scale). Such a strong dip is not apparent in the systems undergoing eccentric collisions. Whereas, in case of the opposide sides of the inclination distribution, inner orbits are more likely brought closer together by CE evolution, thereby inducing circular mergers. Systems undergoing circular mergers are dominant; their contribution to the total SNe Ia is found to be $(99.0 \pm 1.7)\%$ and $(99 \pm 2)\%$ for Model 1 and Model 2 respectively. There are also systems undergoing eccentric collisions, but with a smaller contribution. Their fractional contribution is found to be $(0.8 \pm 0.1)\%$ for Model 1, and $(1.0 \pm 0.1)\%$ for Model 2.

Models	Channel	DD (%)	SD (%)	SCM (%)	CM (%)	He+CO (%)	CO+CO (%)
Model 1	Triple	99.3 ± 1.7	0.7 ± 0.1	90.7 ± 20.06	9.3 ± 4.9	96.6 ± 1.7	3.4 ± 0.2
	Binary	99.4 ± 1.9	0.6 ± 0.1	93.7 ± 23.8	6.3 ± 4.5	99.3 ± 1.9	0.7 ± 0.1
Model 2	Triple	99.1 ± 1.7	0.9 ± 0.1	86.4 ± 19.1	13.6 ± 5.9	96.7 ± 1.7	3.3 ± 0.2
	Binary	99.3 ± 1.9	0.7 ± 0.1	90.0 ± 20.7	10.0 ± 5.2	99.3 ± 1.9	0.7 ± 0.1
Model 3	Triple	99.5 ± 4.3	0.5 ± 0.2	75.0 ± 57.3	25.0 ± 28.0	97.7 ± 4.2	2.3 ± 0.5
Model 4	Triple	100.0 ± 6.8	0.0	0.0	0.0	79.7 ± 5.8	20.3 ± 2.4
Model 5	Triple	99.7 ± 3.4	0.3 ± 0.1	80.0 ± 53.7	20.0 ± 21.9	97.4 ± 3.4	2.6 ± 0.4
Model 6	Triple	99.5 ± 3.4	0.5 ± 0.1	66.7 ± 43.03	33.3 ± 27.2	96.8 ± 3.4	3.2 ± 0.4

DD - Percentage of DD SNe Ia of the total number of SNe Ia
SD - Percentage of SD SNe Ia of the total number of SNe Ia
SCM - Percentage of sub-Chandrasekhar mass SD SNe Ia of the total number of SD SNe Ia
CM - Percentage of Chandrasekhar mass SD SNe Ia of the total number of SD SNe Ia
He+CO - Percentage of mergers/collisions of He white dwarf and CO white dwarf of the total number of DD SNe Ia
CO+CO - Percentage of mergers/collisions of CO white dwarf and CO white dwarf of the total number of DD SNe Ia

Table 2.4: Contribution of different progenitors to SNe Ia. The 'Binary' channel here refers to the inner binaries of the triple population, evolved without the tertiary star.

2.4.3 DD and SD SNe Ia

It is interesting to analyze the contribution of DD and SD channels to SNe Ia. From our study, the DD channel surpasses the SD channel in great numbers. The percentage of systems undergoing DD SNe Ia is $(99 \pm 2)\%$ and $(99 \pm 2)\%$ for Model 1 and Model 2 respectively whereas the SD SNe is $(0.7 \pm 0.1)\%$ for Model 1 and $(0.7 \pm 0.1)\%$ for Model 1. When I carried out an in-depth analysis into the various sub channels contributing to DD SNe Ia, I find that the majority of them are He white dwarf and CO white dwarf mergers, and there is also a non-negligible contribution from CO-CO white dwarf mergers. Fig. 2.11 shows the relative contributions from He-CO white dwarfs and CO-CO white dwarfs. The detail numbers are displayed in Table 2.4. The contribution of SD sub channels is analyzed in the next section.

2.4.4 Chandrasekhar and Sub-Chandrasekhar mass SNe Ia

As described in Section 2.2.1, there are two possible scenarios of single degenerate SNe Ia taken into account in our simulations. The first scenario involves the accretor (CO white dwarf) gaining mass by accreting mass from a non-degenerate donor star and exploding as SNe Ia when the white dwarf reaches the Chandrashekar mass limit ($1.44\,M_\odot$). In the second case, the CO white dwarf undergoes stable accretion via Roche lobe overflow. Here, the donor is a H poor, He burning stripped star. The white dwarf undergoes dou-

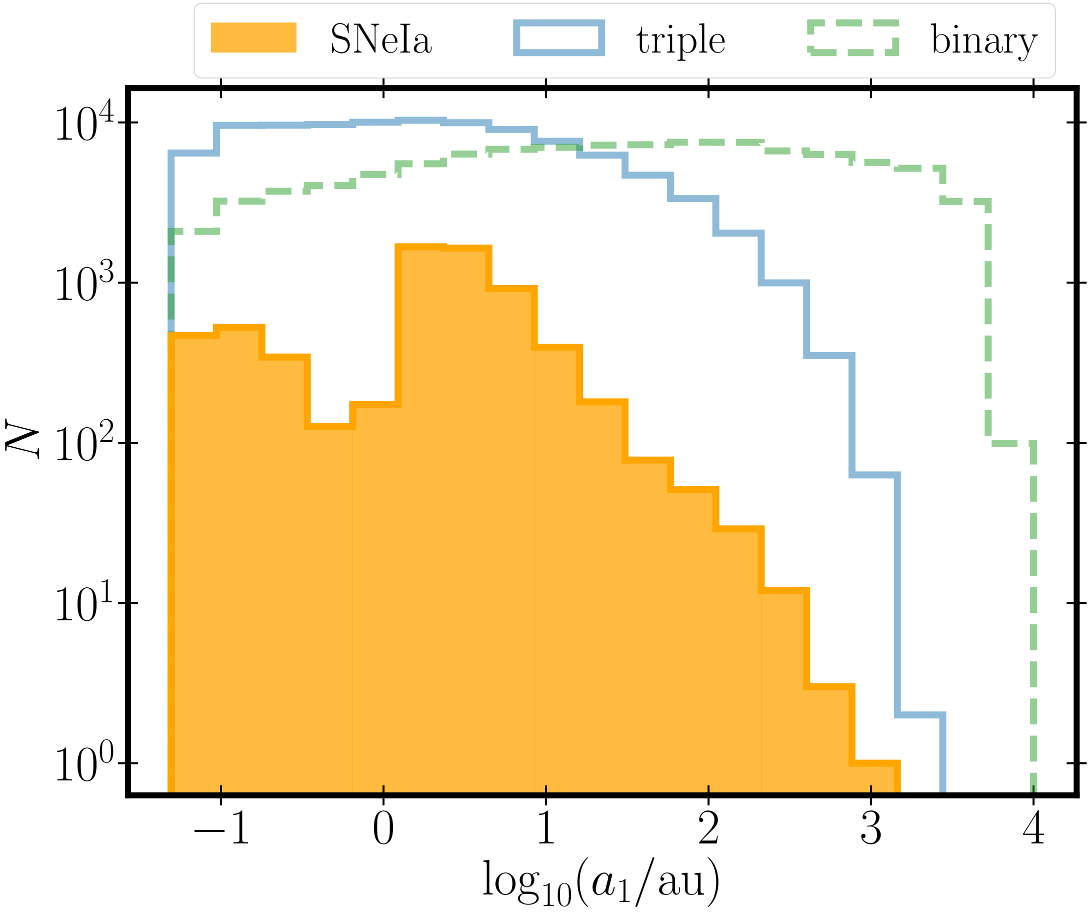

Figure 2.13: Initial inner semimajor axis distribution of our triple population (Model 1 - solid blue line), isolated binary population (dashed green line) and systems that explode as SNe Ia from triple evolution channels (filled yellow columns).

ble detonation and explodes as SNe Ia, well before the Chandrasekhar mass is reached. These two scenarios involve different evolutionary pathways (see, e.g., Ruiter 2020). From our Model 1 simulations of single degenerate SNe Ia, the percentage of systems undergoing Chandrashekhar mass and sub-Chandrashekhar mass are $(9 \pm 5)\%$ and $(90 \pm 20)\%$ respectively. From the Model 2 simulations, the percentage of systems undergoing Chandrashekhar mass and sub-Chandrashekhar mass are $(14 \pm 6)\%$ and $(86 \pm 19)\%$ respectively. It is apparent from the statistics that the contribution of sub-Chandrasekhar mass SNe Ia dominate the fraction of single degenerate SNe Ia over Chandrasekhar mass SNe Ia.

2.4.5 Isolated binary evolution

In order to understand the contribution of the triple evolution channel to the SNe Ia rate, it is important to compare to the rate attributed to the binary evolution channel. I constructed our initial binary population to be fully consistent with our sampling of the triple population. Specifically, I assumed the Kroupa (2001) IMF for the primary mass distribution; the secondary mass, eccentricity, and period distributions follow the functional distributions from Moe & Di Stefano (2017). I used the same SNe Ia prescriptions as for our triple runs and, for consistency, the same population synthesis code MSE to evolve these binary systems for 10 Gyr. The estimated time integrated SNe Ia rate from our binary system calculations is $(3.2 \pm 0.1) \times 10^{-4}$ $\mathrm{M}_{\odot}^{-1}$. The corresponding DTD from the binary evolution channel is shown in Fig. 2.7 with the red dotted line.

2.4.6 Properties of the third star

I examined the nature of the third star at the moment when the inner binary explodes as SNe Ia. I find that, in about 1 per cent of systems, two unbound stars collide during a phase of dynamical instability leading to SNe Ia, 20 per cent of stars are newly formed binaries as result of the merger of the inner binary and the tertiary component, 30 per cent of systems have an unbound third star, and 49 per cent of systems have a bound third star. The mass distribution of the tertiary star in those cases when it is still bound at the moment of the SNe Ia explosion is shown in left panel of Fig. 2.12; most of the tertiaries have masses less than 1 $\mathrm{M}_{\odot}$, peaking at $\approx 0.5\,\mathrm{M}_{\odot}$. The outer semimajor axis distribution for the cases when the tertiary star is still bound at the time of the SNe Ia explosion is shown in right panel of Fig. 2.12; the outer semimajor axis is found to be distributed broadly up to more than a million au, but peaking at a semimajor axis of about 10^3 au. In most of the cases, fly-bys are responsible for these wide orbits while in a small number of cases, CE evolution in the inner binary can also create these wide orbits. It is also noted that these outer orbits are mostly eccentric and expected to be typically short-lived. In addition, I point out that it would be very difficult to detect these ultra-wide orbits.

2.5 Discussion

2.5.1 The effect of the tertiary star

In order to investigate the effect of the tertiary on the formation of SNe Ia, I investigated three different data sets: runs with the hierarchical triple population, runs with the inner binary of the triples population (after removing the tertiary star from the triple system) and runs with the isolated binary population. I find that the time-integrated SNe Ia rates from hierarchical the triple population, inner binary of triple population and isolated binary population cases are $(3.60 \pm 0.04) \times 10^{-4}\mathrm{M}_{\odot}^{-1}$, $(2.90 \pm 0.04) \times 10^{-4}\mathrm{M}_{\odot}^{-1}$, and $(3.2 \pm 0.1) \times 10^{-4}\mathrm{M}_{\odot}^{-1}$, respectively. This shows that the hierarchical triple population slightly yields the highest contribution to the SNe Ia rate.

The tertiary star is contributing to the SNe Ia in different ways: Firstly, the stability configuration of the hierarchical triple population demands the inner binaries of the hierarchical triple population to be in tighter orbits than those of the isolated binary population.

I can also see from Fig. 2.13 that these tight inner binaries contribute the most to SNe Ia explosions. Secondly, the tertiary star can assist in shrinking the inner binary orbit and bringing them closer to lead to either a circular merger via tides, stable mass transfer, and/or CE, or an eccentric collision. One can see these two contribution of the tertiary in two different peaks in the yellow column of Fig. 2.13.

Hamers et al. (2013) carried out a similar study by restricting the initial conditions to systems with $a_1(1 - e_1^2) > 12\,\mathrm{au}$ and estimated the SNe Ia rates from triples to be on the order of $10^{-6}\,\mathrm{M}_\odot^{-1}$. Our rates agree with Hamers et al. (2013) for systems with $a_1(1 - e_1^2) > 12\,\mathrm{au}$. The isolated binary population rates from our calculations are similar to that of Claeys et al. (2014). Putting our results in perspective, the time integrated rates from the isolated binary and triple channels in our simulations are $(3.2 \pm 0.1) \times 10^{-4}\mathrm{M}_\odot^{-1}$ and $(3.60 \pm 0.04) \times 10^{-4}\mathrm{M}_\odot^{-1}$ respectively. The observed time integrated rate from Maoz et al. (2012) is $(1.3 \pm 0.2) \times 10^{-3}\mathrm{M}_\odot^{-1}$. The combined rates from the triple and binary channels thus contribute to about ~ 52 per cent of the observed rate, of which the largest contribution comes, somewhat surprisingly, from triple systems. The discrepancy between the observed and theoretical rates demands the exploration of other SNe Ia progenitors, though it should be noted that there are significant uncertainties in our models, which I address in the next Section.

2.5.2 Uncertainties in the models

Fig. 2.7 shows the DTD of DD SNe Ia with solid blue line, dashed green line, and dotted red line representing the corresponding DTD from Model 1, Model 2, and isolated binary population, respectively. From Fig. 2.7, it is evident that the total rate and DTD are not affected by the underlying q_{out} distribution. However, as shown by Fig. 2.14, the CE efficiency parameter α_{CE} does strongly affect the number of SNe Ia and hence the rates. A higher efficiency parameter ($\alpha_{\mathrm{CE}} = 10$) results in more early mergers and thereby fewer SNe Ia than a lower efficiency ($\alpha_{\mathrm{CE}} = 1$). Furthermore, a low efficiency parameter ($\alpha_{\mathrm{CE}} = 0.1$) results in less transfer of orbital energy during CE evolution, thereby reducing the number of close binaries that could lead to SNe Ia explosions. The effects of fly-bys and lower metallicity are negligible in producing SNe Ia. I have used multiplicity fractions from Moe & Di Stefano (2017) while normalizing the rates for every models. Uncertainties in the multiplicity fractions, as well as the precise values for the upper and lower mass of the synthesized population, propagate into errors in the mass normalisation, which I have not considered here for simplicity. I further note as a caveat that all uncertainties that apply to single and binary star evolution (including the criteria for what exactly produces a SNe Ia transient), also apply here.

2.5.3 Predominance of circular mergers

As described in Section 4.2, according to our results, SNe Ia attributed to circular mergers via CE are dominant compared to those following eccentric collisions. This is in strong contrast to Dong et al. (2015), who suggested that head-on white dwarf collisions in isolated

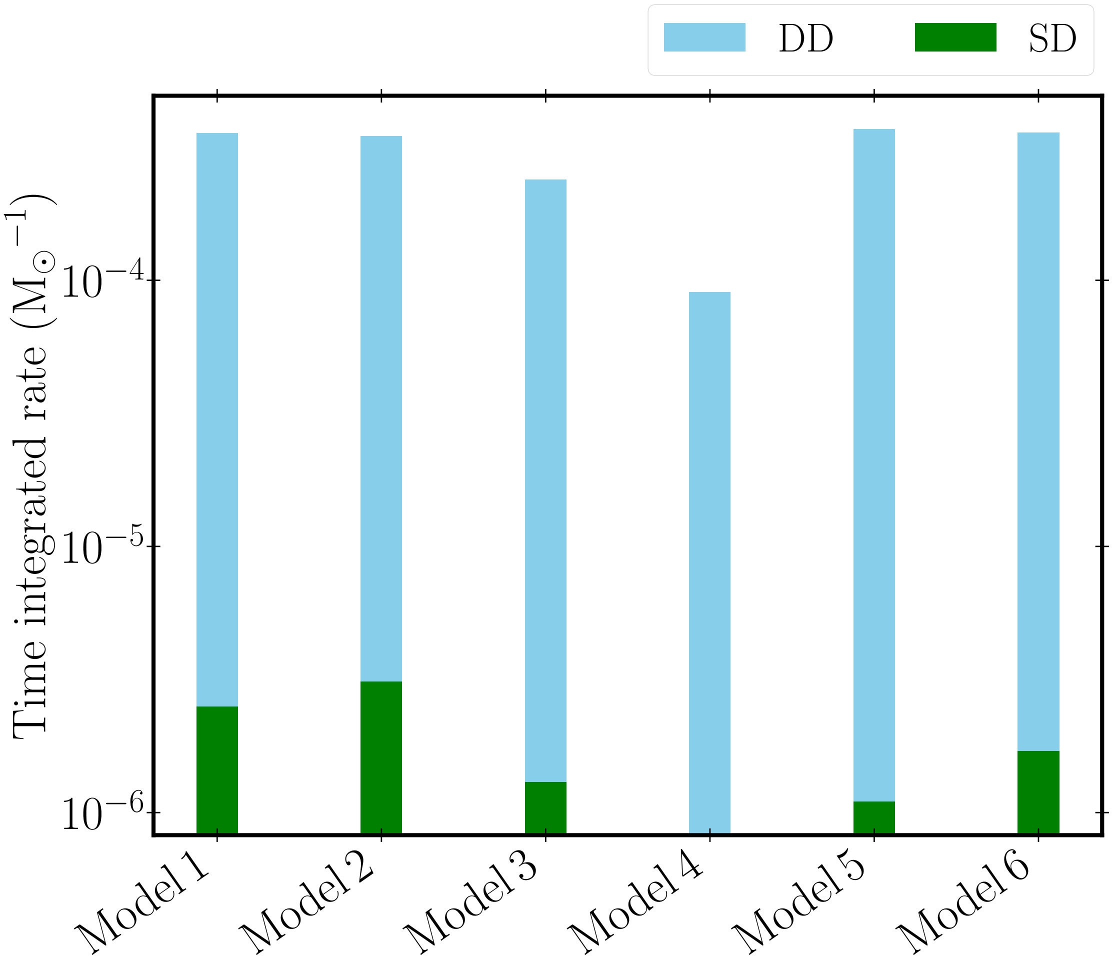

Figure 2.14: Impact of different models on the SNe Ia rate. See Table 2.1 for a description of the models.

triples are the dominant channel for producing SNe Ia, and agrees with previous works (Hamers et al., 2013; Toonen et al., 2018) which found that the rate of head-on collisions in white dwarf-white dwarf systems is too low to explain the observed SNe Ia rate.

About 6% of total evolved triple systems did not complete due to the set restricted wall time of 5 hrs. Fig. 2.15 shows the wall time distribution of systems that explode as SNe Ia. It is evident that the majority of the systems that explode as SNe Ia have a wall time within 1 hr; any contribution from systems with longer wall-time is negligible.

Even though the SNe Ia rate from the triple evolution channel is found to contribute similarly to that of binary evolution channel, the combined rate from triples and binaries is still inadequate to explain the complete the observed rate. Thus, a detailed study on other possible SNe Ia progenitors and contribution of SNe Ia from higher order systems should be done in the future.

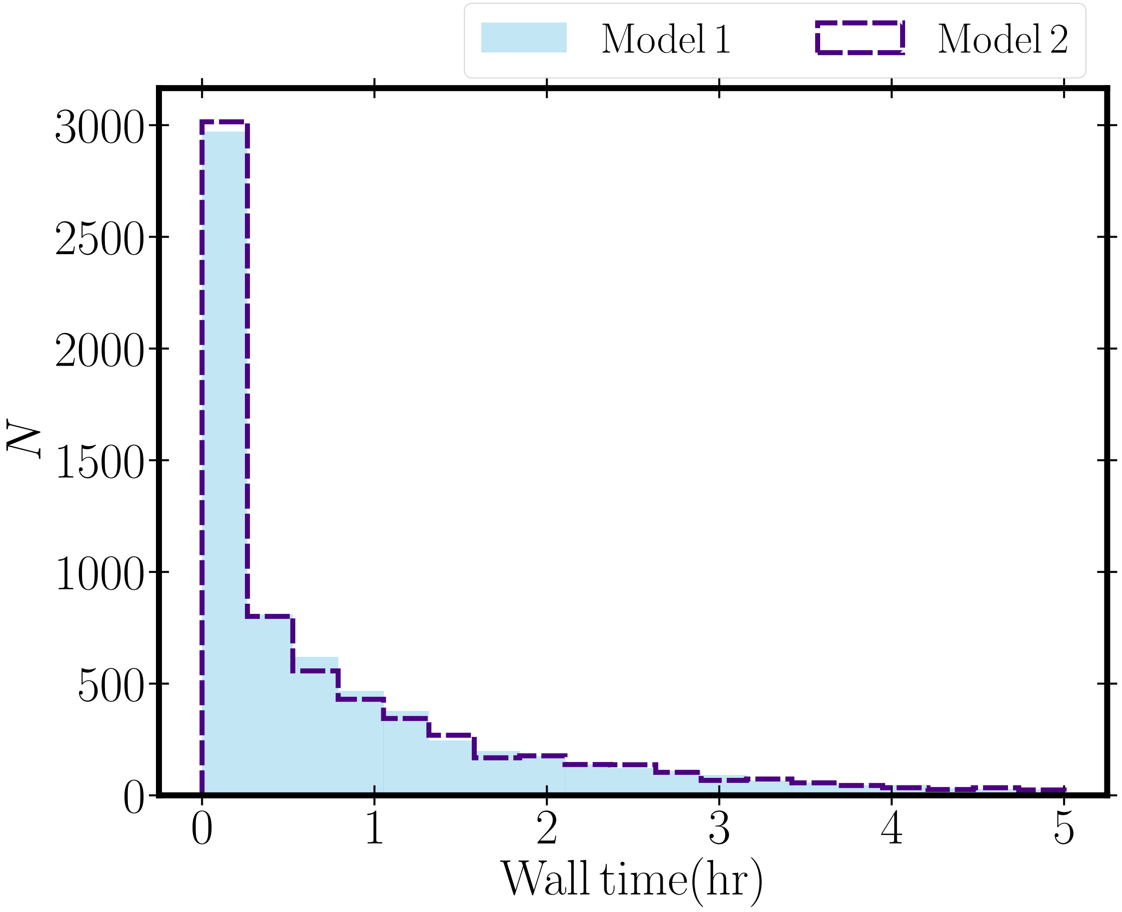

Figure 2.15: Wall time for systems that explode as SNe Ia.

2.6 Conclusions

I studied rates of SNe Ia explosions in hierarchical triple systems by performing evolutionary population synthesis calculations. The triple populations were constructed following Kroupa (2001) and Moe & Di Stefano (2017), and I only considered initially dynamically stable systems, using the stability criterion from Mardling & Aarseth (2001). The systems in which one or more of the stars are filling their Roche lobe at the beginning of the main sequence were ignored. Our sampled triples were evolved using the evolutionary population synthesis code MSE (Hamers et al., 2021) for a period of 10 Gyr, and a statistical analysis was carried out. The results are summarized as follows.

1. I found 5 unique formation channels to produce SNe Ia.
    (a) Unbound tertiary: a triple evolution channel in which the tertiary gets unbound when it collapses into a neutron star. The other reasons for the tertiary star to get unbound includes dynamical instability, and CE in the inner binary system.

   (b) Double merger: a triple system in which the inner binary components merge to form a new massive star, which then later interacts with the tertiary star to produce a SNe Ia explosion.
   (c) TCE: a triple system in which the massive tertiary transfers mass on top of the inner binary resulting in exchange, merger or dynamical instability. The newly formed components then interact to produce a SNe Ia explosion at a later time.
   (d) Eccentric collision: in a triple star system, when the mutual inclinations are large, the inner binary undergoes eccentricity enhancements due to secular evolution. This can increase the eccentricity of the inner binary, of which the components then collide to form a SNe Ia.
   (e) Dynamical instability: unlike the isolated binary channel, this triple evolution channel can produce SNe Ia without undergoing a CE phase. This is a purely dynamical channel in which the the triple system undergoes dynamical instability to explode as SNe Ia.

2. Head-on eccentric collisions of white dwarfs contribute only about 1 per cent (Model 1) to the total SNe Ia, while the rest are all circular mergers that involve CE evolution.

3. When there occurs a SNe Ia in the inner binary, the third star is found to be bound in ~ 49 per cent of systems. The mass distribution of the bound star peaks around 0.5 $M_\odot$, and the outer orbital semimajor axis is distributed over a broad range of about few million au, peaking at about 10^3 au.

4. I estimated the delay time distribution for single and DD SNe Ia, which was presented in Fig. 2.7, and Fig. 2.8 respectively. The time-integrated rate of SNe Ia from the triple evolution channel is found to be slightly higher than that of the binary evolution channel, although this conclusion is affected by uncertainties in the models.

5. Previously, (Hamers et al., 2013; Toonen et al., 2018) considered triples with only wide inner binaries and found a comparatively low contribution of triples to the SNe Ia rate. However, when the complete set of parameters is included, it is evident that the triple channel is an important channel in producing SNe Ia explosions.

6. According to our models, the combined rate from the triple and binary evolution channels contributes to about 52 per cent of the observed SNe Ia rate.

Chapter 3

Evolution of binaries containing a hot subdwarf and a white dwarf

Submitted to Astronomy & Astrophysics, Rajamuthukumar et al. (2025)

3.1 Introduction

Hot subdwarfs are stripped He stars that burn He in their core with little to no H envelope (Heber, 1986, 2016). Studies such as Han et al. (2002, 2003) suggest that binary interactions such as stable or unstable mass transfer plays a major role in the formation of hot subdwarfs. Observations provide evidence that most of the hot subdwarfs are found with binary companions (e.g., Pelisoli et al., 2020). Further, a significant fraction of hot subdwarfs are found in close orbits ($P_{\mathrm{orb}} \sim 10\,\mathrm{days}$) with white dwarfs, which are likely post common envelope systems (Han et al., 2002, 2003).

Compact binaries containing hot subdwarfs and white dwarfs have gained significant interest following the discovery of a super-Chandrasekhar binary by Maxted et al. (2000b). This binary is particularly interesting as a potential Type Ia supernova progenitor (but, see also Ergma et al. 2001 for other outcomes). The number of discoveries of binaries containing hot subdwarfs with white dwarf companions has steadily increased (e.g., Napiwotzki et al., 2004; Geier et al., 2013; Vennes et al., 2012). Large spectroscopic studies have been characterizing binaries containing hot subdwarfs (e.g., Schaffenroth et al., 2022). In addition to those detached binaries, Kupfer et al. (2020b,a) identified binaries in which the hot subdwarf is Roche-lobe filling. Furthermore, some of recent the observed binaries such as CD-30°11223 (Vennes et al., 2012; Geier et al., 2013) and HD 265435 (Pelisoli et al., 2021) are verification binaries for LISA (for more details see Kupfer et al. 2024) and suggested progenitors of double donation supernovae (Kupfer et al., 2022).

Interacting hot subdwarf + white dwarf binaries could potentially result either in an explosion only in the He shell of the white dwarf (a He nova, Kato et al. 2000; Gianninas et al. 2010; Piersanti et al. 2014) or a thermonuclear explosion of a white dwarf (probably as a supernova type Ia, Whelan & Iben 1973; Iben & Tutukov 1984). The thermonuclear

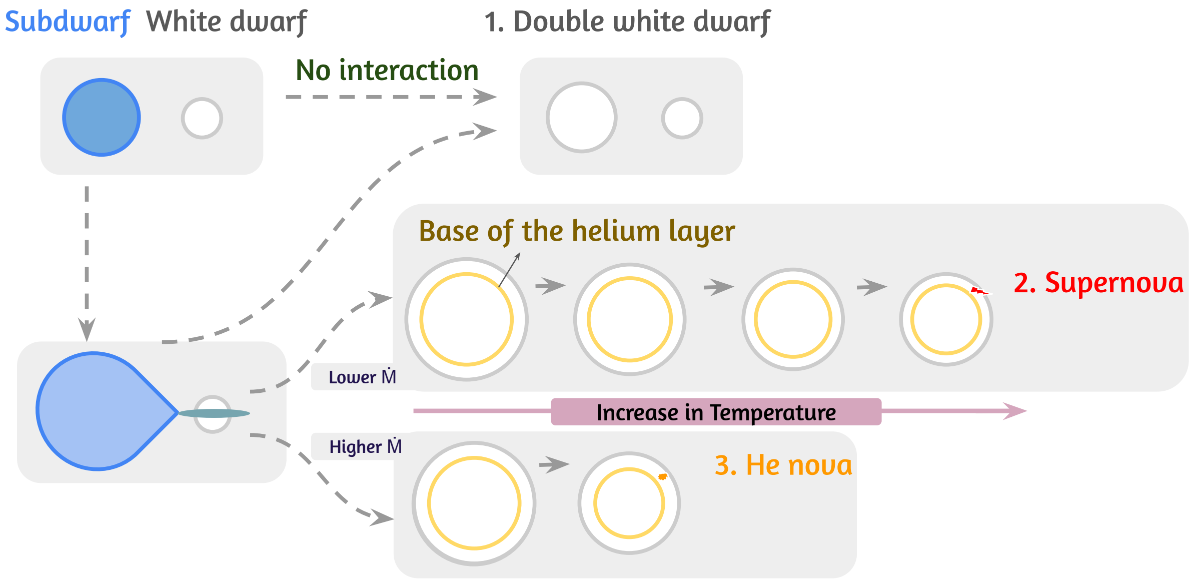

Figure 3.1: A schematic diagram representing possible evolution channels of a hot subdwarf + white dwarf binary to a double white dwarf, a double detonation supernova or a He nova. Double detonation supernovae and He novae result from systems that undergo mass transfer and later experience thermonuclear instability in the He layer on the surface of the white dwarf. The differentiation between double detonation supernova and He nova is based on the He layer's critical density (see Sec. 3.2.1). Double white dwarfs result from systems that either evolve in isolation or involve episodes of accretion but do not enter unstable nuclear burning.

explosion of the white dwarf could result from a Chandrasekhar mass explosion (Yoon & Langer, 2003; Wang et al., 2009; Brooks et al., 2016) or from a sub-Chandrasekhar mass double detonation explosion due to He accretion. In the double detonation mechanism, He-accreting white dwarfs undergo the first detonation in the He shell that triggers the second detonation in the C/O core leading to a thermonuclear supernova.

The He donor channel as a mechanism to produce a double detonation was already investigated in the early 1980s by Taam (1980a,b), Nomoto (1982a,b). Later studies by Livne (1990), Livne & Glasner (1990), Langer (1991), Livne & Glasner (1991), Fink et al. (2007), and Fink et al. (2010) further explored He-accreting white dwarfs and established that they are promising channels for SNe Ia. However, they also estimated that single degenerate double detonations require thick He shells which likely will lead to spectra representing a peculiar supernova Ia. The light curve of ZTF18aaqeasu (also known as SN 2018byg and ATLAS 18pqq), De et al. (2019), suggests that it is a double detonation supernova with a massive He shell ($\sim 0.15\,\mathrm{M}_\odot$). This thick He shell aligns with predictions by Bauer et al. (2017) for a hot subdwarf + white dwarf binary (CD-30°11223). On the contrary, studies by Sim et al. (2010), Kromer et al. (2010), and Woosley & Kasen (2011) also explored channels that would enable the synthetic spectra to resemble a "normal" Type Ia supernova. Furthermore, Wang et al. (2013) and Neunteufel et al. (2016) probe the He star + white dwarf binary channels as a potential single-degenerate double detonation mechanism. In addition, some studies explored the effects of white dwarf rotation (Yoon & Langer, 2004a) and magnetic fields (Neunteufel et al., 2017) on He ignition.

He donor channels are also interesting as a mechanism to produce hypervelocity runway stars such as US 708. Should there be a full explosion of the white dwarf, the hot subdwarf can be ejected at very high velocities (Justham et al., 2009; Wang & Han, 2009). This mechanism can explain some of the observed population of hypervelocity runaway stars with velocities of $\sim 1000\,\mathrm{km\,s^{-1}}$ (Geier et al., 2015; Brown et al., 2015; Neunteufel, 2020; Neunteufel et al., 2022).

Given the increasing number of observed hot subdwarf and white dwarf binaries, interest in understanding the fate of these systems has been growing. Our galaxy contains at least $10^3 - 10^4$ hot subdwarf + white dwarf binaries that are likely to interact within the subdwarf lifetime (Bauer & Kupfer, 2021). Despite detailed modeling studies of individual systems, the literature still lacks a broad study of binary spatial configurations that lead to double detonation supernovae. The purpose of this paper is to map the initial binary configurations of hot subdwarf and white dwarf binaries to their fates: double detonation supernovae, He novae, and double white dwarfs.

In this study, I use the 1D stellar evolution code MESA to simulate a dense grid of hot subdwarf + white dwarf binaries. Unlike some of the previous studies, I also model the accreting white dwarf. I simultaneously evolve both the donor and accretor, including binary interactions, aiming to address two main objectives: 1) Identifying the region of initial parameter space that distinguishes the fate of the systems, and determining whether they evolve into double detonation supernovae, He novae, or double white dwarfs, and characterize the properties of any surviving system or object 2) Investigating the velocities of the runaway hot subdwarf in the event of double detonation supernovae, thereby providing constraints to observed runaway stars.

The paper is structured as follows: In Section 3.2 I explain our methods. Section 3.3 illustrates examples of three distinct outcomes under consideration: a double detonation supernova, He nova, or a double white dwarf. I present the fate of the binaries across our parameter space in Section 3.4. In Section 3.5 I give more details about the final state of the binaries, and in particular, runaway velocities in 3.5.2. I discuss the results in Section 3.6 and conclude in Section 3.7.

3.2 Methods

In this section, I describe the physical assumptions used in this study. I use Modules for Experiments in Stellar Astrophysics (modified[1] MESA version r23.05.1 Paxton et al. 2011,

---

[1] The composition of the accretion stream is modified to change the mass fraction of H to He throughout accretion. See later in Sec. 3.2 for more details. This is done by modifying the

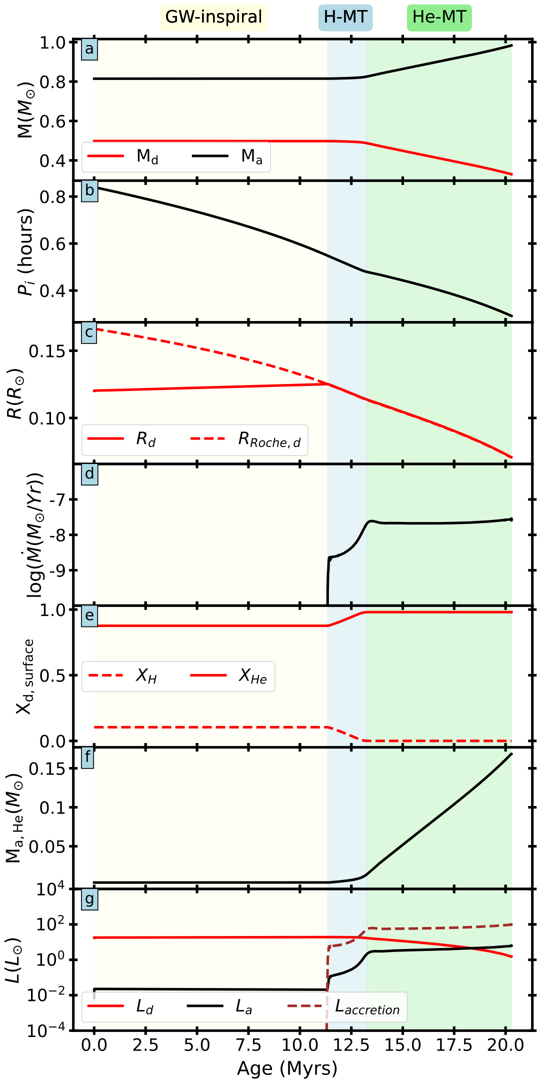

Figure 3.2: An example of a binary with $\mathrm{M_d} = 0.5\,\mathrm{M}_\odot$, $\mathrm{M_a} = 0.8\,\mathrm{M}_\odot$, and $\mathrm{P_i} = 0.84$ hours, where a thermonuclear explosion occurs in the white dwarf (accretor). The background colors yellow, blue, and green represent the gravitational-wave inspiral phase (GW-inspiral), H mass transfer phase (H-MT), and He mass transfer phase (He-MT), respectively. Panels (a) through (f) show the evolution of various parameters: (a) **Mass Evolution:** M_a (accretor) and M_d (donor); (b) **Orbital Period Evolution**; (c) **Radius Evolution:** R_d (donor's radius) and $R_{roche,d}$ (Roche radius of the donor); (d) **mass transfer rate**; (e) **Evolution of surface mass fraction:** X_H (hydrogen) and X_{He} (helium) in the donor; (f) **He Mass on the Accretor**; (g) **Luminosity Evolution:** L_a (accretor), L_d (donor), and $L_{\mathrm{accretion}}$ (accretion). The accretor gains mass at the rate of $\sim 10^{-8}\,\mathrm{M}_\odot\mathrm{yr}^{-1}$, resulting in the He ignition in the He layers denser than the assumed critical density for detonation ($> 10^6\,\mathrm{g\,cm^{-3}}$).

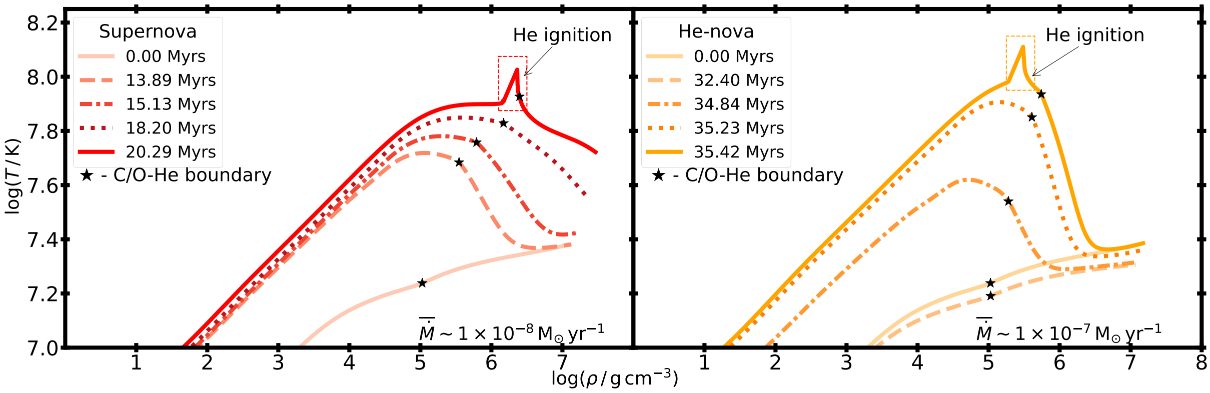

Figure 3.3: Each curve depicts the evolution of the temperature-density profile of the accreting white dwarf at various times, as indicated in the legend, for a system that undergoes double detonation supernova (left panel) and a He nova (right panel). The black star indicates the C/O-He boundary, that moves to higher density as the white dwarf accretes and contracts. In the left panel, the white dwarf accretes at the rate of $\sim 10^{-8}\,\mathrm{M_\odot yr^{-1}}$, igniting the high density regions of the He shell ($> 10^6\,\mathrm{g\,cm^{-3}}$), and so I classify the outcome as a double detonation supernova. In the right panel, the accretor's evolution is initially dominated by the cooling of the white dwarf. After the accretion starts, the white dwarf accretes at $\sim 10^{-7}\,\mathrm{M_\odot yr^{-1}}$. The white dwarf experiences compressional heating, causing the low-density ($< 10^6\,\mathrm{g\,cm^{-3}}$) layers to ignite explosively. I then classify this system as a He nova.

2013, 2015, 2018, 2019; Jermyn et al. 2023) to model the binary evolution of hot subdwarf + WD binaries.

Convective Treatment: I use the `Schwarzschild` stability criterion to determine the regions that are unstable to convection. Further, mixing by convection is followed using the mixing length theory (Böhm-Vitense, 1958), with `mixing_length_alpha = 2` and `MLT_option = 'TDC'`, the time-dependent convection model based on Kuhfuss (1986). For convection treatments in the He core of hot subdwarf, I employ “predictive mixing", which allows the core to grow while avoiding breathing pulses during the late stages of He core burning. For details on convection in hot subdwarfs in general, see Ostrowski et al. (2021).

Nuclear Network: When evolving the binary system, I use `basic_plus_ fe56_ni58.net` for hot subdwarf stars and a custom `nco.net` from Bauer et al. 2017 (included in the Zenodo repository) for WDs. For the hot subdwarf, the nuclear network `basic_plus_fe56_ni58.net` contains stable isotopes ^{56}Fe and ^{58}Ni in addition to the basic isotopes ^{1}H, ^{3}He, ^{4}He, ^{12}C, ^{14}N, ^{16}O, ^{20}Ne, ^{24}Mg. This has been chosen to account for all isotopes and reactions from He burning. For the WD, the nuclear network includes the NCO ($^{14}\mathrm{N}(e^-,\nu)^{14}\mathrm{C}(\alpha,\gamma)^{18}\mathrm{O}$) chain, in which the electron capture to ^{14}N in high densities ($\sim 10^6\,\mathrm{g\,cm^{-3}}$), leads to the formation of ^{14}C. This ^{14}C can further capture an alpha particle

---

`binary_mdot.f90` file. All files including the modified `binary_mdot.f90` can be found at Zenodo.

inducing a thermonuclear runaway in the accretor (Bauer et al., 2017).

Stellar winds: To account for mass loss during the red giant branch, I use the Reimers prescription (Reimers, 1975) from MESA and switch to the T-Blöcker prescription (Bloecker, 1995) during the asymptotic giant branch phase. Further, I assume no winds during the hot subdwarf phase. The mass and luminosity of these low-mass stripped stars are too low to drive strong winds that would affect the binary evolution and hence the results (Krtička et al., 2016).

Hot subdwarf: A hot subdwarf star is a low mass core He burning star with a very thin ($\lesssim 10^{-2}\,\mathrm{M}_\odot$; Heber 2016) H envelope. To create starting models for hot subdwarfs, I first evolve single stars from the pre-main sequence until He ignition. The hot subdwarf gets stripped either during a mass transfer phase or a CE phase. In this work, I approximate the mass loss during the mass-transfer or CE phase by applying a high wind mass loss rate, while freezing the nuclear reactions in the core. The stripping continues until the total mass of H in the envelope is $3 \times 10^{-4}\,\mathrm{M}_\odot$[2] In our models, hot subdwarf stars originating from low-mass progenitors ($< 2.3\,\mathrm{M}_\odot$) have degenerate He cores, leading to He ignition via a core He flash. In contrast, hot subdwarf stars with progenitors $> 2.3\,\mathrm{M}_\odot$ ignite He gradually without undergoing a core He flash. The initial zero-age main sequence (ZAMS) masses of hot subdwarfs are chosen from the range $1\,\mathrm{M}_\odot$ to $5.95\,\mathrm{M}_\odot$ to include both degenerate and non-degenerate core He ignition. The hot subdwarf stars in our models are in the mass range of $0.33\,\mathrm{M}_\odot$ to $0.8\,\mathrm{M}_\odot$. The lower limit of $0.33\,\mathrm{M}_\odot$ represents the minimum mass required for core He ignition. The most massive model, $0.8\,\mathrm{M}_\odot$ expands to a giant-like phase reaching the radii of approximately $10\,\mathrm{R}_\odot$. Notably, our hot subdwarf models include $0.47\,\mathrm{M}_\odot$, which is considered the canonical mass for such stars (Han et al., 2002; Heber et al., 2003). Table. 3.1 gives the details of the donor masses.

White dwarf: I create carbon oxygen WDs (0.7 to $1.0\,\mathrm{M}_\odot$) after modifying the `make_co_wd` test suite to cool until the age of 3×10^8 years. The modified test suite `make_co_wd` evolves a single star from the pre-main sequence phase to the WD phase. The mass range of the WD spans from 0.7 to $1.1\,\mathrm{M}_\odot$, chosen to align with the existing observations and to anticipate the potential explosive fate of these systems. The massive $1.1\,\mathrm{M}_\odot$ WD is created by rescaling the $1.0\,\mathrm{M}_\odot$ WD using the MESA inlist parameter `relax_mass_scale`, which rescales to the new mass without altering the composition profile. All the WD models are further refined to convert all H to ^{4}He, avoiding the extra computational cost of evolving through classical novae at the onset of mass transfer, which is not the focus of this study.

Binary Evolution: The mass transfer rate follows MESA's Kolb scheme (Kolb & Ritter, 1990; Paxton et al., 2015). I assume conservative mass transfer for our models. Thus, the mass transfer rate is always equal to the accretion rate. The entropy of the accreted material is determined by matching the entropy of the outer shell of the accretor. Further, the WDs undergoing accretion are expected to undergo compressional heating, which MESA incorporates into evolutionary models through its energy equation and thermodynamically consistent EOS (see Jermyn et al. 2023). Exploring the effects on non-conservative mass transfer, tidal heating, and spin-up of the accretor is left to future work.

---

[2] This H mass is chosen to prevent thin-shell instabilities in the donor.

Parameter	Range	Values
$M_{\text{hot subdwarf}}$	$0.33\,M_\odot$ to $0.8\,M_\odot$	0.33, 0.35, 0.39, 0.40, 0.47, 0.50, 0.55, 0.60, 0.65, 0.70, 0.75, 0.80
$M_{\text{whitedwarf}}$	$0.7\,M_\odot$ to $1.1\,M_\odot$	0.70, 0.75, 0.80, 0.85, 0.90, 0.95, 1.00, 1.10
P_i	36 minutes to 7.2 hours	Logarithmically spaced (30 values)

Table 3.1: Initial parameters (masses and orbital periods) for hot subdwarfs and white dwarfs. For more details, see Sec. 3.2.

The donor starts transferring the envelope, which adds H and heats the surface of the WD, resulting in classical novae. Simulating and evolving through these novae is computationally expensive and not the focus of this paper. Therefore, I modify the accretion stream to convert the mass fraction of H and ^{3}He to the mass fraction of ^{4}He. Furthermore, the initial composition profile of the WD model is further modified to convert ^{3}He to ^{4}He to avoid further production of H through nuclear reactions.

I initiate our hot subdwarf and WD models in a range of periods starting from 36 minutes to 7.2 hours. This range is chosen to encompass the mass transfer during various core He fractions for all our donors, including phases like shell burning phase, and thermal pulses. Additionally, the period range allows for donors to evolve without interaction to become a WD. Further details of the grid can be found in the Table 3.1.

The evolution is followed until either the accretor reaches the ignition conditions (see Sec. 3.2.1) or the donor evolves to a WD making a double white dwarf. I terminate our simulations as double white dwarfs if the binary system is non-interacting and the radius of the hot subdwarf decreases to $0.03\,R_\odot$. Once this radius is attained, all the hot subdwarf-turned WDs in our simulations enter the cooling track.

I do not include the effects of convective overshooting while creating hot subdwarfs and WDs. I further assume no gravitational settling, meaning that the hot subdwarf/WD atmosphere contains not only hydrogen but also contamination from heavier elements. Nevertheless, the mass fraction of these elements is likely too low to significantly impact the binary evolution or the final fate of the system.

3.2.1 Conditions for ignition

I evolve our binaries either until He ignition occurs in the accretor or when the non-interacting hot subdwarf evolves into a white dwarf. The thermonuclear explosion of a C/O white dwarf is a multidimensional phenomenon (Pakmor et al., 2024). However, our simulations use hydrostatic 1D MESA calculations, which do not fully capture the multidimensional nature of the explosion or the nature of nuclear burning processes. Therefore, for the binaries in which He ignition occurs in the accretor, I post-process to classify the detonation events. I use an approximate criterion to classify outcomes as either “detonation” or “non-detonation”. In this classification scheme, I assume all “detonations” trigger a second detonation in the core of the white dwarf, leading to a double detonation supernova (Fink et al., 2010; Boos et al., 2021; Gronow et al., 2021). Conversely, “non-detonations” result in a He nova, where the He shell is expelled but the white dwarf itself remains intact.

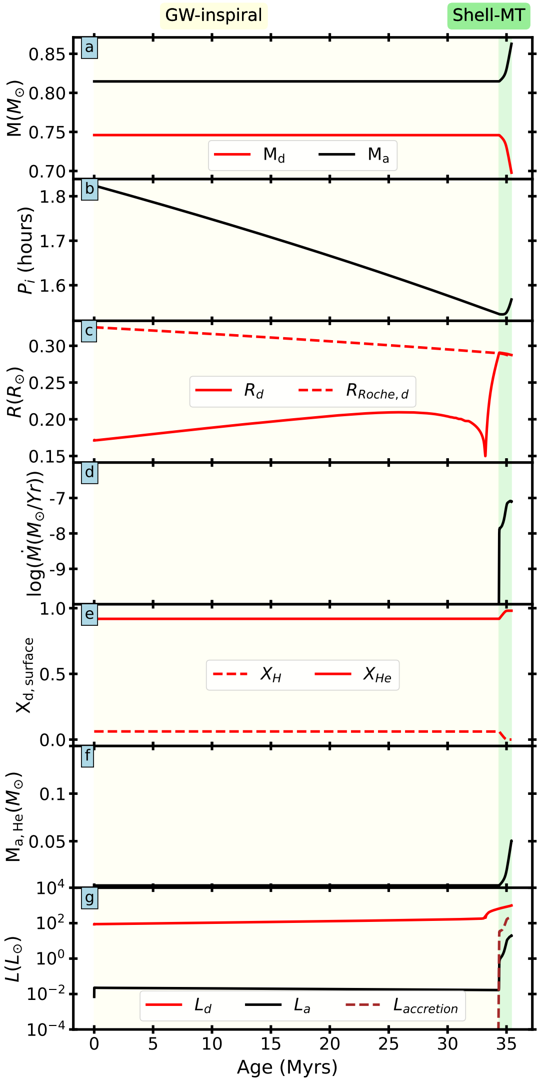

Figure 3.4: An example of a binary with $M_d = 0.75\,M_\odot$, $M_a = 0.8\,M_\odot$, and $P_i = 1.9$ hours, where a He nova occurs in the white dwarf (accretor). The panels display the evolution of different parameters as in Fig. 3.2. The background colors yellow, and green represent the gravitational-wave inspiral phase (GW-inspiral), and mass transfer phase during the He shell burning phase (Shell-MT), respectively. The accretor accretes with a relatively high accretion rate of $\sim 10^{-7}\,M_\odot \mathrm{yr}^{-1}$, resulting in the ignition in the He layers less dense than the assumed critical density for detonation ($< 10^6\,\mathrm{g\,cm^{-3}}$).

From the attempts to understand the distinguishing criteria between detonation and deflagration, previous works have shown that this classification is correlated to various factors such as ignition temperature-dependent critical density (Woosley & Kasen, 2011), and density of the ignition region (Woosley & Weaver, 1994). From Woosley & Weaver (1994), the He flashes in the degenerate surface of the white dwarf heavily depend on the density of the ignition region. They found that for the systems undergoing detonation, the minimum density of the He shell was $\rho = 6.8 \times 10^5\,\mathrm{g\,cm^{-3}}$. Furthermore, most of the systems that experienced detonations were characterized by densities above $\rho = 10^6\,\mathrm{g\,cm^{-3}}$. In this work, I adopt a critical density $\rho_c = 10^6\,\mathrm{g\,cm^{-3}}$. I classify all systems that undergo He ignition at densities below this critical as non-detonations (He novae), and those igniting above this density as detonations leading to thermonuclear supernovae.

3.3 Description of example systems

In this section, I discuss examples of the three potential outcomes for hot subdwarf + white dwarf binaries as double detonation supernovae, He novae, and double white dwarfs. Fig. 3.1 shows a schematic diagram for three different fates. Double detonation supernovae and He novae result from systems that undergo mass transfer and later experience thermonuclear instability in the He layer on the surface of the white dwarf. I differentiate a double detonation supernova from He nova based on the He layer's critical density (see Sec. 3.2.1). Double white dwarf systems result from binaries that either do not come into contact or involve episodes of accretion that fail to ignite the He layers of the white dwarf.

3.3.1 Supernova

I first examine a system that evolves into a double detonation supernova. For this example, I initiate a hot subdwarf ($0.5\,\mathrm{M_\odot}$) and a white dwarf ($0.8\,\mathrm{M_\odot}$) binary system with an orbital period of 0.84 hours, assuming the hot subdwarf has just started core He burning. Figure 3.2 illustrates the evolution of key system properties: (a) the mass of the donor and the accretor, (b) the orbital period of the binary, (c) the radius of the donor, (d) the mass transfer/accretion rate, (e) the surface mass fractions of H and He in the donor, (f) the He mass in the accretor, and (g) the luminosity of the donor, accretor, and the accretion process which I estimate as accretion luminosity

$$L_{\mathrm{acc}} \approx \frac{G\,M_{\mathrm{WD}}\,\dot{M}}{R_{\mathrm{WD}}}, \tag{3.1}$$

where G is the gravitational constant, M_{WD} is the mass of the white dwarf, $\dot{M}$ is the mass transfer rate, and R_{WD} is the radius of the white dwarf.

For the initial 11 million years, gravitational wave radiation shortens the binary orbital period until the onset of mass transfer at ~ 0.55 hours. The hot subdwarf has a convective He burning core and an H-rich envelope. Mass transfer in typical hot subdwarf + white dwarf binaries occurs in two phases: envelope mass transfer and He core mass transfer

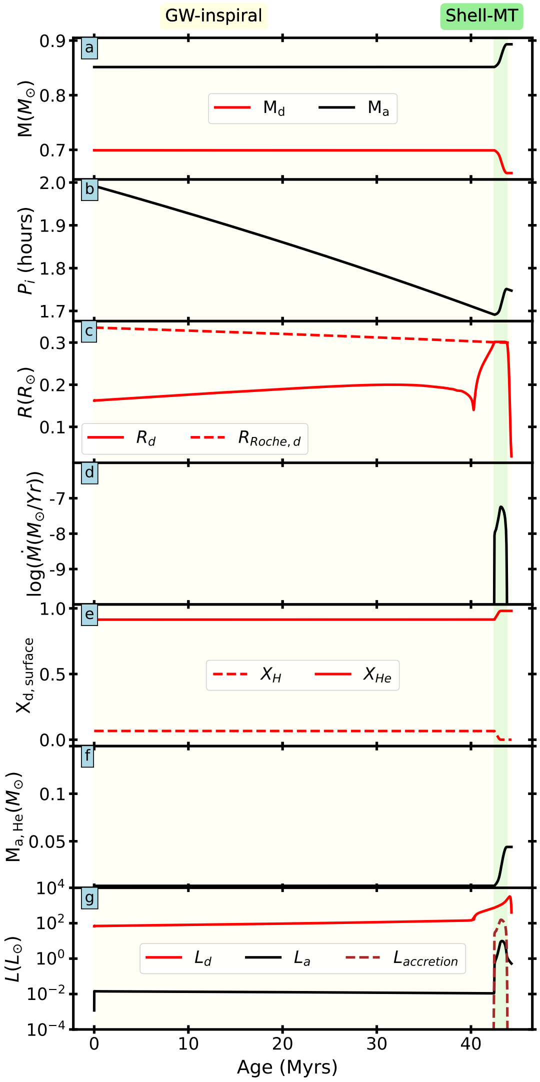

Figure 3.5: Evolutionary aspects of a binary with $M_d = 0.7\,M_\odot$, $M_a = 0.85\,M_\odot$, and $P_i = 2$ hours, where the donor evolves into a white dwarf, forming a double white dwarf system. The panels display the evolution of different parameters as in Fig. 3.2. The background colors yellow, and green represent the gravitational-wave inspiral phase (GW-inspiral), and mass transfer phase during the He shell burning phase (Shell-MT), respectively. This system is detached for most of its lifetime, and undergoes one episode of accretion that fails to ignite the He layer of the accretor, resulting in a double white dwarf. This double white dwarf is expected to merge in 86 million years which might lead to a Type Ia supernova.

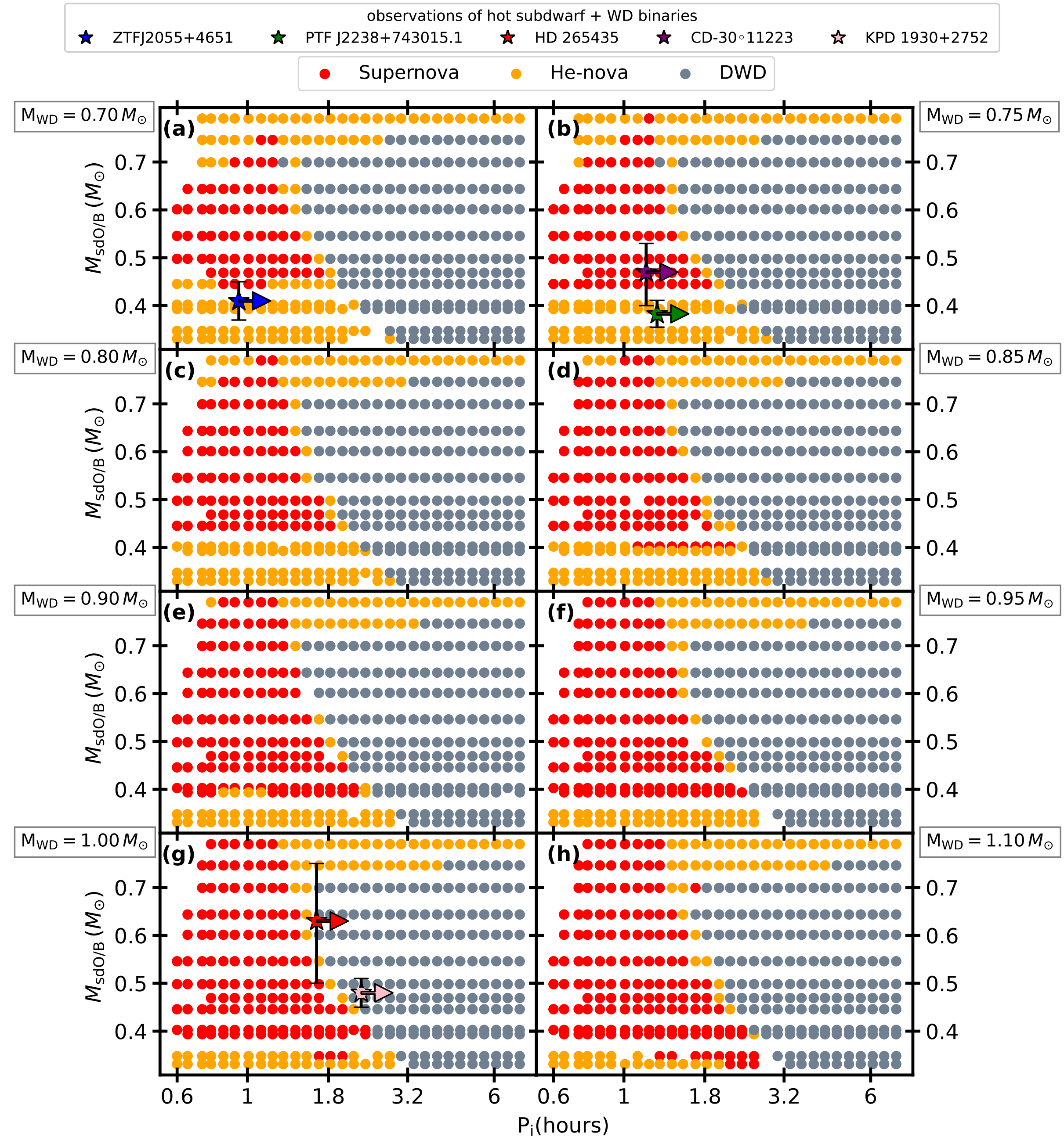

Figure 3.6: Mapping of outcomes (supernova, He nova, and double white dwarf) across the initial parameter space. The x-axis represents the initial orbital period, and the y-axis represents the initial donor mass ($M_{sdO/B}$). The 8 sub-panels describe different white dwarf masses, as labeled, that increase from the top left to the bottom right. Red points denote double detonation supernovae, orange points indicate He novae and grey points represent double white dwarfs. The stars highlight observed hot subdwarf + white dwarf binary systems (see Table 3.2), with arrows indicating that initial orbital periods must be longer than the observed values. The lower mass donors ($< 0.4\,M_\odot$) only lead to double detonation supernovae with higher mass accretors ($> 0.9\,M_\odot$). For details, see Sec. 3.4.

(Bauer & Kupfer, 2021). Initially, the donor transfers its H-rich envelope for about 2 million years at a relatively slow mass-transfer rate of about $\sim 10^{-9}\,\mathrm{M_{\odot}yr^{-1}}$. After the envelope is stripped off, the donor transitions to transferring He for the next 7 million years, with the mass-transfer rate increasing to $\sim 10^{-8}\,\mathrm{M_{\odot}yr^{-1}}$(see panel d of Fig. 3.2), accumulating a dense He layer ($\sim 0.16\,\mathrm{M_{\odot}}$) on the surface of the accretor. Throughout the accretion process, the rates are too low for stable He burning and growth of the C/O core, instead He accumulates as the He envelope.

In the left panel of Fig. 3.3, I see the time evolution of the accretor's temperature-density ($T - \rho$) profile. At the start, the temperature decreases monotonically from the center ($\rho \sim 10^{7}\,\mathrm{g\,cm^{-3}}$) to the surface. After He accretion starts at about 14 Myr, a temperature inversion occurs due to compressional heating from the accretion (e.g., Nomoto 1982a; Townsley & Bildsten 2004). As the accretor continues to accrete He at a steady rate of $\sim 10^{-8}\,\mathrm{M_{\odot}yr^{-1}}$, the combination of compressional heating and temperature diffusion continues to compress and heat the underlying layers, shifting the maximum temperature to deeper He layers with densities $\rho \sim 2 \times 10^{6}\,\mathrm{g\,cm^{-3}}$. This eventually leads to thermonuclear instability in the degenerate He layers, resulting in the runaway fusion of He via the NCO chain (marked as He ignition in Fig. 3.3). I stop our simulation at this point.

To understand the dominant process that contributes to reaching the He ignition conditions, I use the analytic expressions described below. I can estimate the adiabatic compression, at constant entropy, using the definition of the third adiabatic index (Hansen et al., 2004)

$$\left(\frac{\partial \ln T}{\partial \ln \rho}\right)_s \equiv \Gamma_3 - 1 \tag{3.2}$$

where T represents the temperature, ρ is the density, and Γ_3 is the third adiabatic index . The timescale for compressional heating can be estimated as

$$t_{\mathrm{comp}} = \frac{T}{\dot{T}} = \frac{\rho}{\dot{\rho}} \cdot \left(\frac{1}{\Gamma_3 - 1}\right). \tag{3.3}$$

I estimate the heat diffusion timescale using

$$t_{\mathrm{th}} = \frac{H^2}{D_{\mathrm{th}}} \tag{3.4}$$

where $H = P/\rho g$ is the local pressure scale height, P is the pressure, and g is the gravitational acceleration. $D_{\mathrm{th}} = 4acT^3/3\kappa\rho^2 c_P$ is the coefficient of thermal diffusion, where a is the radiation constant, c is the speed of light, κ is the opacity, and c_P is the specific heat at constant pressure.

The neutrino cooling timescale is estimated using

$$t_{\mathrm{neu}} = \frac{c_P T}{\epsilon_{\mathrm{neu}}} \tag{3.5}$$

where ϵ_{neu} is the energy loss rate due to neutrino emission.

Comparing the timescales for compressional heating, heat diffusion, and neutrino cooling based on the profiles of these quantities from our MESA model, I estimate that heat diffusion is the dominant process in setting the shape of the temperature profile that drives He ignition in the double detonation supernova case described above.

He ignition in this model occurs at densities $\rho \sim 2 \times 10^6\,\mathrm{g\,cm^{-3}}$, which is greater than the adopted critical density (see Sec. 3.2.1). Thus I classify this He ignition as a detonation and I expect that triggers a subsequent core detonation in the white dwarf (Polin et al., 2019), consequently destroying the white dwarf in a thermonuclear supernova. Immediately before the detonation, the white dwarf has a mass of $\sim 0.96\,\mathrm{M_\odot}$ with a thick He shell $\sim 0.16\,\mathrm{M_\odot}$ and thick He shell likely will lead to a red, faint transient (Kromer et al., 2010; Polin et al., 2019).

3.3.2 He nova

Next, I focus on a binary system that leads to a He nova. The specific system starts with a $0.75\,\mathrm{M_\odot}$ hot subdwarf donor, a $0.8\,\mathrm{M_\odot}$ white dwarf accretor, and an orbital period of 1.9 hours. Fig. 3.4 shows the same key binary evolution properties as shown in the previous section. The stars remain detached throughout the core He burning phase of the hot subdwarf. After about 34 million years, the hot subdwarf exhausts its core He fuel, expands to a He-shell burning phase, and fills its Roche lobe, commencing mass transfer.

The accretor gains mass at a higher rate ($\sim 10^{-7}\,\mathrm{M_\odot yr^{-1}}$) compared to the double detonation supernova example, resulting in the transfer of $0.05\,\mathrm{M_\odot}$ of He over 1 million years. I note that the mass transfer rates in this scenario are about an order of magnitude larger compared to the supernova example. At these higher rates, the timescale of compressional heating (Eq. 3.3) is shorter than the time scale of heat diffusion (Eq. 3.4). Thus, the accretion compresses and heats the less dense layers, eventually triggering a thermonuclear instability. This leads to unstable He burning via the 3α process. I stop our simulations at this point.

The right panel of Fig. 3.3 depicts the evolution of the $T-\rho$ profile of the accretor and marked regions show the He ignition. Since the He ignition occurs at densities $\rho \sim 2.5 \times 10^5\,\mathrm{g\,cm^{-3}}$, which is less than the critical density (see Sec. 3.2.1), I expect that this system does not create a detonation when it ignites. While I do not evolve systems beyond the initial thermonuclear instability, previous studies have found various outcomes for the systems undergoing He novae. Some studies (Yungelson, 2008; Nelemans, 2010; Brooks et al., 2015) have found that for systems that survive the initial thermonuclear instability, subsequent evolution is unlikely to lead to a supernova via double detonation. Instead, the continued mass transfer will lead to weaker He shell flashes. However some studies (Hachisu & Kato, 2001; Neunteufel et al., 2016) have found evidence for He-novae being progenitors of Type Ia supernova. Thus, the deterministic fate of these systems can be stated only after full evolution through all the nova outbursts.

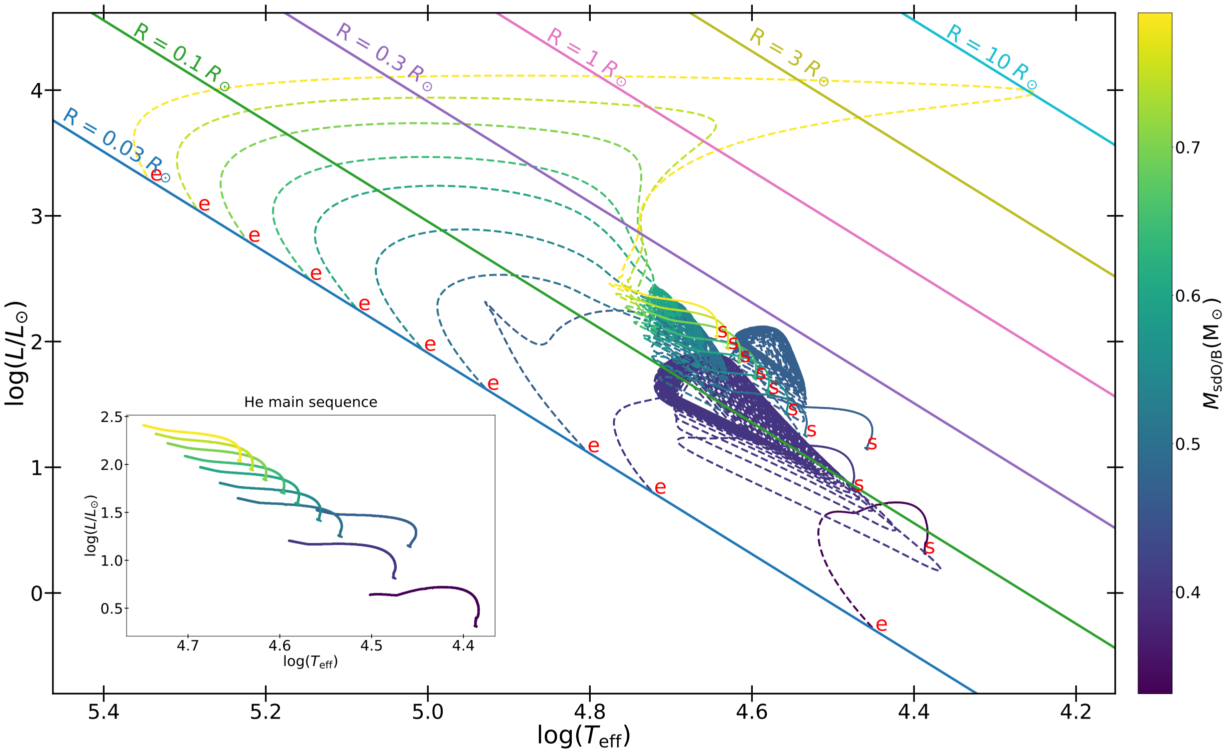

Figure 3.7: The evolution of selected single hot subdwarf stars is shown in the HR diagram. The annotated red letters “s" and “e" indicate the start and end of the evolution respectively. Different colors represent different masses of hot subdwarf stars, as indicated by the color bar. The constant radius lines illustrate the radius evolution of the hot subdwarf stars during their He shell burning phase. The inset represents a zoomed-in view of the He main sequence phase. Details of the evolution of hot subdwarf as single stars are explained in Sec. 3.2

3.3.3 Double white dwarf

Finally, I look at a system that does not ignite explosively and evolves into a double white dwarf binary. Fig. 3.5 shows the binary evolution properties of the system. The system starts as a hot subdwarf ($0.7\,\mathrm{M}_{\odot}$) and a white dwarf ($0.85\,\mathrm{M}_{\odot}$) binary system with an orbital period of 2 hours, assuming the hot subdwarf has just started core He burning. The system comes into contact during the giant-like phase of the hot subdwarf after evolving without interaction for about 42 million years.

The system undergoes one episode of accretion with a rate of $\sim 10^{-7}\,\mathrm{M}_{\odot}\mathrm{yr}^{-1}$ depositing $\sim 0.04\,\mathrm{M}_{\odot}$ of He on the surface of the accretor. However, the mass transfer stops afterward as the donor runs out of He and evolves into a white dwarf, resulting in a double white dwarf. The accretor (originally a white dwarf) in this double white dwarf has a massive shell due to accretion, unlike those formed through single stellar evolution. I terminate our simulation when the donor's radius decreases to $0.03\,\mathrm{R}_{\odot}$ and the system is no longer

Observed system	**Orbital Period (min)**	$M_{\textbf{hot subdwarf}}\,(\mathrm{M}_\odot)$	$M_{\textbf{WD}}\,(\mathrm{M}_\odot)$	**Reference**
ZTFJ2055+4651	56.34785 ± 0.00026	0.41 ± 0.04	0.68 ± 0.05	Kupfer et al. (2020b)
PTF J2238+743015.1	76.341750 ± 0.000001	0.383 ± 0.028	0.725 ± 0.026	Kupfer et al. (2022)
HD 265435	99.09918 ± 0.00029	$0.63^{+0.13}_{-0.12}$	1.01 ± 0.15	Pelisoli et al. (2021)
CD-30°11223	70.53	$0.47^{+0.07}_{-0.06}$	0.74 ± 0.02	Geier et al. (2013); Deshmukh et al. (2024)
KPD 1930+2752	137	0.48 ± 0.03	1.0 ± 0.03	Maxted et al. (2000b); Geier et al. (2007)

Table 3.2: Observed systems with their orbital periods, hot subdwarf masses, and white dwarf masses.

interacting (for more details, see Sec. 3.2). As seen in panel (b) of Fig. 3.5, the orbital period increases due to mass transfer. However, the magnitude of this increase is not very significant compared to the overall shortening from the initial orbital period (2 hours). The resulting double white dwarf has masses of $\sim 0.66\,\mathrm{M}_\odot$ and $\sim 0.89\,\mathrm{M}_\odot$, with an orbital period of 1.75 hours. This double white dwarf is expected to merge in 86 million years. Given that one of the white dwarfs has a mass of $\sim 0.9\,\mathrm{M}_\odot$, the example system could potentially lead to a Type Ia supernova triggered by the merger (Pakmor et al., 2021).

3.4 The fate of binaries across our parameter space

I construct a grid of binaries varying in initial accretor masses, orbital periods, and donor masses. The ranges of donor mass ($\mathrm{M_{hotsubdwarf}}$), accretor mass ($\mathrm{M_{WD}}$), and initial orbital periods ($\mathrm{P_i}$) are listed in Table 3.1 (see also Sec. 3.2). Fig. 3.6 presents the main results, showing the fates of the systems as a function of their initial parameters. Each point represents the outcome of a MESA model of a hot subdwarf + white dwarf binary. Eight panels correspond to different initial white dwarf masses. Within each panel, I vary the initial masses for the donor and different initial orbital periods. Systems are color-coded based on their outcomes: red points indicate systems that end in double detonation supernovae, orange points represent systems that lead to He novae, and grey points denote systems that evolve into double white dwarfs. The stars of different colors mark observed systems within our parameter space (see Table 3.2, Maxted et al. 2000b; Geier et al. 2007, 2013; Kupfer et al. 2020a; Pelisoli et al. 2021; Deshmukh et al. 2024).

3.4.1 Effect of the donor mass on the mass transfer rate

In this section, I present the different evolutionary phases of hot subdwarfs and how they vary with the initial mass of the hot subdwarf. This difference is crucial for understanding the results of binary evolution, as it is one of the causes that determine the point of contact during mass transfer.

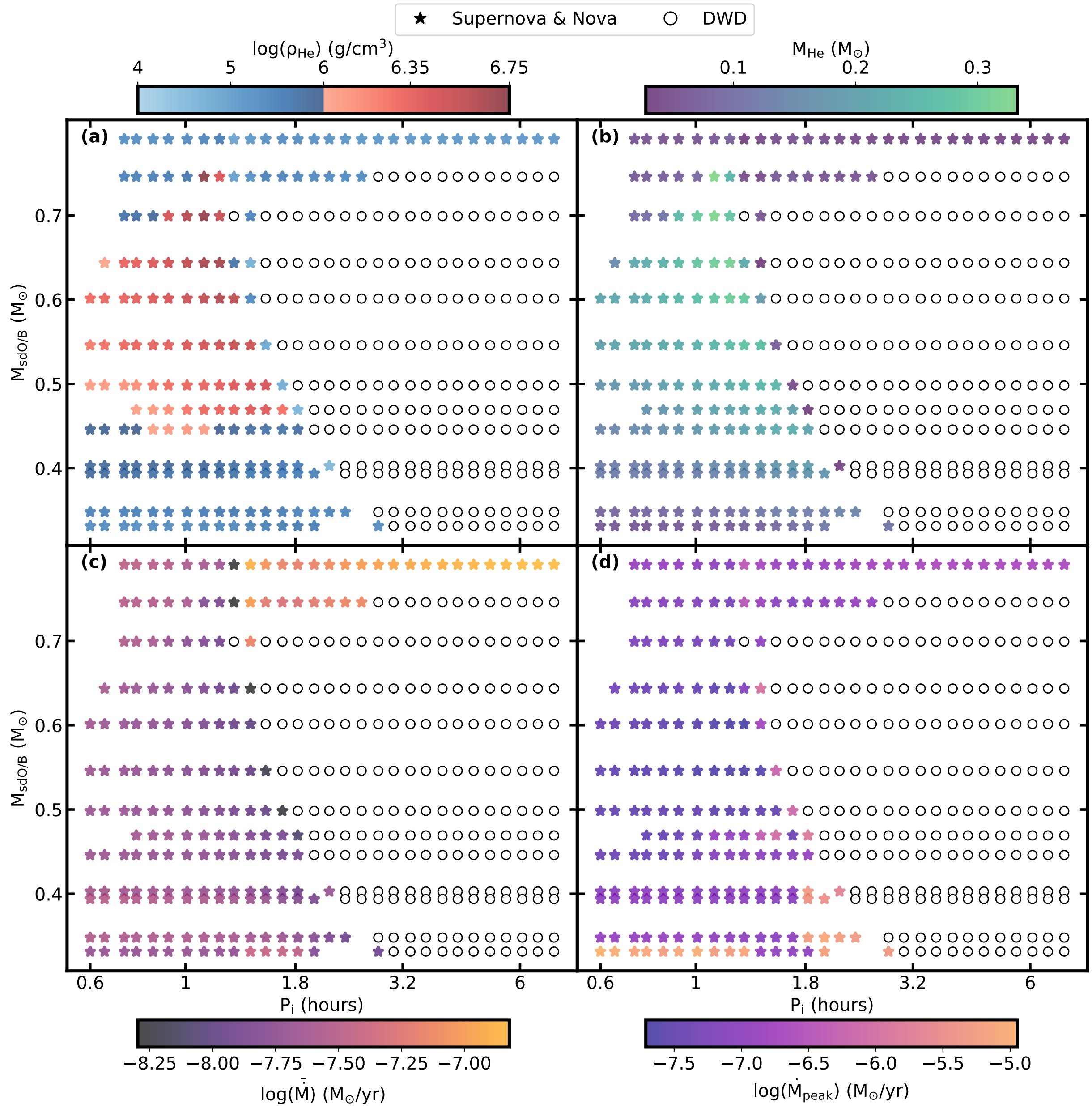

Figure 3.8: Critical properties of systems that undergo He ignition in binaries with an accretor of an initial mass of 0.7 $M_\odot$. The figure shows (a) the density of the He layer at the location of ignition, (b) the total mass of He accumulated on the white dwarf, (c) the time-averaged accretion rate from the time when the accretion rate was greater than $10^{-10}\,M_\odot\,\mathrm{yr}^{-1}$ until the He ignition and (d) the peak accretion rate at which the white dwarf gains mass. Systems classified as double detonation supernovae experience steady accretion with lower average and peak rates, leading to the accumulation of more He and ignition at a denser ($> 10^6\,\mathrm{g\,cm^{-3}}$) layer.

Fig. 3.7 illustrates the HR diagram for the evolution of hot subdwarf stars in isolation. Low-mass hot subdwarf stars ($< 0.6\,\mathrm{M}_\odot$) begin by burning He in the core, enter a thermally pulsing phase once core He is exhausted, and eventually evolve into white dwarfs with thick He shells. In our MESA models, these stars experience periodic thermal pulses because the He shell burning is unstable. The pulses cause the star to undergo significant expansions and contractions, leading to variability in the luminosity. Conversely, high-mass hot subdwarf stars ($> 0.6\,\mathrm{M}_\odot$) start with core He burning and transition to stable He shell burning upon exhausting core He. After the shell-burning phase, these stars also become white dwarfs with thick He shells.

For accretor and donor masses $< 0.75\,\mathrm{M}_\odot$, I observe an average accretion rate of approximately $10^{-8}\,\mathrm{M}_\odot\,\mathrm{yr}^{-1}$ during the core He burning phase of the donor (see panel (c) of Fig. 3.8). During the He shell burning, thermally pulsing phase, and proto-white dwarf (where donor's luminosity comes from residual heat rather than fusion) phase, the peak mass transfer rate ranges from about $10^{-7}\,\mathrm{M}_\odot\,\mathrm{yr}^{-1}$ to $10^{-6}\,\mathrm{M}_\odot\,\mathrm{yr}^{-1}$ (see panel (d) of Fig. 3.8). If mass transfer starts during the core He burning phase, the accretion rates are generally slow enough to allow accumulation of large He shells that result in He ignition in the deeper, denser ($\rho > 10^6\,\mathrm{g\,cm^{-3}}$) (see panel (a) of Fig. 3.8) layers of the accretor, resulting in a double detonation supernova. Conversely, if mass transfer occurs during the He shell burning, thermally pulsing phase, or proto-white dwarf phase of the donor, He ignition occurs in the less dense ($\rho < 10^6\,\mathrm{g\,cm^{-3}}$) (see panel (a) of Fig. 3.8) layers of the accretor, leading to a He nova. For donor masses $> 0.75\,\mathrm{M}_\odot$, where there is the possibility of the donor mass being greater than that of the accretor in low mass accretors (for example, a $0.7\,\mathrm{M}_\odot$ white dwarf and a $0.75\,\mathrm{M}_\odot$ white dwarf), the mass transfer rate depends on the mass of the accretor (for more details, see Sec. 3.4.2).

In our simulations, mass transfer ceases only when the donor exhausts its He or when I stop the simulation when it reaches one of the specified outcomes. In the following subsection, I use systems containing 0.7 white dwarf as examples and explain them in detail.

Explanation to evolutionary fates with a $0.7\,\mathrm{M}_\odot$ white dwarf

Panel (a) of Fig. 3.6 displays outcomes from a grid of binary systems featuring a $0.7\,\mathrm{M}_\odot$ accretor and various donors at different initial masses and binary orbital periods. Fig. 3.8 displays the critical properties of the systems that undergo He ignition in binaries with an accretor of an initial mass of $0.7\,\mathrm{M}_\odot$. The figure illustrates (a) the density of the He layer at the location of ignition, (b) the total mass of He accumulated on the white dwarf, (c) the time-averaged accretion rate for times when the instantaneous accretion rate was greater than $10^{-10}\,\mathrm{M}_\odot\,\mathrm{yr}^{-1}$, and (d) the peak accretion rate at which the white dwarf gains mass.

First, I describe systems containing low-mass hot subdwarf donors (ranging from $0.33\,\mathrm{M}_\odot$ to $0.40\,\mathrm{M}_\odot$). For these systems, He ignition occurs in white dwarfs when the initial orbital periods are less than 3 hours. In contrast, no He ignition occurs for initial orbital periods longer than 3 hours. Of the binaries where the accretor undergoes He ignition, the system comes into contact and starts transferring mass during the core He burning phase of the donor and continues as the donor evolves into a white dwarf. Throughout the core He burning phase, they accrete at the rate of $\sim 10^{-8}\,\mathrm{M_\odot\,yr^{-1}}$. When the donor transitions into a proto-white dwarf, the mass transfer rates peak at $\sim 10^{-6}\,\mathrm{M_\odot\,yr^{-1}}$, resulting in He ignition in less dense ($< 10^{6}\,\mathrm{g\,cm^{-3}}$) layers of the white dwarf. This ignition occurs at densities less than the critical density (see Sec. 3.2.1), classifying all of them as He novae. Systems with low-mass donors ($0.33\,\mathrm{M_\odot}$ to $0.40\,\mathrm{M_\odot}$) and initial orbital periods longer than ~ 3 hours never interact before the hot subdwarf becomes a white dwarf. The initial orbital periods of the double white dwarf systems range from 3 to 7.2 hours. These systems are expected to merge due to gravitational wave radiation in a time ranging from 81 million years to 7.9 billion years. The time until a binary system merges due to gravitational wave radiation (Peters, 1964) is calculated by

$$t_{\mathrm{merge}} = \frac{5}{256}\frac{c^5}{G^3}\frac{a^4}{M_a M_d (M_a + M_d)} \tag{3.6}$$

where c is the speed of light in a vacuum, and a denotes the semi-major axis of the orbit.

For slightly more massive donors than described in the previous paragraph ($0.45\,\mathrm{M_\odot} \leq \mathrm{M_d} \leq 0.6\,\mathrm{M_\odot}$), He ignition occurs for initial orbital periods less than 2 hours. For initial orbital periods longer than 2 hours, the binary system fails to ignite the He layers of the white dwarf. For systems that experience He ignition, donors in this mass range initiate mass transfer either during the core He burning stage or during the thermally pulsing phase, depending on the initial orbital period. If mass transfer begins during the core He burning phase and proceeds with steady accretion at a rate of approximately $10^{-8}\,\mathrm{M_\odot\,yr^{-1}}$, it can lead to He ignition in layers of the white dwarf where densities exceed the critical density criterion, leading to classification as a double detonation supernova. Conversely, if mass transfer begins during the core He burning phase and continues as the donor transitions to a white dwarf, or if it starts during the thermally pulsing phase, the peak accretion rates range from $\sim 10^{-7}\,\mathrm{M_\odot\,yr^{-1}}$ to $\sim 10^{-6}\,\mathrm{M_\odot\,yr^{-1}}$. This results in He ignition in the less dense layers of the white dwarf, leading to these systems being classified as He novae. For initial orbital periods between 2 and 3 hours, the white dwarf experiences episodic accretion during the thermally pulsing phase of the donor before the donor exhausts its He. However, this accretion does not lead to He ignition, resulting in the formation of a double white dwarf system. For systems with donor masses in the range of $0.45\,\mathrm{M_\odot} \leq \mathrm{M_d} \leq 0.6\,\mathrm{M_\odot}$ and initial orbital periods ranging from 3 to 7.2 hours, double white dwarfs are expected to merge within 3.8 million years to 6.1 billion years.

For more massive donors ($0.6\,\mathrm{M_\odot} \leq \mathrm{M_d} \leq 0.75\,\mathrm{M_\odot}$), He ignition in the accretor occurs for shorter initial orbital periods (less than 1.5 hours). For initial orbital periods longer than 1.5 hours, the binary system fails to ignite the white dwarf. For systems that undergo ignition, if the mass transfer commences during the core He burning phase, the white dwarf gains mass at a steady rate of $\sim 10^{-8}\,\mathrm{M_\odot\,yr^{-1}}$, leading to ignition in He layers with densities greater than the critical density criteria, classifying these systems as double detonation supernovae. For systems undergoing mass transfer during the shell He burning phase, or during the core He burning phase that continues into the shell He burning phase, the peak accretion rate ranges from $\sim 10^{-7}\,\mathrm{M_\odot\,yr^{-1}}$ to $\sim 10^{-6}\,\mathrm{M_\odot\,yr^{-1}}$. This results in ignition in the less dense He layers of the white dwarf, classifying these systems as He novae. For donor masses between $0.6\,\mathrm{M_\odot}$ and $0.7\,\mathrm{M_\odot}$ and initial orbital periods of 1.5 to 2.5 hours, the system undergoes episodes of accretion during the shell burning phase of the donor before the donor exhausts He. For initial orbital periods greater than 2.5 hours, the donor and accretor do not interact and evolve in isolation to become a double white dwarf. These double white dwarfs will eventually merge in approximately 2 million years to 4.8 billion years.

A $0.8\,\mathrm{M_\odot}$ donor whose mass is higher than the accretor ($q > 1; q = \mathrm{M_a}/\mathrm{M_d}$) transfers mass at a high average accretion rate ($\sim 10^{-7}\,\mathrm{M_\odot\,yr^{-1}}$) at all initial orbital periods within our range. This high accretion rate ignites the less dense layers of the white dwarf, but the rates are not high enough for the steady burning of He. I therefore classify this system as a He nova. Our initial orbital period range is insufficient for these systems to evolve in isolation to become double white dwarfs.

As the donor mass increases, the rate of He burning also increases, leading to a shorter core He burning phase. During this phase, these binaries come into contact after losing angular momentum due to gravitational wave radiation. Because of the shorter core He burning phase at higher masses, there is less time for gravitational wave radiation to shrink the orbit. Consequently, the range of initial orbital periods that result in double detonation supernovae becomes smaller with higher donor masses, while the range for double white dwarfs becomes larger.

3.4.2 Effect of the initial accretor mass on the accretion outcome

The initial accretor mass can affect the fate of the binary for two reasons. Firstly, massive white dwarfs have a denser He shell compared to low-mass white dwarfs. For instance, the base of the He shell prior to accretion in our $1.0\ \mathrm{M_\odot}$ white dwarf is denser ($\rho \sim 2 \times 10^5\,\mathrm{g\,cm^{-3}}$) compared to that in a $0.7\,\mathrm{M_\odot}$ white dwarf ($\rho \sim 0.8 \times 10^5\,\mathrm{g\,cm^{-3}}$). He ignition is highly dependent on both temperature and density. As a result, the mass of the He required to ignite the $1.0\,\mathrm{M_\odot}$ accretor is significantly lower than that required for the $0.7\,\mathrm{M_\odot}$ accretor. As a result, for a given accretion rate, the time needed to ignite He is the $1.0\,\mathrm{M_\odot}$ accretor is shorter compared to the $0.7\,\mathrm{M_\odot}$ accretor. This effect is explained below by comparing binaries with two different accretors $0.7\,\mathrm{M_\odot}$ and $1.0\,\mathrm{M_\odot}$ but with the same donor mass $0.4\,\mathrm{M_\odot}$ and same initial orbital period of 36 minutes.

With a low-mass donor ($0.4\,\mathrm{M_\odot}$) and an initial orbital period of 36 minutes, the $1.0\,\mathrm{M_\odot}$ white dwarf gains mass during the donor's core He burning phase at an average mass transfer rate of $10^{-8}\,\mathrm{M_\odot\,yr^{-1}}$, accumulating approximately $0.09\,\mathrm{M_\odot}$, which is sufficient to trigger He ignition. The density of the He ignition is greater than the critical density, making the outcome for this system classified as a double detonation supernova. However, with the same donor and initial orbital period, a $0.7\,\mathrm{M_\odot}$ white dwarf accretor begins to gain mass during the donor's core He burning phase but accumulates about $0.11\,\mathrm{M_\odot}$ at the similar average rate. This is insufficient to heat the He layers for ignition, given the lower density of the He shell in the $0.7\,\mathrm{M_\odot}$ white dwarf compared to the $1.0\,\mathrm{M_\odot}$ white dwarf. As

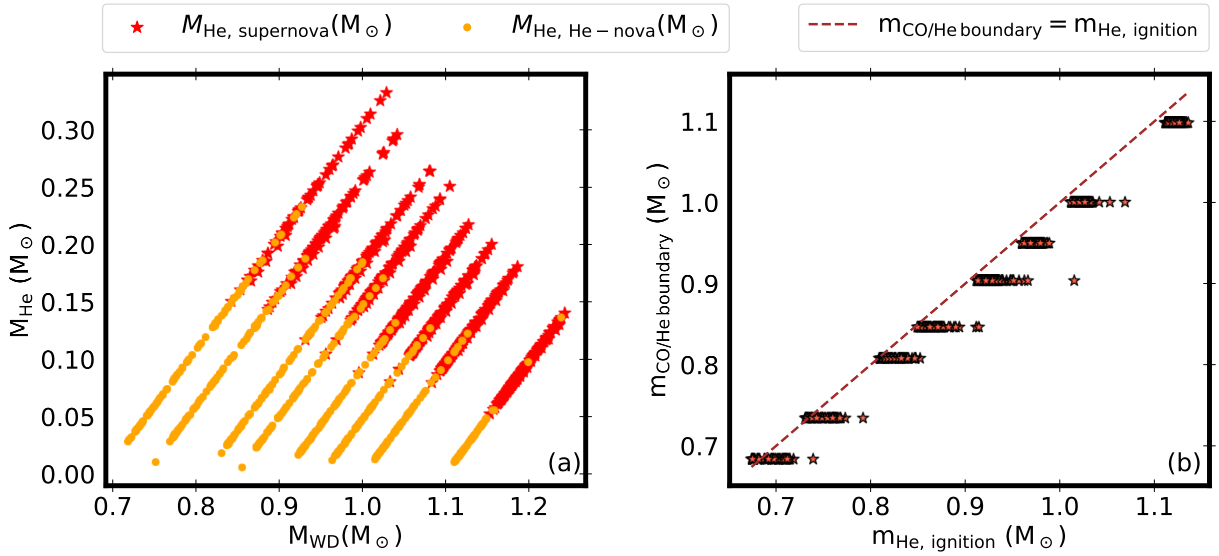

Figure 3.9: He masses (panel a) and mass coordinates (panel b) for systems that undergo double detonation supernovae and He novae. Panel (a) shows the mass of the He shell at the time of ignition versus the total mass of the white dwarf for systems undergoing double detonation supernovae and He novae. The minimum He mass required for He ignition in our simulations, at high densities greater than the assumed critical density is $\sim 0.05\,\mathrm{M_\odot}$. Panel (b) displays the mass coordinate of the ignition point against the mass coordinate of the C/O - He boundary, where the C/O - He boundary is defined as the layer containing less than 10 % He.

a result, mass transfer continues as the donor transitions into a white dwarf. During this transition, the mass transfer rate increases to around $10^{-7}\,\mathrm{M_\odot\,yr^{-1}}$, accumulating a total of approximately $0.12\,\mathrm{M_\odot}$, leading to He ignition in the less dense layers of the $0.7\,\mathrm{M_\odot}$ white dwarf. The density of the He ignition is less dense than the critical density. Hence I classify these systems as He novae.

Secondly, the mass ratio has a direct effect on the mass transfer rate. The mass ratio affects the response of the Roche radius to the mass transfer and hence the mass accretion rate. Bauer & Kupfer (2021) studies the phases of mass transfer in hot subdwarf + white dwarf binaries. In particular, they present an analytic expression to estimate the Roche radius response to the mass transfer as $(\mathrm{d}\log R_{\rm RL}/\mathrm{d}\log M_d) \approx -\frac{5}{3} + 2.1q$. Let us compare binaries with two different initial accretor masses, $0.7\,\mathrm{M_\odot}$ and $1.0\,\mathrm{M_\odot}$, but with the same donor of $0.8\,\mathrm{M_\odot}$ and same initial period of 36 minutes. For an accretor of $0.7\,\mathrm{M_\odot}$ and a donor of $0.8\,\mathrm{M_\odot}$, the mass ratio q is greater than 1, but for a $1.0\,\mathrm{M_\odot}$ accretor, $q < 1$. For a larger mass ratio as in $0.7\,\mathrm{M_\odot}$ accretor and a $0.8\,\mathrm{M_\odot}$ donor, the Roche lobe contracts as the donor loses mass, resulting in an increased mass transfer rate. Whereas for a $1\,\mathrm{M_\odot}$ accretor, the Roche radius of the donor increases in response to mass loss, leading to a relatively smaller accretion rate, leading to a double detonation supernova.

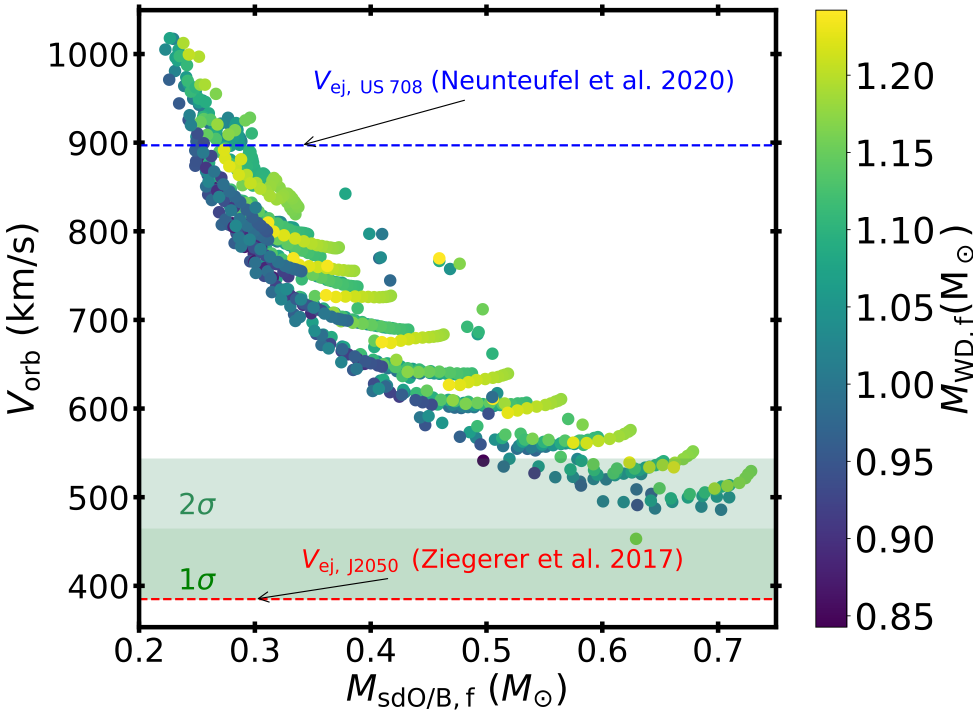

Figure 3.10: Orbital velocities of the donor at the time of the explosion of the white dwarf. The blue line and red line indicate inferred ejection velocities of the observed He-rich stars US708 (Neunteufel 2020) and J2050 (Ziegerer et al. 2017) respectively. The dark and light green shaded regions represent the 1 σ and 2 σ uncertainties to J2050. Low-mass donors with high-mass accretors result in the highest possible orbital velocities. The outliers with higher velocities for the same initial donor mass indicate the donor is a proto-white dwarf at the time of He ignition.

3.4.3 Outliers

In this section, I present two interesting outlier systems that deviate from the overall trends of the grid in Fig. 3.6. The detailed evolution diagram can be found in the appendix B.

Double white dwarf with massive He shell

I explain how a $0.7\,\mathrm{M}_\odot$ accretor accumulates $\sim 0.18\,\mathrm{M}_\odot$ of He. The binary system, comprising a $0.7\,\mathrm{M}_\odot$ donor, a $0.7\,\mathrm{M}_\odot$ accretor, and an initial orbital period of $\sim$ 1.3 hours, undergoes two episodes of accretion. The first mass transfer episode begins during the donor's core He burning phase, which heats the accretor, but pauses when the donor contracts due to core He depletion, allowing the accretor to cool. The second mass transfer episode occurs as the donor expands during its shell-burning phase, leading to the total accumulation of $\sim 0.18\,\mathrm{M}_\odot$ of He in the accretor.

Supernova during the late giant phases of accretion

I explain the formation of a double detonation supernova during shell burning phase of a donor. A binary with a $0.7\,\mathrm{M}_\odot$ donor, a $1.1\,\mathrm{M}_\odot$ accretor, and an initial orbital period of ~ 1.7 hours comes into contact during the late shell burning phase of the donor. Unlike He nova systems with shorter orbital periods around 1.5 hours (where accretion rates reach about $10^{-7}\,\mathrm{M}_\odot\,\mathrm{yr}^{-1}$), this system begins interacting during a later expansion phase, where the donor's expansion rate is slower, resulting in lower accretion rates of around $10^{-8}\,\mathrm{M}_\odot\,\mathrm{yr}^{-1}$. This lower accretion rate leads to He ignition in the dense layers of the white dwarf, ultimately getting classified as a double detonation supernova.

3.5 Final state of the binaries and observables

In this section, I present the final state of the binaries from our simulations, including the mass of the He shell of the white dwarf at the time of the explosion and the orbital velocity at time of the explosion that should be comparable to the runaway velocity of the surviving star. Additionally, I present the mass of He shell of both the donor and the accretor for systems that end up as double white dwarfs.

3.5.1 He shell masses at ignition

He-accreting white dwarfs are one of the progenitors of double detonation supernovae. Sub-Chandrasekhar explosions can occur when explosive burning in the He shell of the white dwarfs triggers a second detonation within the white dwarf, resulting in a thermonuclear supernova. However, the He mass required for the first detonation is uncertain. Previous studies (Woosley & Kasen, 2011; Sim et al., 2012) suggest that in a single degenerate scenario, a He shell of 0.1 - 0.2 $\mathrm{M}_\odot$ is required to trigger the first detonation. But such a massive He shell would lead to the production of titanium, chromium, and nickel, leading to deviation from normal supernova Ia spectra (Kromer et al., 2010; Sim et al., 2012; Shen et al., 2021; Collins et al., 2022). Here, I present the He shell masses for the systems that undergo double detonation supernovae.

Fig. 3.9 shows the He masses in systems that undergo double detonation supernovae and He novae. Panel (a) shows the mass of the He shell of the white dwarf at the time of ignition versus the mass of the white dwarf for systems that undergo double detonation supernovae and He novae. In systems undergoing a double detonation supernova, the more massive the accretor, the less helium mass is required for helium ignition. For systems that undergo double detonation supernova, the He shell masses during the first ignition range from $0.05\,\mathrm{M}_\odot$ to $0.33\,\mathrm{M}_\odot$. Panel (b) of Fig. 3.9 shows the mass coordinate of ignition (m_{He}) versus the mass coordinate of the C/O - He boundary ($\mathrm{m}_{\mathrm{CO/Heboundary}}$). I define the C/O - He boundary as the layer where the He mass fraction falls below 10 %. The dashed line shows the points where the mass coordinate of the C/O - He boundary equals the mass coordinate of He ignition. I observe the location of the He ignition in most cases is above the C/O - He boundary.

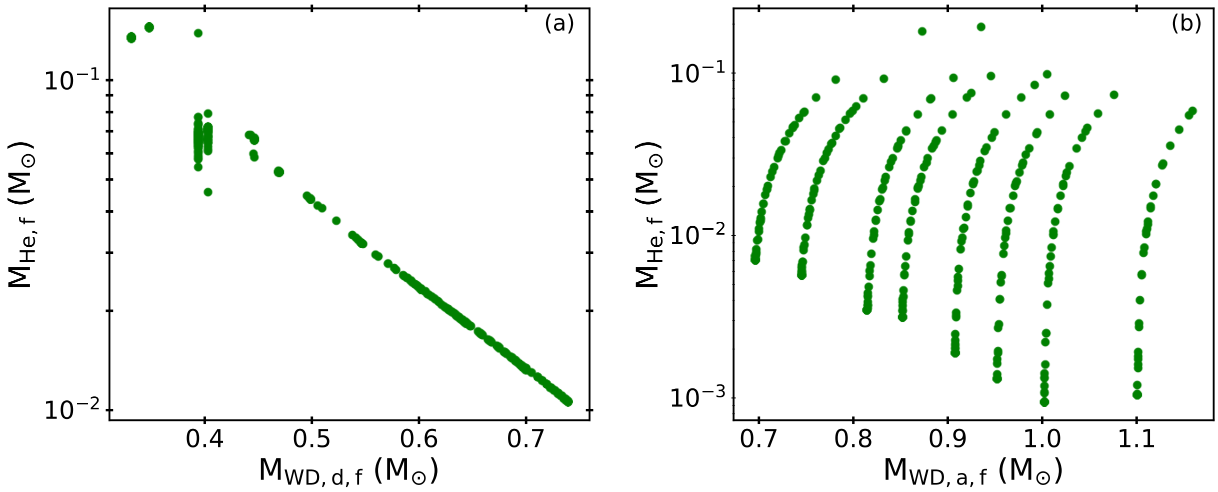

Figure 3.11: He shell masses for both the donor white dwarf, which was originally a hot subdwarf (panel a) and the accretor white dwarf, which was originally a white dwarf (panel b) in double white dwarf systems. Panel (a) displays the mass of the donor white dwarf versus the mass of its He shell. Panel (b) shows the accretor white dwarf versus the mass of its He shell. The maximum mass of the accreted He shell is $\sim 0.18\,M_\odot$.

Among the systems that result in double detonation supernovae, there is a variation in He shell masses. The system for which I find the least massive He shell originates from a binary with a $0.35\,M_\odot$ donor and a $1.1\,M_\odot$ accretor with an initial orbital period of ~ 1.3 hours begins mass transfer while the donor is still burning He in its core. Before undergoing He ignition, the accretor accumulates $\sim 0.05\,M_\odot$ of He on its surface through steady accretion ($10^{-8}\,M_\odot\,yr^{-1}$). However, the ignition point is not at the base of the He layer. The mass of the envelope above the ignition point is $0.02\,M_\odot$, located well above the base of the He layer but the densities at ignition are larger than the critical density. Hence I classify this system as a double detonation supernova.

A system resulting in the most massive He shell originates from a binary with a $0.75\,M_\odot$ donor and a $0.7\,M_\odot$ accretor with an initial orbital period of ~ 1 hour, which starts mass transfer while the donor is burning He in the core. The accretor accumulates $\sim 0.33\,M_\odot$ of He through steady accretion ($10^{-8}\,M_\odot\,yr^{-1}$). Here too, the ignition point is above the base of the He layer, with the envelope mass above the ignition point being $0.31\,M_\odot$, but with densities greater than the critical density. Thus, I also classify this system as a double detonation supernova.

3.5.2 Runaway velocities

A He-rich star, US 708, was originally observed by Usher et al. (1982) and later observed by SDSS. Hirsch et al. (2005) measured the velocity of the star and suggested that its high velocity might result from interactions in the Galactic center. Justham et al. (2009) proposed that this velocity could be attributed to the orbital velocity of a hot subdwarf star after its white dwarf companion underwent a Type Ia supernova explosion. This hypothesis was supported by Geier et al. (2015), and Brown et al. (2015), who demonstrated that the trajectory of the hot subdwarf star cannot be traced back to the Galactic center. Given the increasing number of hypervelocity runaway stars discovered by *Gaia* and the upcoming data releases, I anticipate more detections of these stars.

Since our grid includes models that might lead to white dwarf explosions, I present here the orbital velocities of these donor stars at the time of the explosion of the white dwarf. The orbital velocities range from $\sim 453\,\mathrm{km\,s^{-1}}$ to $\sim 1018\,\mathrm{km\,s^{-1}}$. Fig. 3.10 shows the orbital velocity of these donor stars as a function of hot subdwarf mass. The colors represent the current white dwarf mass at the time of the explosion. Neunteufel (2020) estimated the ejection velocity of US 708 after taking into account the updated proper motion measurements from Gaia Collaboration et al. (2018). With the inferred ejection velocity to be 894 $\mathrm{km\,s^{-1}}$, and assuming a Chandrasekhar mass supernova, they estimate the mass of US 708 to be in the range $0.34\,\mathrm{M_\odot} < M_{\mathrm{US708}} < 0.37\,\mathrm{M_\odot}$ (see the blue line in Fig. 3.10). In Fig. 3.10 the red line and green shaded regions show the estimated ejection velocities of J2050 (a spectroscopic twin of US 708; Ziegerer et al. 2017), which are $385 \pm 78\,\mathrm{km\,s^{-1}}$. From our models, there is one surviving donor with a mass of $0.63\,\mathrm{M_\odot}$ that lies within their $1\,\sigma$ range, and 69 models within the mass range $0.5\,\mathrm{M_\odot} < M_{\mathrm{d}} < 0.73\,\mathrm{M_\odot}$ fall within their $2\,\sigma$ range.

The He star is expected to receive kick velocities of 10-100 $\mathrm{km\,s^{-1}}$ from the ejecta (Liu et al., 2023). However, this is much lower compared than the pre-explosion orbital velocity of the star. Hence, the runway velocities are predominantly determined by the pre-explosion orbital velocities (Liu et al., 2023; Braudo & Soker, 2024). A proto-white dwarf can also be ejected from these binaries if the mass transfer phase is prolonged or begins at a later phase, allowing the donor sufficient time to advance in its evolution toward a white dwarf phase. In Fig. 3.10, the outliers that have higher velocities than hot subdwarfs of the same mass represent these proto-white dwarfs.

3.5.3 He shell masses for double white dwarf

In this subsection, I present the properties of the systems that end up as double white dwarfs. These are systems where either the hot subdwarf star and the white dwarf evolve without interaction or where episodes of accretion on the white dwarf fail to ignite the He shell.

Figure 3.11 presents the final He shell mass for both the donor (panel a) and the accretor (panel b) white dwarfs. If the initial orbital period of the binary is large enough to allow for the isolated evolution of the donor, it evolves into a white dwarf with a thick He shell. Panel (a) of Figure 3.11 shows the mass of the donor white dwarf versus the mass of its He shell.

About 24 % of white dwarfs of all the double white dwarfs undergo accretion either during the thermally pulsing phase or the shell burning phase of the donor, accumulate a range of He masses on the white dwarf, ranging from $\sim 9.5 \times 10^{-4}\,\mathrm{M_\odot}$ to $\sim 0.18\,\mathrm{M_\odot}$. Panel (b) of Figure 3.11 shows the mass of the accretor white dwarf versus the mass of its He shell.

The system that accumulates the maximum He mass (~$0.18\,\mathrm{M}_\odot$) without He ignition starts with a $0.7\,\mathrm{M}_\odot$ donor, a $0.7\,\mathrm{M}_\odot$ accretor, and an initial orbital period of ~1.3 hours. This system undergoes two phases of mass transfer: the core He burning phase and the He shell burning phase of the donor. This system is explained in detail in Section 3.4.3. Since the He shell masses are estimated through detailed modeling of binary evolution, these systems provide realistic input for 3D merger simulations, including those that lead to SNe Ia.

3.6 Discussion

I simulated the binary evolution of hot subdwarf and white dwarf binaries to study their potential as progenitors of double detonation supernovae, He novae, and double white dwarfs. In this section, I discuss the possible characteristics of double detonation supernovae resulting from our hot subdwarf + white dwarf models, compare our results with previous works, and discuss caveats and limitations inherent in our approach.

3.6.1 Charateristics of double detonation supernovae

I estimated the He shell masses at ignition for systems that undergo double detonation supernova. From Sec. 3.4, I observe that the He masses required for double detonations range from $\sim 0.05\,\mathrm{M}_\odot$ to $\sim 0.33\,\mathrm{M}_\odot$. Previous literature suggests that the spectra from these events will be enriched with titanium (Ti), chromium (Cr), and nickel (Ni), and will not align with the typical SNe Ia spectra (Kromer et al., 2010; Fink et al., 2010; Götberg et al., 2020). According to Townsley et al. (2019), and Boos et al. (2021), thin He shells with masses around $0.01\,\mathrm{M}_\odot$ are required to replicate SNe Ia spectra. Therefore, these systems are unlikely to represent normal type Ia supernovae but could result in other peculiar type I supernova transients. Kupfer et al. (2022) estimated the rate of double detonation supernovae with thick He shells to be $4 \times 10^{-6}\,\mathrm{yr}^{-1}$, which is 1% of the complete SNe Ia rate estimated by Sullivan et al. (2006).

3.6.2 Caveats and limitations

In our binary models, I assume conservative mass transfer with no mass lost from the system. This is an initial approximation, as the He retention efficiency of the accretor is still poorly constrained. Further studies are needed to understand the effects of mass loss and angular momentum loss due to mass ejection from the system. Additionally, I assume that any angular momentum gained by the accretor during the accretion process is transferred back to the orbit. These systems, when in contact, are extremely compact and are commonly expected to be tidally synchronized. Studies such as Fuller & Lai (2014) indicated that tides may be efficient enough to prevent the accretor from spinning up beyond the orbital frequency, and most of the angular momentum gained by the accretor could therefore be transferred back to the orbit. However, other studies have investigated the consequences if the white dwarf can be significantly spun up. For example, Yoon et al. (2004) studied rotational spin-up due to He accretion in white dwarfs and found that He shell burning is more stable in rotating white dwarfs compared to non-rotating cases. Similarly, Neunteufel et al. (2017) investigated magnetic and rotating white dwarfs and found that lower mass white dwarfs ($0.54 - 0.8\,\mathrm{M}_{\odot}$) could accumulate 50% more mass compared to non-rotating cases before the He ignition.

In our models, stellar winds from hot subdwarfs do not affect the fate of the binary. I tested the effect of the stellar winds by implementing the wind prescription from Krtička et al. (2016).

White dwarf explosions are a multidimensional phenomenon (Pakmor et al., 2024). Our classification between He novae and double detonation supernovae is based on a critical density criterion. However, there is a continuous distribution of ignition densities for systems undergoing double detonation supernovae and He novae, indicating that further research is necessary to understand this better. In addition, a He nova is not a final state of the system. Any system classified as He nova can further evolve to either explode the white dwarf or become a double white dwarf. Simulating through He novae involves mass loss assumptions and is computationally expensive. Hence, more work is needed to understand this classification better. I tested the convergence of our models for the number and grid pattern of double detonation supernovae, He novae and double white dwarfs by incrementally increasing both the time step and mesh resolution.

3.6.3 Current and future observations

The observed system PTF J2238+743015.1 is marked in panel (b) of Fig. 3.6. A recent study modeling PTF J2238+743015.1 by Piersanti et al. (2024) considers the rotational spin-up of the white dwarf due to accretion and finds that the shear heating from this process could raise the surface temperature of the accretor, making it less dense and preventing it from undergoing a double detonation supernova. Consequently, the accretor would fail to detonate the He layers during He accretion. This contrasts with the modeling of PTF J2238+743015.1 by Kupfer et al. (2022), which, using a non-rotating accretor similar to our work, proposes that the binary would end up detonating the white dwarf. While our models do not include the spin-up of the accreting white dwarf or possible associated shear heating, I consider it likely that tides will prevent the white dwarf from spinning up to near critical rotation (see also arguments in Bauer & Kupfer 2021). Our models therefore allow for the possibility of a supernova detonation for this system, but the relatively low observed mass of the hot subdwarf donor favors a He nova as more likely.

Another system in panel (b) of Fig. 3.6 is CD-30°11223 (Vennes et al., 2012; Geier et al., 2013). Modeling by Deshmukh et al. (2024) proposes that the binary would come into contact before the hot subdwarf star becomes a white dwarf. They also predict that the accretor would undergo detonation in the He layers, which agrees with panel (b) of Fig. 3.6.

The observed binary in panel (a) of Fig. 3.6 is ZTFJ2055+4651, one of the Roche-lobe filling hot subdwarf + white dwarf binaries. Modeling by Kupfer et al. (2020a) suggests that the donor is currently in the Roche-lobe filling stage and will later evolve into a white dwarf, resulting in a double white dwarf system. From our analysis (Fig. 3.6), the system could lie in the transition phase between He nova and double detonation supernova. However, since the initial orbital period is longer than the observed orbital period, it is still possible that the system would end up as a double white dwarf, in agreement with Kupfer et al. (2020a).

The other observed systems in panel (g) of Fig. 3.6 (Maxted et al., 2000b; Geier et al., 2007; Pelisoli et al., 2021) are at the threshold of multiple possibilities, indicating that the fate of these systems is very sensitive to their initial conditions.

One of the main difficulties in observing these binaries is that the companion is a massive white dwarf. Massive white dwarfs are difficult to observe in electromagnetic observations due to their ultra-compact nature and resulting faintness. However, a sufficiently close massive hot subdwarf is bright ($10-100\,\mathrm{L}_\odot$) and can be observed by photometric brightness from Gaia's color-magnitude diagram (for the latest volume completed sample of observed hot subdwarfs, see Dawson et al. 2024). In addition, due to their short orbital periods, these systems exhibit ellipsoidal modulations due to the tidal deformation of the hot subdwarf. These can be observed using ZTF (Bellm et al., 2019), and BlackGEM (Bloemen et al., 2016), OGLE (Udalski et al., 2015) and Gaia (Gaia Collaboration et al., 2016).

Large surveys such as 4MOST (de Jong et al., 2014), WEAVE (Dalton et al., 2012), and the Milky Way mapper survey included in SDSS-V (Kollmeier et al., 2017) will provide us with RV variability to detect the binary companion.

3.7 Conclusion

I simulated a grid of binary models containing a hot subdwarf and a white dwarf. Both the hot subdwarf and white dwarf were simultaneously evolved using MESA, incorporating their binary evolution and stable mass transfer via Roche-lobe overflow. Our orbital period spans a wide period range (36 minutes $\lesssim P_\mathrm{orb} \lesssim 7.2$ hours) to accommodate interacting and non-interacting systems. For shorter orbital periods, the binary components come into contact before the hot subdwarf becomes a white dwarf (see Sec. 3.4.1 for more details). I identify several phases of mass transfer, including mass transfer during the core He burning phase, the shell He burning phase, and late thermal pulses. The initial parameter space for systems that end up as double detonation supernovae, He novae, and double white dwarfs are shown in Fig. 3.6. In systems where the white dwarf explodes, the runaway velocities of the donor can reach up to $\sim 1018\,\mathrm{kms}^{-1}$. Fig. 3.10 shows the calculated orbital velocities of donor stars as a function of the hot subdwarf mass. Systems with larger orbital periods tend to evolve into double white dwarfs. I present the most important conclusions here.

1. I present the most up-to-date dense grid of MESA models for hot subdwarf + white dwarf binaries that lead to the formation of double detonation supernovae, He novae, or double white dwarfs. Fig. 3.6 shows the mapping of these outcomes across initial parameter space.

2. I find that the systems initiate mass transfer during core He burning, shell He burning, and thermally pulsing phase of the donor. In addition, there is also a non-negligible fraction of systems that undergo two phases of mass transfer, which leads to He ignition on the accretor. These systems begin mass transfer during the core He burning phase and later ignite the He shell of the accretor when the mass transfer rate increases during the shell-burning phase of the donor. See Sec. 3.4.1 for more details.

3. In addition to the runaway velocities of hot subdwarfs, I also estimate the runaway velocities of proto-white dwarfs, which tend to have a higher runaway velocities compared to that of a hot subdwarf of similar mass. For more details, see Fig. 3.10.

4. I estimated the He shell masses at the time of He ignition for the systems that undergo double detonation supernova (see Fig. 3.9). The minimum mass required for He detonation in our models is $\sim 0.05\,\mathrm{M}_{\odot}$. In most of the cases, the ignition point is found to be above the base of the He layer.

5. Double white dwarf resulting from this hot subdwarf + white dwarf binaries have thicker He shells compared to if the white dwarfs had formed from single stars (see Fig. 3.11). This may affect the outcomes of double white dwarf mergers, and so SNe Ia. The white dwarf with the most massive He shell in our double white dwarf systems is a $\sim 0.88\,\mathrm{M}_{\odot}$ white dwarf containing a $\sim 0.18\,\mathrm{M}_{\odot}$ He shell. For more details, see Sec. 3.4.3.

I compiled the existing observations of hot subdwarf + white dwarf binaries that fall within the parameter space of our grid and marked them accordingly in Fig. 3.6. The marked region aligns well with the detailed modeling of these systems. Therefore, this grid will provide a first-order estimate of the potential outcomes for future hot subdwarf + white dwarf binary observations. Since our double white dwarf properties are estimated through detailed binary evolution calculations, this grid also serves as the realistic input for 3D merger simulations, including that could lead to a Type Ia supernova.

Chapter 4

Role of triple evolution in the formation of LISA double white dwarfs

Submitted to Astronomy & Astrophysics, Rajamuthukumar et al. (2025)

4.1 Introduction

Observations indicate that triple star systems are common across various stellar evolutionary stages, including main-sequence stars, evolved giant stars, brown dwarfs, and black holes (Eggleton & Tokovinin, 2008; Moe & Di Stefano, 2017; Kervella et al., 2017; Triaud et al., 2020; Lillo-Box et al., 2021; Burdge et al., 2024). In particular, white dwarfs have been found in triple systems with main-sequence stars (for a review within 20 pc, see Toonen et al. 2014), other white dwarfs (Maxted et al., 2000a; Perpinyà-Vallès et al., 2019), neutron stars (Ransom et al., 2014), and brown dwarfs (Rebassa-Mansergas et al., 2022). However, the observed number of white dwarfs in triple systems remains significantly lower than theoretical predictions, possibly due to observational biases. Indeed, Shariat et al. (2024) propose that many observed local double white dwarfs could have originated from triples. For example, a recent spectroscopic study of wide double white dwarfs by Heintz et al. (2024) reveals some systems in which the more massive white dwarf companion has a shorter cooling age compared to the less massive one, which contradicts the initial-final mass relation if both stars were formed simultaneously in a non-interacting binary. One proposed explanation is that the progenitors of the double white dwarf were originally in a triple system, where the massive white dwarf was formed by the merger of two stars, resulting in a shorter cooling age. Furthermore, triples could significantly contribute to the rate of SNe Ia, making a substantial contribution to that from isolated binary stars (Katz et al., 2011; Hamers et al., 2013; Rajamuthukumar et al., 2023).

Hierarchical triple systems are characterized by a close inner orbit and with a tertiary component in a wider orbit. When the orbits of the inner and outer stars are sufficiently inclined, the gravitational perturbation from the tertiary star can cause large-amplitude von Zeipel-Lidov-Kozai (ZLK) oscillations (von Zeipel, 1909; Lidov, 1962; Kozai, 1962) oscillations of the inner binary eccentricity whilst the semi-major axis is unchanged. This process can play a key role in the formation of close binaries. The combination of ZLK oscillations with dissipative effects like tidal friction (Kiseleva et al., 1998b; Eggleton & Kiseleva-Eggleton, 2001b; Fabrycky & Tremaine, 2007) and gravitational-wave radiation can lead to a reduction in the inner binary's orbital semi-major axis. Thus, perturbations from the tertiary star can facilitate close-binary processes such as mass transfer, common-envelope phases, mergers, and collisions in the inner binary (Fabrycky & Tremaine, 2007; Perets & Kratter, 2012; Shappee & Thompson, 2013; Hamers et al., 2013; Michaely & Perets, 2014; Antonini et al., 2017; Toonen et al., 2020; Hamers & Thompson, 2019; Stegmann et al., 2022b,a).

Gravitational waves from compact double white dwarfs (with frequencies ranging from 10^{-4} to 10^{-1} Hz) detectable with the upcoming Laser Interferometer Space Antenna (LISA) mission offer a unique way to explore these triple systems (Amaro-Seoane et al., 2023). By detecting the gravitational-wave signals from double white dwarfs, LISA could uncover a population of systems formed through the triple evolution channel which are inaccessible to electromagnetic observations. This capability has the potential to provide new insights into the formation mechanisms of double white dwarfs, their contribution to SNe Ia (Iben & Tutukov, 1984; Korol et al., 2024), and the broader implications for the chemical evolution of the Galaxy (Pagel, 1997).

LISA is expected to detect $\sim \mathcal{O}(10^6)$ of Galactic double white dwarfs as part of an unresolved confusion gravitational-wave background and individually resolve around 10^3 – 10^4 of the 'loudest' double white dwarfs (e.g., Korol et al., 2017; Lamberts et al., 2019; Wilhelm et al., 2021; Thiele et al., 2023; Li et al., 2023; Tang et al., 2024). While these previous studies has focussed on double white dwarfs formed from the evolution of isolated binary stars, increasing evidence suggests that hierarchical triple systems, in which a close inner binary is orbited by a distant tertiary companion, may also play a significant role in the formation of double white dwarfs (Toonen et al., 2020; Heintz et al., 2024; Shariat et al., 2024).

There is mounting observational evidence that stars often form with bound companions, with a binary fraction of 30 % and a triple fraction of 10 % for F and G-type stars (i.e. with masses $\sim 1\,\mathrm{M}_{\odot}$, Eggleton & Tokovinin (2008); Raghavan et al. (2010); Tokovinin (2014); Moe & Di Stefano (2017); Offner et al. (2023). Moreover, the inner binaries in triple systems tend to be in closer orbits than the binaries found in isolated systems, which increases the probability for some binary interactions (Toonen et al., 2020). In this paper, I show that triple systems offer a greater number of evolutionary pathways for forming short-period inner binaries compared to isolated binary systems.

Approximately 10% of white dwarfs are found in double white dwarfs (binary systems where both components are white dwarfs) (Maxted & Marsh, 1999; Maoz et al., 2018; Napiwotzki et al., 2020)

Previous studies have explored the potential for detecting tertiary companions in LISA data (e.g., Seto, 2008; Robson et al., 2018; Tamanini & Danielski, 2019). Similar to electromagnetic observations, the motion of the double white dwarf around the center of mass of the triple system modulates the gravitational-wave frequency through the Doppler effect. This modulation causes a periodic shift in the gravitational-wave frequency, oscillating around the intrinsic frequency of the inner binary. Recent studies have focused on leveraging this effect to detect sub-stellar mass tertiaries, such as exoplanets and brown dwarfs (Tamanini & Danielski, 2019; Danielski et al., 2019; Kang et al., 2021; Katz et al., 2022). Thus, previous studies have primarily focused on either the isolated binary population of double white dwarfs or the detection possibilities of the third star. Our work is the first evolutionary population synthesis study of Galactic double white dwarfs resulting from triple evolution. In addition, our study accesses the impact of the triple evolution channel to the LISA's astrophysical noise background, thereby influencing the ρ of all other gravitational-wave sources.

I aim to quantify the contribution of the triples to the population of double white dwarfs detectable by LISA. I combine population synthesis models using the Multiple Star Evolution (`MSE`) code (Hamers et al., 2021) with cosmological simulations from the `TNG50` project (Nelson et al., 2019; Pillepich et al., 2019) to construct a representative model of the Galactic double white dwarf population. Our study addresses two critical questions: 1) What fraction of double white dwarfs detectable by LISA originates from the triple evolution channel? 2) Can LISA detect the dynamical effects of the third star in these triple systems?

The paper is structured as follows. In Section 4.2, I explain our methodology. Section 4.3 describes the evolutionary pathways of triples that lead to the formation of LISA double white dwarfs. I detail the population properties of LISA double white dwarfs from isolated binaries and triples in Section 4.4, investigating prospects for direct detection of the third star in Section 4.4.4. Finally, I discuss the results in Section 4.5 and summarise our findings in Section 4.6.

4.2 Methods

All simulations are performed using the publicly available population synthesis code `MSE`[1] (Hamers et al., 2021). Our set of simulations of hierarchical triples consists of a main run with a choice of default parameters and three model-variant runs. In each simulated data set, I evolve the triples from the start of the zero-age-main-sequence until a maximum integration time $t_{\max} = 14\,\mathrm{Gyr}$. The main triple data set consists of 10^5 systems, where I adopt a common envelope efficiency parameter $\alpha_{\mathrm{CE}} = 1$, and all three stars are assumed to have formed at solar metallicity $Z = \mathrm{Z}_{\odot} = 0.02$. This initial population results in 3×10^3 LISA double white dwarfs, with a $\sim 2\%$ Poisson uncertainty in this number. In each of the three model-variant runs, I simulate 10^4 systems and either vary the common envelope efficiency parameter as $\alpha_{\mathrm{CE}} = 0.1$ and 10 or change the metallicity of the stars to sub-solar $Z = 0.1\,\mathrm{Z}_{\odot}$. The effects of the chosen parameters are discussed in Section 4.5. In addition to the triple runs, I simulate a population of 10^5 isolated binaries to compare

---

[1] `https://github.com/hpreece/mse`.

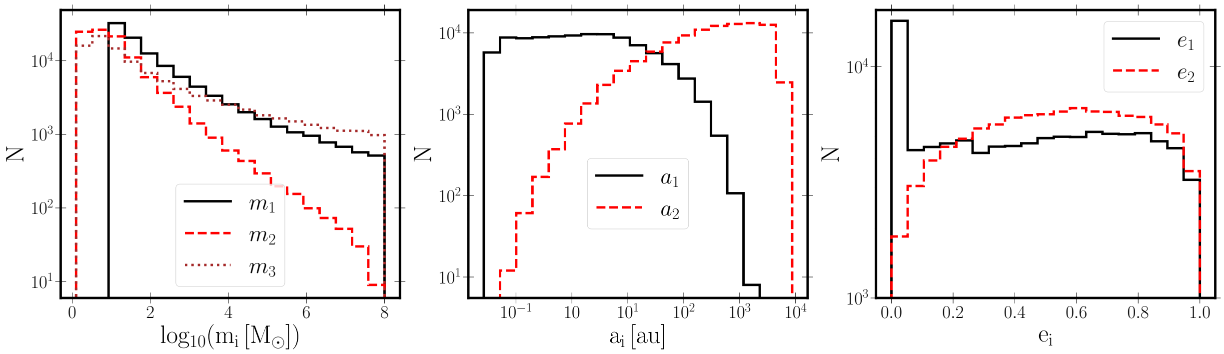

Figure 4.1: Initial parameter distributions. The left panel shows the mass distributions (m_i), where m_1 and m_2 denote the masses of the inner binary components, and m_3 represents the mass of the tertiary. The middle panel displays the semi-major axis distributions(a_i) for the inner (a_1) and outer (a_2) orbits, respectively. The right panel illustrates the eccentricity distributions(e_i) of the inner (e_1) and outer (e_2) orbits, respectively. See Section 4.2.2 for more details.

the impact of tertiary companions. Additionally, I model the inner binaries of all triples without their tertiary stars to assess their influence on the resulting LISA double white dwarf population. I expect that the isolated binary population differs significantly from the inner binary population of triples (Rajamuthukumar et al., 2023). The primary distinction is that the inner binaries have much more compact semi-major axes due to the dynamical stability constraints imposed by the tertiary star.

This section details the physics of the single, binary, and triple evolution incorporated into `MSE`, and outlines our initial distributions for the stellar populations. Additionally, I provide an overview of the Milky Way-like galaxy selected from the cosmological simulation `TNG50`. This Milky Way-like galaxy are then used to seed double white dwarfs in the galaxy. The methodology for constructing the Galactic double white dwarf population from triples is also explained here, while further details on building the Galactic double white dwarf population from isolated binaries are provided in the appendix.

4.2.1 Multiple stellar evolution code (MSE)

I use the population synthesis approach using the code `MSE` to model the stellar evolution, binary interactions (tides, mass transfer, etc.), dynamical perturbations from higher-order companions in multiple systems, and fly-bys from ambient stars. `MSE` is a `C/C++` code with a `Python` interface that can handle any number of stars as long as they start in a hierarchical arrangement. `MSE` uses a hybrid approach that switches between the secular approximation for dynamically stable orbits (that satisfy the criterion of Mardling & Aarseth 2001) and direct N-body integration using `MSTAR` (Rantala et al., 2020) for dynamically unstable orbits. Throughout the evolution post-Newtonian terms are included to 2.5 order in the secular approximation and to 3.5 order for the direct N-body integration.

To follow the evolution of single stars, `MSE` relies on the fitting formulae from Tout et al. (1996); Hurley et al. (2000), while binary interactions such as tides, wind mass transfer, stable mass transfer episodes, and common envelope (CE) evolutions are computed using modified prescriptions of Hurley et al. (2002). I briefly explain the physical handling of these key processes below. For more detailed explanations see Hamers et al. (2021).

Stable mass transfer: In `MSE`, mass transfer stability is determined either by the critical mass ratio criterion or by comparing mass transfer and dynamical timescales. The critical mass ratio depends on the donor's stellar type (Hamers et al., 2021). I assume fully conservative mass transfer ($\beta_{\rm MT} = 1$), meaning no mass is lost from the system. While `MSE` generally follows Hurley et al. (2002) for binary interactions, it differs in treating mass transfer in eccentric orbits. Hurley et al. (2002) assumes tides are always efficient in circularizing the orbit. However, in triple systems, the eccentricities are excited secularly. I follow the analytical model from Hamers & Dosopoulou (2019) to model mass transfer at periastron in eccentric orbits.

Common envelope evolution: Unstable mass transfer/CE evolution in `MSE` follows the $\alpha_{\rm CE}$ prescription (Paczynski, 1976; van den Heuvel, 1976; Livio & Soker, 1988; Iben & Livio, 1993; Hurley et al., 2002). The code solves for orbital energies before and after the CE phase, parameterizing the envelope ejection efficiency by $\alpha_{\rm CE}$ and assuming a binding energy factor of $\lambda = 1$. For the main runs, I adopt $\alpha_{\rm CE} = 1$ and I assume that the common envelope material is lost in a timescale of 10^3 yr. The post-CE semi-major axis is determined from the corresponding orbital energy.

Merger/collision: A "failed" CE can result in the merger of two stars. This occurs if the post-CE semi-major axis is too small for either star to avoid Roche lobe overflow. Beyond post-CE mergers, `MSE` also accounts for physical collisions when the sum of the stellar radii exceeds the semi-major axis or when a periapsis collision occurs in an eccentric orbit. The properties of the merger remnant are assigned following Hurley et al. (2002).

Contact evolution: If both stars simultaneously fill their Roche lobes, `MSE` assumes a CE phase if both are giant stars. Otherwise, a merger is assumed.

Triple common envelope (TCE) evolution: Mass transfer from a third star onto the inner binary can lead to a TCE. If CE conditions are met for the third star, `MSE` employs "circumstellar triple CE evolution", allowing the third star to fill its Roche lobe around the inner binary and undergo unstable mass transfer. This follows a similar approach to the prescription proposed by Comerford & Izzard (2020). The final outer semi-major axis is estimated using an $\alpha_{\rm CE}$ prescription, assuming the inner binary remains intact and does not change. However, CE modeling is inherently uncertain (see Ivanova et al. 2013 for a review), and TCE evolution is even more so, requiring cautious interpretation of results. For hydrodynamical simulations of triple CE outcomes, see e.g. Glanz & Perets (2020).

Fly-bys: `MSE` also includes the gravitational perturbations from stellar fly-bys in the vicinity of the system using the impulsive approximation. The fly-by mass is sampled from a Kroupa initial mass function (Kroupa, 2001), and encounters are randomly sampled within an encounter sphere of radius $R_{\rm enc} = 10^5\,au$ with velocities drawn from a Maxwellian velocity distribution with dispersion $\sigma_\star = 30$ km s^{-1}. The number density of fly-bys accounts for the low-density environments, assuming $n_\star = 0.1\,{\rm pc}^{-3}$. These fly-bys become significant for the evolution of the system if the semi-major axis of the outer orbit exceeds about 10^3 au (Jiang & Tremaine, 2010; Grishin & Perets, 2022; Stegmann et al., 2024).

4.2.2 Initial conditions

Here, I describe the initial distribution of our synthetic population of stars. I denote the masses of the inner binary components as m_1 and m_2, where $m_1 \geq m_2$, and the mass of the tertiary companion as m_3. Semi-major axes are denoted as a_1 for the inner binary and a_2 for the outer binary. Orbital eccentricities are denoted as e_1 and e_2, respectively. Figure 4.1 shows the distribution of the parameters of the initial triple population.

I draw the primary mass m_1 from a Kroupa initial mass function (Kroupa, 2001) between 1 and $8\,\mathrm{M}_\odot$. Furthermore, I follow functions from Moe & Di Stefano 2017 to sample the orbital period ($0.2 \leq \log(T_1/\mathrm{days}) \leq 8$) and secondary mass ($0.08\,\mathrm{M}_\odot \leq m_2 \leq m_1$) of the inner binary, and calculate the semi-major axis a_1 from Kepler's law. Similarly, the orbital period of the outer binary also follows Moe & Di Stefano 2017, where I assume that the inner binary is represented as a single star with a mass of $m_1 + m_2$. I allow the tertiary mass m_3 to be more massive than the total mass of the inner binary in certain cases, and an extrapolated mass ratio distribution from Moe & Di Stefano 2017 is used to sample m_3. In addition, I sample the eccentricities of the inner (e_1) and outer (e_2) orbits from Moe & Di Stefano 2017 and randomly sample the spatial orientations of the inner and outer orbital frames from isotropic distributions.

I reject any star whose radius exceeds the Roche-lobe radius on the zero-age main-sequence (Eggleton, 1983) and reject any system which would be dynamically unstable (Vynatheya et al., 2022) at the start of the simulation. Any Roche lobe overflow or dynamical instabilities are modeled using prescriptions in `MSE` during the evolution (see Section 4.2.1 for more details).

4.2.3 Construction of Galactic double white dwarf population

I use a Milky Way-like galaxy from the large-scale cosmological magneto-hydrodynamical simulations `TNG50` (Nelson et al., 2019; Pillepich et al., 2019). With a comoving volume of $(50\,\mathrm{Mpc})^3$ the `TNG50` simulation box contains about 100 Milky Way-like galaxies with a total mass of $10^{14}\,\mathrm{M}_\odot$. To select a suitable Milky Way-like galaxy, I randomly choose one of the six halos with a total mass $1 - 2 \times 10^{12}\,\mathrm{M}_\odot$ and whose central galaxy has a stellar mass $5 - 7 \times 10^{10}\,\mathrm{M}_\odot$. Additionally, I examine the galaxy's stellar projection to confirm disk dominance. The mass of the selected galaxy (Galaxy ID = 476266) is $\sim 5 \times 10^{10}\,\mathrm{M}_\odot$ which is consistent with our Milky Way galaxy (e.g. Bland-Hawthorn & Gerhard, 2016). I extract present-day properties such as age, stellar mass, and 3D-position of the star particles. I place our observer at a randomly assigned Sun-like position in the disk, 8.2 kpc from the Galactic center. I then measure the distances to all LISA-detectable double white dwarfs from each star particle to this location. I combine these Galactic properties with the simulated triples to construct a representative Galactic double white dwarf population as follows.

From the 10^5 simulated triples with `MSE`, I select those which form double white dwarfs that emit gravitational waves in the LISA frequency bandwidth (10^{-4} Hz – 0.1 Hz) during their evolution. I use this sample to assemble the entire Galactic LISA double white dwarf population in each star particle of the selected `TNG50` Milky Way-like galaxy. In our simulated sample all the stars are assumed to be formed simultaneously. To allow for continuous star formation I seed the number of LISA double white dwarfs per star particle ($N_{\mathrm{DWD},\star}$) based on the age and stellar mass ($M_\star$) of the star particle as:

$$N_{\mathrm{DWD},\star} = \frac{N_{\mathrm{DWD,\ MSE}}}{M_{\mathrm{tot,\ MSE}}} \times M_\star, \tag{4.1}$$

where $N_{\mathrm{DWD,\ MSE}}$ is the total number of all double white dwarfs in `MSE` which emit gravitational waves in the frequency bandwidth of LISA at a simulation time equal to the age of the star particle and $M_{\mathrm{tot,\ star\ particle}}$ is the mass of the star particle at $z = 0$, which is obtained from the `TNG50` simulation. The total stellar mass of the simulated population is given by

$$M_{\mathrm{tot,\ MSE}} = \frac{N_{t,\,\mathrm{in\,range}}}{f_{t,\,\mathrm{in\,range}} \cdot f_t} \cdot \left[f_t \cdot \bar{m}_t + f_b \cdot \bar{m}_b + (1 - f_t - f_b) \cdot \bar{m}_s \right], \qquad \text{for } f_t \neq 0, \tag{4.2}$$

where $N_{t,\,\mathrm{in\,range}} = 10^5$ is the number of simulated triple systems with `MSE`, $f_{t,\,\mathrm{in\,range}}$ is the fraction of triples in this range relative to a wider mass range of stars ($0.08\,\mathrm{M}_\odot - 100\,\mathrm{M}_\odot$), and the triple fraction $f_t = 0.2$, binary fraction $f_b = 0.3$, and single star fraction $1 - f_t - f_b = 0.5$ represent the fractions of triple, binary, and single systems in a full stellar population (Moe & Di Stefano, 2017). I assumed a more optimistic triple fraction than currently estimated from observations to account for the incompleteness. However, our results can be rescaled for practically any assumed triple fraction. The parameters $\bar{m}_t = 3.5\,\mathrm{M}_\odot$, $\bar{m}_b = 0.9\,\mathrm{M}_\odot$, and $\bar{m}_s = 0.5\,\mathrm{M}_\odot$ denote the numerically computed average masses of triple, binary, and single systems, respectively. The first term of Eq. (4.1) represents the total contribution to the stellar mass from triple systems, scaled by their fraction in the population and their average mass. The second term accounts for the contribution from binary systems and the third term represents the mass contribution from single stars. The multiplicative term $N_{t,\,\mathrm{in\,range}}/(f_{t,\,\mathrm{in\,range}} \cdot f_t)$ re-scales the number of simulated triples in the simulated mass range ($1 - 8\,\mathrm{M}_\odot$) to the total number of stellar systems in the full mass range ($0.08 - 100\,\mathrm{M}_\odot$), accounting for the fraction of triples in the full population (f_t) and their relative contribution to the restricted range ($f_{t,\,\mathrm{in\,range}}$).

Using Eq. (4.1), I seed the number $N_{\mathrm{DWD},\star}$ of LISA-detectable double white dwarfs corresponding to each star particle and randomly select them from our simulated sample (for $N_{\mathrm{DWD},\star} > N_{\mathrm{DWD,\ MSE}}$ a star particle contains some sampled double white dwarfs more than once). Additionally, I assume that all double white dwarfs are located at a star particle's center of mass.

4.3 Key processes that shape the triple evolutionary pathways

In this section, I present a brief overview of the five key processes characteristic of triple evolution that shape the evolutionary pathways leading to the formation of LISA double white dwarfs:

1. *Induced mass transfer:* The perturbation from the tertiary star triggers mass transfer in the inner binary, altering its timing or evolutionary phase compared to an isolated binary. This process ultimately leads to the formation of a short-period LISA double white dwarf.
2. *Outer binary channel:* The inner binary stars merge and form a new rejuvenated star which then evolves with the tertiary star to become a LISA double white dwarf.
3. *Ejected tertiary:* The tertiary star aids the formation of the inner double white dwarf but becomes unbound before it enters the LISA frequency bandwidth.
4. *Triple common envelope:* The third star initiates mass transfer onto the inner binary, leading to the formation of a LISA double white dwarf.
5. *Inner binary channel:* The tertiary companion remains bound to the inner binary throughout its evolution but is too distant to significantly affect the formation of a double white dwarf; this channel is effectively that of the isolated binary channel.

I show a schematic diagram for primary processes that drive evolutionary pathways leading to LISA double white dwarfs from triples in Figure 4.2. In the following subsections, I discuss these processes in greater depth with detailed examples. All uncertainities presented below are estimated by scaling up the fractional Poisson error from the intrinsic population evolved with MSE. Figure 4.3 shows that the processes are not mutually exclusive. For instance, about 4.8% of Galactic LISA double white dwarfs from triples undergo a TCE phase and induced mass transfer, leading to a merger in the inner binary. Hence, the relative percentages quoted below do not add up to 100 %.

4.3.1 Induced mass transfer

When comparing the triple runs to the inner binary runs (where the inner binary from the same triple population evolves without the tertiary star; see Section 4.2). I find that approximately 9.0 % ± 0.1 % of the Galactic LISA double white dwarfs undergo a mass transfer episode solely induced by the presence of a third star. These inner binaries would not have interacted over a Hubble time without the presence of the tertiary star. About 52 % ± 1 % of Galactic LISA double white dwarfs initiate mass transfer at a different time due to the influence of a tertiary star. Thus, a total of 61% of systems experience induced mass transfer (see Figure 4.3). In contrast, the corresponding isolated binaries would either

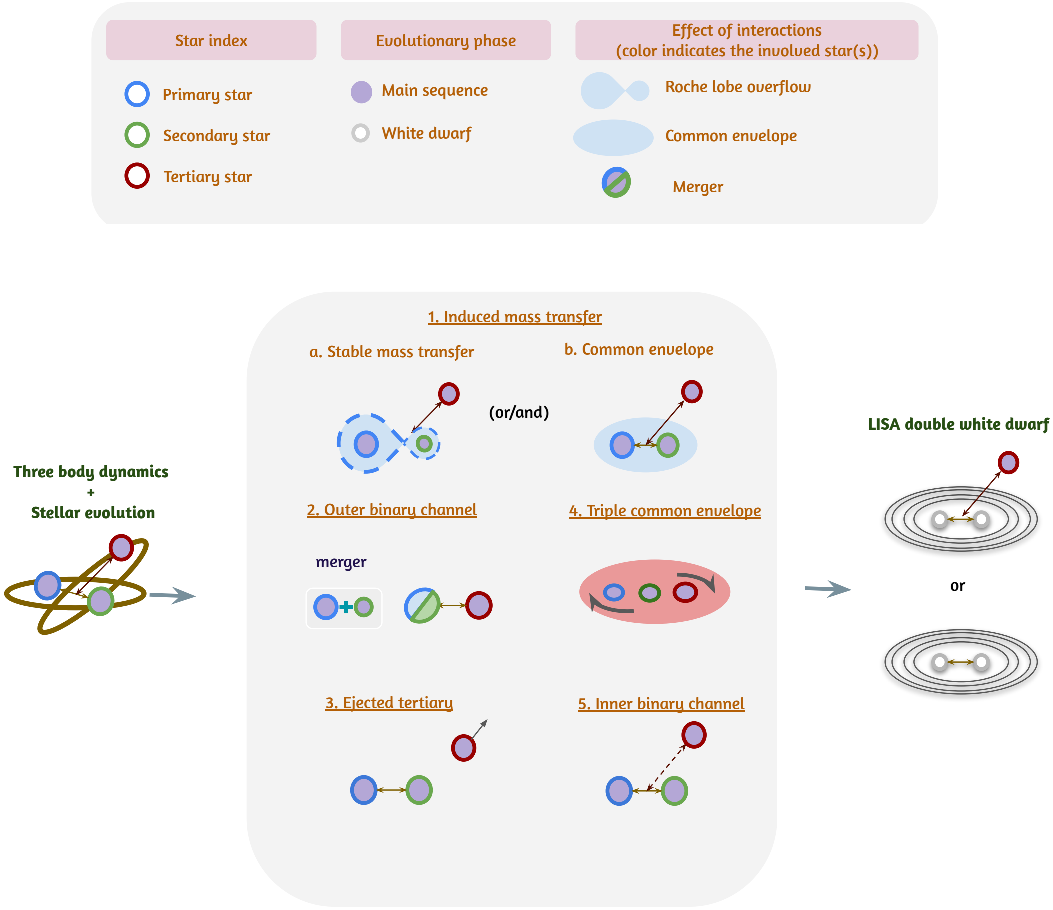

Figure 4.2: A schematic diagram of possible key processes that drive the evolutionary phases of a triple evolution leading to the formation of a double white dwarf in the LISA frequency bandwidth. The diagram showcases key stages, including mass transfer, common envelope phases, ZLK oscillations that enhance eccentricity, and eventual binary evolution. The tertiary star plays a critical role in shaping the inner binary's dynamics, either by inducing orbital changes or facilitating interactions that lead to the formation of the LISA double white dwarf. The circles represent the index of the star, with blue, green, and red indicating the primary, secondary, and tertiary stars, respectively. The filling inside each circle represents the star's evolutionary phase: purple for the main-sequence and white for a white dwarf. A dashed arrow denotes a distant tertiary star that is too far to significantly influence the inner binary. A multi-colored circle represents a post-merger star, with the two colors signifying the components that have merged.

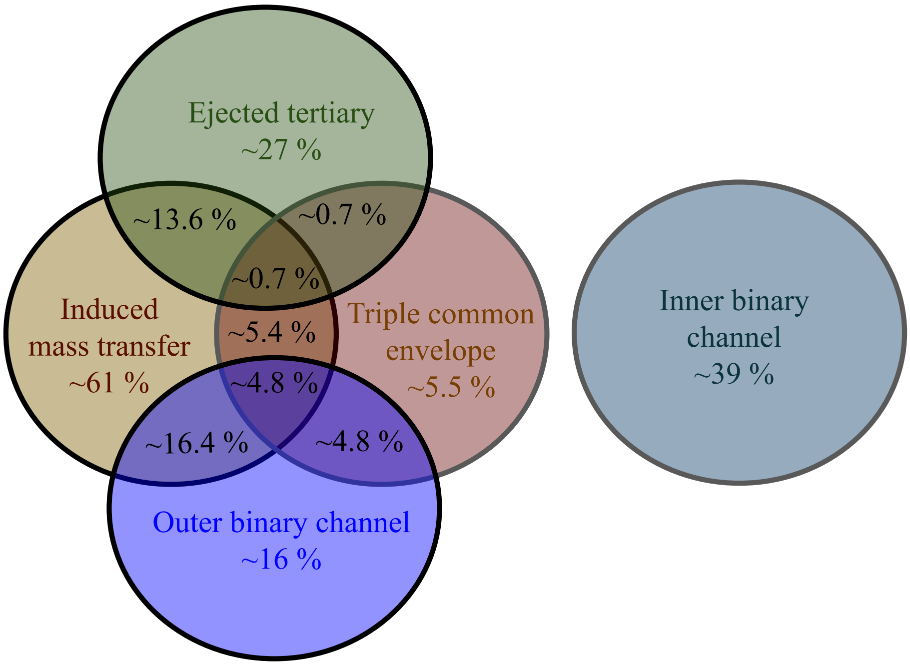

Figure 4.3: A Venn diagram illustrating the overlap of the different evolutionary processes. Among the five processes, the Inner Binary channel is the only one that does not require mandatory assistance from the tertiary star to produce a LISA double white dwarf. In contrast, the other four processes rely on the tertiary star to bring the system into the LISA frequency bandwidth. These processes are not mutually exclusive and exhibit significant overlap.

not undergo mass transfer or interact at a different time. This timing difference for the onset of mass transfer is crucial for driving the merger in the inner binary or forming a short-period inner binary that can enter the LISA frequency bandwidth within Hubble time (see the below example for more details). Also, I note that only a negligible fraction ($\sim 10^{-6}$) of systems undergo stable mass transfer without eventually becoming unstable.

As examples I show the evolution of a triple system and the inner binary without the tertiary star in Figure 4.4. The triple system starts with $m_1 = 1.61\,\mathrm{M}_\odot$, $m_2 = 1.28\,\mathrm{M}_\odot$, and $m_3 = 1.16\,\mathrm{M}_\odot$ as the tertiary star. The inner binary is initially eccentric, with an eccentricity $e_1 = 0.18$ and a semi-major axis $a_1 = 42.6\,\mathrm{au}$, while the tertiary orbit is much wider, with a semi-major axis of $a_2 \approx 2980\,\mathrm{au}$ and an eccentricity of $e_2 = 0.26$. The initial mutual inclination between the inner and outer orbits is $99°$. Without the tertiary star the system evolves as an isolated binary. The relatively large initial semi-major axis allows the binary components to evolve into white dwarfs without a mass transfer episode. During the course of evolution of the binary mass loss due to winds further widens the system, as shown in Figure 4.5. The system continues to lose orbital energy via gravitational-wave radiation but remains too wide ($a \approx 32.1\,\mathrm{au}$) to enter the LISA frequency bandwidth within a Hubble time. However, with the third star present, the system undergoes significant

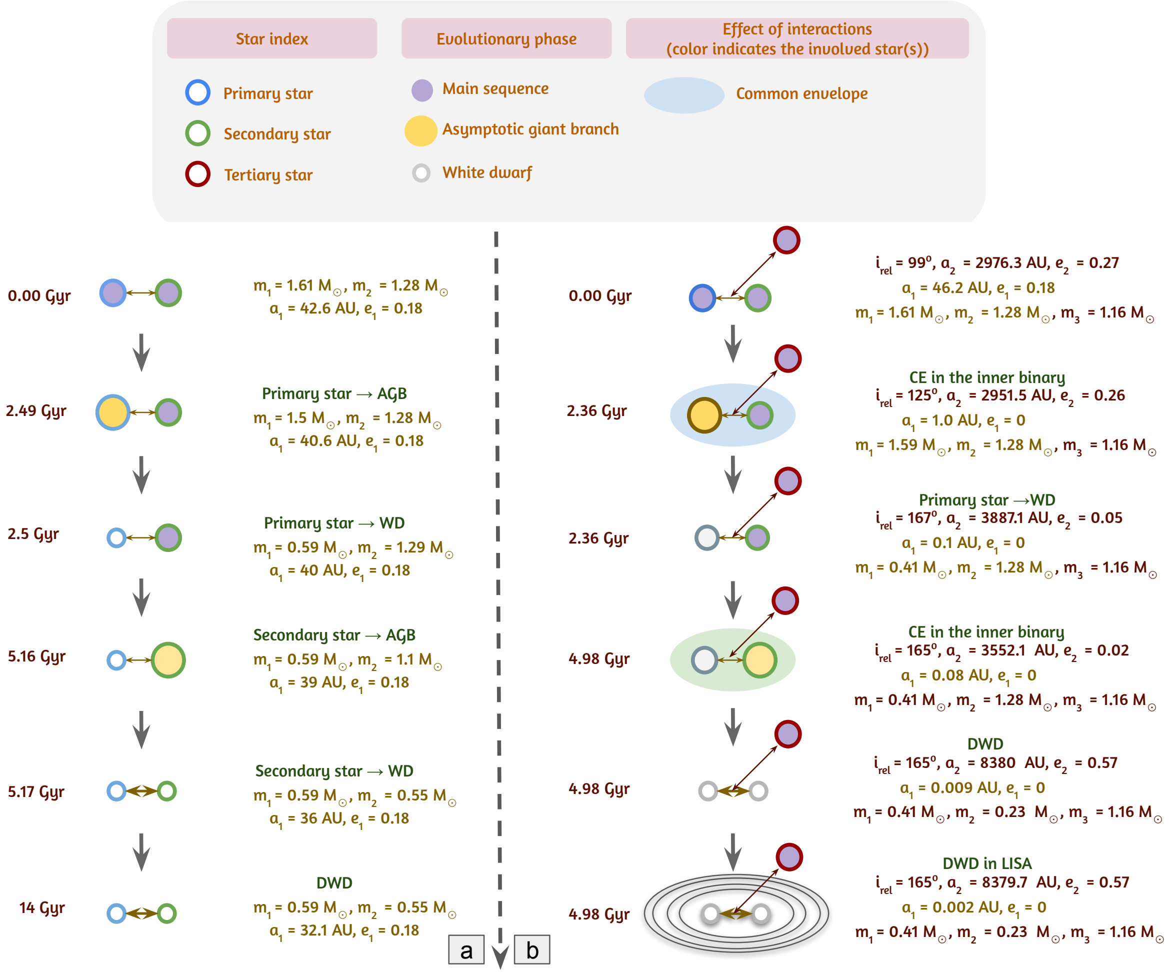

Figure 4.4: Comparison of the evolution of a triple system with and without a tertiary star. Panels (a) and (b) illustrate the evolution of the inner binary with and without the third star respectively. In the system with the tertiary star, mass transfer is induced by perturbations from the third star, allowing the system to eventually enter the LISA frequency bandwidth. When evolved without a tertiary star the binary components remain too far apart to interact. Such a system does not enter the LISA frequency bandwidth. The legends are similar to those in Figure 4.2. In addition, the yellow filling represents a star in the Asymptotic giant branch phase.

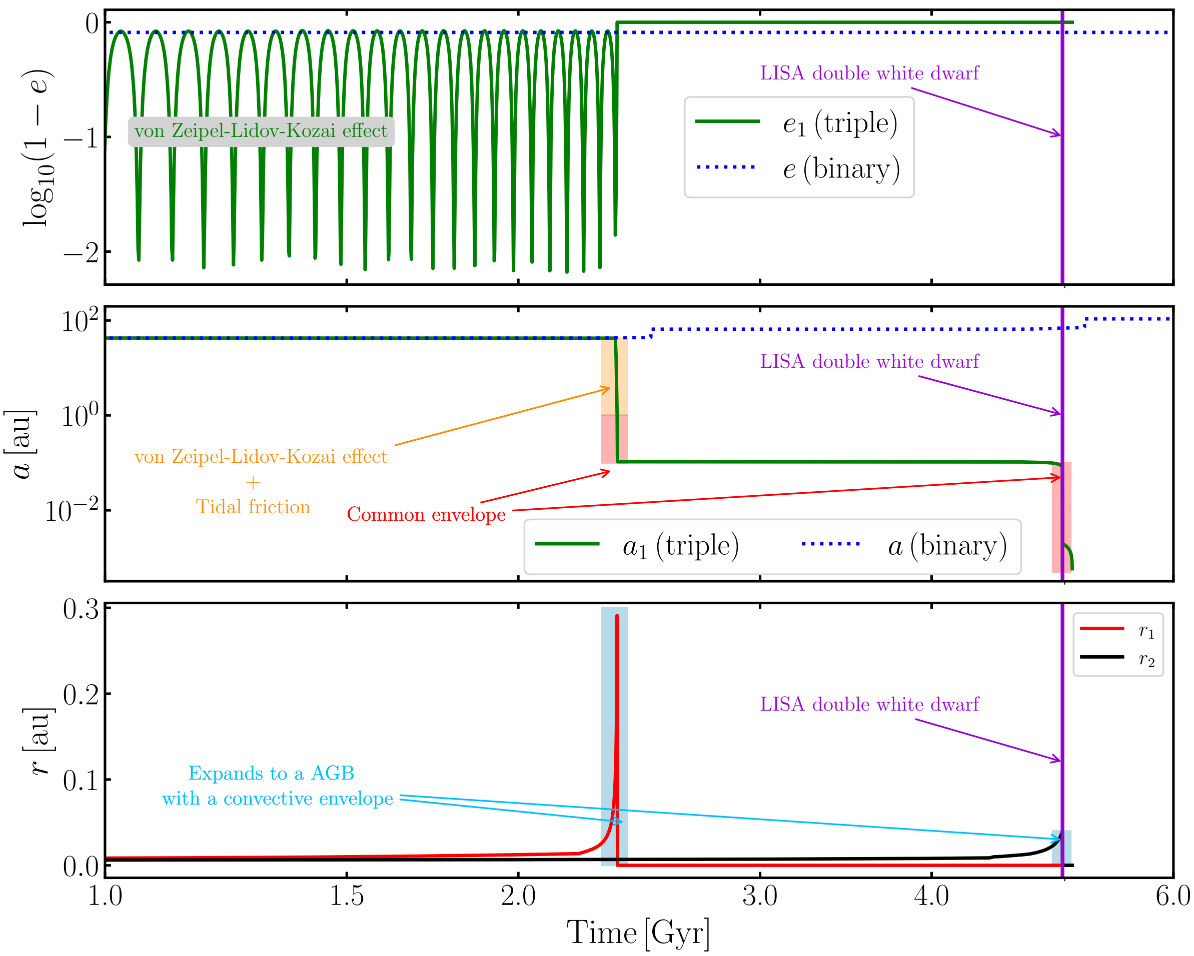

Figure 4.5: Comparative evolution of the properties of the inner binary of the triple with and without a third star. The three panels from top to bottom display the zoomed-in evolution of key parameters: eccentricity, semi-major axis, and radius of the two stars, respectively. In the case of the triple system, the inner binary experiences unstable mass transfer, causing it to shrink further and eventually enter the LISA band. Meanwhile, the inner binary when evolved without a tertiary star undergoes mass loss due to winds, resulting in an increase in its semi-major axis and a widening of the orbit. Here a_1 (triple) and e_1 (triple) represent the semi-major axis and eccentricity of the inner binary evolved with a tertiary star, while a_1 (binary) and e_1 (binary) show the semi-major axis and eccentricity of the same inner binary evolved without the tertiary star. Additionally, r_1 and r_2 represent the radii of the primary and secondary stars in the inner binary, respectively.

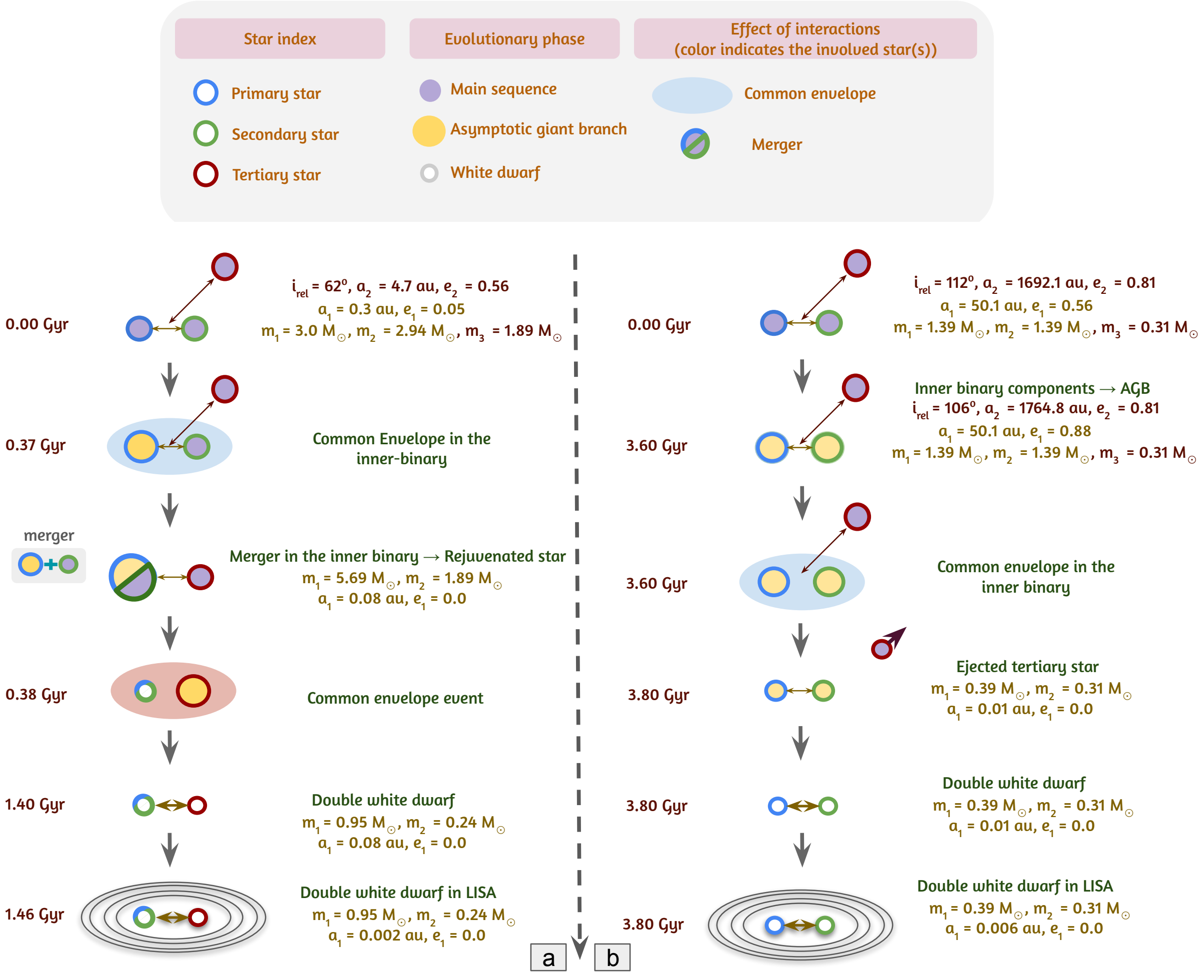

Figure 4.6: Schematic diagrams of systems that enter the LISA frequency bandwidth after following the outer binary channel and those in which the triple eject the tertiary during the course of evolution. Panel (a) depicts an example of systems following the outer binary channel. In this scenario, the inner binary merges to form a rejuvenated star, which later enters the LISA frequency bandwidth along with the tertiary star. Panel (b) illustrates an example system that initially includes a bound third star, which facilitates a common envelope phase in the inner binary but is later ejected. The inner binary subsequently enters the LISA frequency bandwidth.The legends are similar to those in Figure 4.2. In addition, the yellow circle represents a star in the asymptotic giant branch phase.

orbital shrinkage of the inner binary during its evolution and ultimately enters the LISA frequency band. At around 2.2 Gyr, the primary star of the inner binary becomes a red giant with a convective envelope. The ZLK effect, combined with tidal friction (Fabrycky & Tremaine, 2007), shrinks the inner binary's orbit from $a_1 \approx 42.6$ au to 1 au. This shortening allows the primary star to fill its Roche lobe and initiate mass transfer to its companion. The mass transfer becomes unstable due to the high mass ratio and the system enters a CE phase, which further reduces the inner binary's orbit to 0.1 au. This results in a $0.41\,\mathrm{M}_\odot$ white dwarf and a $1.28\,\mathrm{M}_\odot$ main-sequence star. Later, at around 5 Gyr, the main-sequence companion evolves to an AGB star, eventually leading to a second CE phase. This produces a short-period double white dwarf with component masses of $0.41\,\mathrm{M}_\odot$ and $0.23\,\mathrm{M}_\odot$, which enters the LISA frequency bandwidth after a few million years. Thus, in this example, the binary would not be to become a LISA source without the tertiary.

4.3.2 Outer binary channel

About $16.0\,\% \pm 0.3\,\%$ of Galactic LISA double white dwarfs originate from triples where there was a merger of the inner binary stars. I identify four scenarios which lead to mergers. First, if the inner and outer orbital planes are highly inclined with respect to each other, the perturbations from the tertiary companion shrinks the orbit of the inner binary through the combination of the ZKL effect and tides. The tightened triple system has an earlier CE episode than in an isolated binary. The CE evolution results in a merger, forming a rejuvenated star bound to the former tertiary star as a binary system. This binary can evolve into the LISA frequency bandwidth. Second, in comparison to the first, the triples start out with a relatively short-period inner binary and a distant tertiary. Here, the binary comes into contact and merges without the aid of the tertiary star. The merged star further evolves with the tertiary star to enter the LISA frequency bandwidth. Third, a TCE can cause a merger of the inner binary stars (see Section 4.3.4 for more details). Fourth, the orbit of the inner binary can widen due to mass transfer and winds, making the entire system dynamically unstable which eventually leads a chaotic evolution of the orbits and the merger of the inner binary stars.

Panel (a) of Figure 4.6 shows an example where the inner binary merges to form a new star. The system starts with $m_1 = 3\,\mathrm{M}_\odot$ and $m_2 = 2.94\,\mathrm{M}_\odot$, and $m_3 = 1.89\,\mathrm{M}_\odot$ as the tertiary star. The inner binary is initially circular with a semi-major axis $\mathrm{a}_1 = 0.3$ au. The tertiary orbit is relatively tight, with an outer semi-major axis $\mathrm{a}_2 = 4.7$ au and is eccentric with $\mathrm{e}_2 = 0.56$. The mutual inclination between the inner and outer orbits is 62°. The most massive of all three stars is in the inner binary ($m_1 = 3\,\mathrm{M}_\odot$) which, at about 370 Myr, initiates an unstable mass transfer episode onto the secondary resulting in the merger of the two stars. This merger leads to the formation of a new star with a mass $m_r = 5.69\,\mathrm{M}_\odot$. The remaining post-merger binary composed of the rejuvenated star and the tertiary companion subsequently undergoes and survives two more CE episodes: one when the rejuvenated star enters the AGB at about 390 Myr and another when the tertiary companion becomes an red giant star at about 1.4 Gyr. The second CE leads to the formation of a circular double white dwarf with a semi-major axis of 9×10^{-3} au later entering the LISA bandwidth after $\sim 1\,\mathrm{Gyr}$. An isolated binary with the same properties as the inner binary of such triple would not enter the LISA band.

4.3.3 Ejected tertiary

About $27.0\,\% \pm 0.4\,\%$ of Galactic double white dwarfs from triples lost the tertiary star. The unbinding of the tertiary companion primarily occurs due to the following reasons. First, during a CE phase the inner binary's orbit shrinks and loses angular momentum, while the prompt mass loss during the CE unbinds the outer orbit. Second, if the inner binary widens due to mass transfer or stellar winds the system becomes less hierarchical and dynamically unstable. Dynamically unstable orbits lead to chaotic evolution which may eject an object from the system. I provide a specific example of this process below.

Panel (b) of Figure 4.6 shows an example of a system where a tertiary gets ejected after a CE in the inner binary. The system starts with $m_1 = 1.39\,\mathrm{M}_\odot$ and $m_2 = 1.39\,\mathrm{M}_\odot$ as the inner binary components and $m_3 = 0.31\,\mathrm{M}_\odot$ as the tertiary star. The inner binary is initially eccentric with an inner eccentricity $\mathrm{e}_1 = 0.56$ and an inner semi-major axis $\mathrm{a}_1 = 50.1\,\mathrm{au}$. The tertiary orbit is wide, with an outer semi-major axis $\mathrm{a}_2 \approx 1690\,\mathrm{au}$ and is eccentric with $\mathrm{e}_2 = 0.81$. The mutual inclination between the inner and outer orbits is 112°. The inner binary masses are greater than the tertiary star so they evolve on a shorter timescale. The CE occurs in the inner binary during the AGB phase after about 3.6 Gyr. The CE reduces the inner binary semi-major axis to $10^{-2}\,\mathrm{au}$ and unbinds the outer tertiary. The remaining binary components evolve into a double white dwarf system. This double white dwarf binary emits gravitational-waves and later enters the LISA frequency bandwidth after $1\,\mathrm{Myr}$. In this example, even though the binary does not have a bound tertiary star by the time it enters the LISA frequency bandwidth, the tertiary plays a role in shrinking the binary before the CE episode.

4.3.4 Triple common envelope

About $5.5\,\% \pm 0.1\,\%$ of of Galactic double white dwarfs from triples undergo a phase of TCE evolution before entering the LISA frequency band. I identify two possible evolutionary outcomes of a TCE event in our simulations. First, the merger of the inner binary: the inner binary may merge to form a rejuvenated star. The new star forms a binary with the third star which later enters LISA frequency bandwidth. Second, ejection of one component: One of the stars may become unbound from the system, leaving behind a binary formed by the remaining two stars. This binary may enter the LISA band. I explain one of the examples below (see Hamers et al. 2022 for a more detailed study of TCE).

Figure 4.7 shows an example of a TCE where the inner binary merges to form a new binary. The system starts with $m_1 = 1.18\,\mathrm{M}_\odot$, $m_2 = 0.54\,\mathrm{M}_\odot$, and a relatively massive tertiary $m_3 = 5.59\,\mathrm{M}_\odot$. The inner binary is initially circular, with a semi-major axis $\mathrm{a}_1 = 0.05\,\mathrm{au}$. The tertiary orbit is compact, with an outer semi-major axis $\mathrm{a}_2 = 25\,\mathrm{au}$ and highly eccentric with $\mathrm{e}_2 = 0.94$. The mutual inclination between the inner and outer orbit is 160°. Since the tertiary star is massive compared to the inner binary masses, it is the first to reach the AGB phase, in about 92 Myr. The inner binary components are still in the main-sequence.

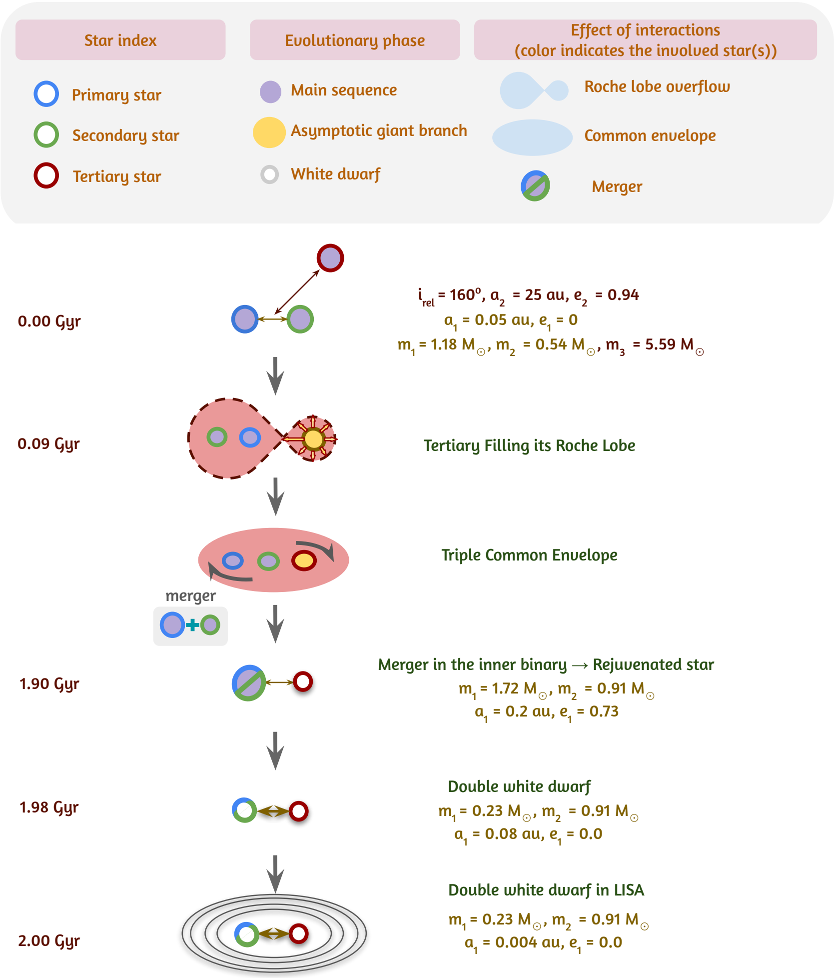

Figure 4.7: Schematic diagram for an example system which undergoes a TCE. In this scenario, the massive star transfers mass onto the inner binary, leading to its merger and the formation of a rejuvenated star. This rejuvenated star later enters the LISA frequency bandwidth along with the tertiary star. The legends are similar to those in Figure 4.2. In addition, the yellow circle represents a star in the asymptotic giant branch phase.

Expansion of the envelope during the AGB phase initiates Roche lobe overflow. The AGB tertiary starts transferring mass onto the inner binary. The mass transfer becomes dynamically unstable owing to a higher mass ratio. The envelope of the AGB tertiary star engulfs both components of the inner binary. The TCE evolution leads to interactions between the three stars. The inner binary merges to form a rejuvenated star which is still bound to the stripped tertiary star. The resulting binary has a large eccentricity of 0.73 and a semi-major axis of 0.2 au.

After approximately 2 Gyr, the rejuvenated star evolves into a red giant which transfers mass onto the white dwarf, initiating another CE phase. The end of this CE phase leaves a circular and compact double white dwarf in a circular orbit with a semi-major axis of $\sim 8 \times 10^{-2}$ au. After a few million years the binary enters the LISA frequency bandwidth due to gravitational-wave emission. Here, TCE plays a significant role as it leads to merging the inner binary. The binary with the post-merger rejuvenated star later enters the LISA frequency bandwidth. Hence, the tertiary star plays a vital role in the evolution of the triple to LISA frequency bandwidth.

4.3.5 Inner binary channel

The inner binary channel is similar to the isolated binary channel, where the binary evolves without a notable contribution from the tertiary star. About 39.0 % ± 0.7 % of the Galactic double white dwarfs from triples in our simulations follow this channel. Here the inner binary undergoes phases of CE before forming a short-period double white dwarf. This double white dwarf later enters the LISA frequency bandwidth with either a wide tertiary or as a binary with an ejected tertiary (for details on ejected tertiary, see Section 4.3.3).

4.4 LISA double white dwarfs: isolated binary vs. triple evolution

Building on the method in Section 4.2.3, where I construct the Galactic population by combining `MSE` with a Milky Way-like galaxy from `TNG50`, I obtain a total of $\sim 7.2 \times 10^6$ Galactic double white dwarfs originating from triples. To compare this result with the isolated binary channel, I adjust our simulation as described in Appendix C. I emphasize that the initial distribution of the isolated binary population is constructed to represent truly isolated binaries and is different from the initial properties sampled to assemble the inner binaries in triple systems (cf. Section 4.2.2). In the isolated binary case, I find that about $\sim 3.8 \times 10^6$ double white dwarfs are produced through isolated binary evolution, yielding a total of $\sim 1.1 \times 10^7$ Galactic double white dwarfs currently emitting gravitational waves within the LISA bandwidth. Thus, approximately 65 % ($\sim 7.2 \times 10^6$) of all Galactic double white dwarf binaries originated from triple systems as illustrated in Figure 4.8. I note that the isolated binary evolution channel only yields circular binaries. In contrast, the triple channel generates a small fraction (3×10^{-6}) of eccentric binaries, which I will discuss below.

Notably, I find that among all the double white dwarfs initially in triples only about half (∼57%) retain a bound tertiary. In the remaining systems the third star either becomes unbound or merges with another star within the system to form a binary. Importantly, all double white dwarfs that retain their tertiary companion in our simulations have the tertiary in a relatively wide orbit. I discuss the potential for detecting the presence of the tertiary companion based on LISA data in Section 4.4.4.

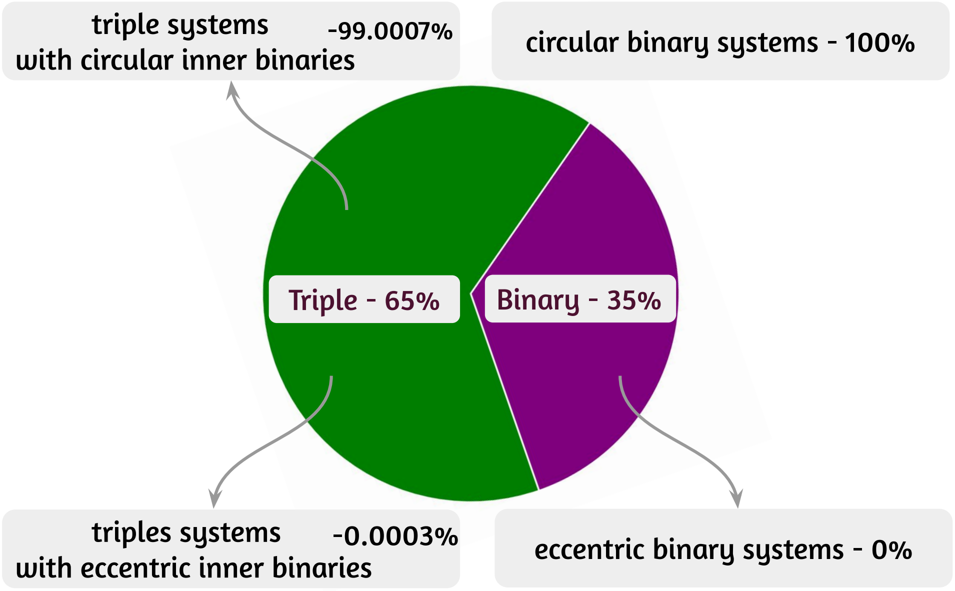

Figure 4.8: Pie chart showing the fraction of eccentric and circular orbits among double white dwarfs from triple systems and isolated binary systems. While isolated binaries do not produce double white dwarfs with eccentric orbits, approximately 3×10^{-6} of LISA-detectable double white dwarfs from triple systems exhibit eccentric orbits.

I recall that I also generated a comparative simulation where the Galactic population only follows the isolated binary channel (i.e., entirely excluding triple channels). In this simulation I obtain a total of $\sim 9.4 \times 10^6$ double white dwarfs emitting at LISA frequencies. All results are summarized in Table 4.1.

In the following subsections I present our estimates for the number of individually resolvable sources and estimate the unresolved stochastic foreground. I discuss the source properties and white dwarf (core composition) types from triple systems then compare them with those from the isolated binary channel.

Category	$N(f < 10^{-4}\,\mathrm{Hz}) \times 10^6$	$N(\rho > 7) \times 10^3$
Triple	7.20 ± 0.13	10.9
Binary	3.80 ± 0.10	6.5
Triple + Binary	11.00 ± 0.16	17.4
Only binaries ($f_t = 0$)	9.40 ± 0.12	14.4

Table 4.1: The table presents the estimated counts of Galactic LISA double white dwarfs from different formation channels: Triple (originating from triple systems), Binary (originating from isolated binaries), Triple + Binary (the combined population from both channels), and Only binaries (isolated binaries with no triples, i.e., a triple fraction $f_t = 0$). Quoted uncertainty estimates represent scaled-up fractional Poisson error from the intrinsic population evolved with MSE.

4.4.1 Detectability with LISA

Circular systems

Double white dwarfs in the LISA band are typically millions of years away from merging. They are continuous, quasi-monochromatic gravitational-wave sources for LISA. Describing these signals requires a set of eight parameters, typically chosen as $\{\mathcal{A}_{\rm gw}, f_{\rm gw}, \dot{f}_{\rm gw}, \lambda, \beta, \iota, \psi, \phi_0\}$ (LISA Consortium Waveform Working Group et al., 2023). Here, $\mathcal{A}_{\rm gw}$ represents the gravitational-wave amplitude, $f_{\rm gw}$ and $\dot{f}_{\rm gw}$ denote the gravitational-wave frequency and its time derivative (or chirp), (λ, β) correspond to the ecliptic longitude and latitude, respectively, ι is the (inner) binary inclination angle with respect to the line-of-sight, ψ is the gravitational-wave polarization angle, and ϕ_0 represents the binary's initial phase. Our population synthesis models provide binary parameters such as component masses, orbital periods and eccentricities, sky positions and distances. I use these to derive gravitation-wave parameters as follows. As discussed above, the overwhelming majority of double white dwarfs in our simulations are circularized.

The gravitational-wave frequency of a circular binary is twice its orbital frequency $f_{\rm orb}$

$$f_{\rm gw} = 2 f_{\rm orb}, \tag{4.3}$$

while the amplitude is given by

$$\mathcal{A}_{\rm gw} = \frac{2(G\mathcal{M}_{\rm c})^{5/3}}{c^4 d} (\pi f_{\rm gw})^{2/3}, \tag{4.4}$$

where G and c are the gravitational constant and speed of light respectively. The amplitude is set by the source's distance d and chirp mass

$$\mathcal{M}_{\rm c} = \frac{(m_1 m_2)^{3/5}}{(m_1 + m_2)^{1/5}}, \tag{4.5}$$

The chirp mass also sets the rate at which the frequency changes due to the gravitational radiation reaction:

$$\dot{f}_{\rm gw} = \frac{96}{5} \frac{(G\mathcal{M})^{5/3}}{\pi c^5} (\pi f_{\rm gw})^{11/3}. \tag{4.6}$$

Equations (4.3), (4.4), and (4.6) define the first three parameters of the set. The ecliptic coordinates (λ, β) are inherited from the `TNG50` Milky Way-like galaxy where the binary was seeded, while the remaining three parameters are assigned randomly: ι is sampled from a uniform distribution in $\cos\iota$, and ψ and ϕ_0 are sampled from flat distributions.

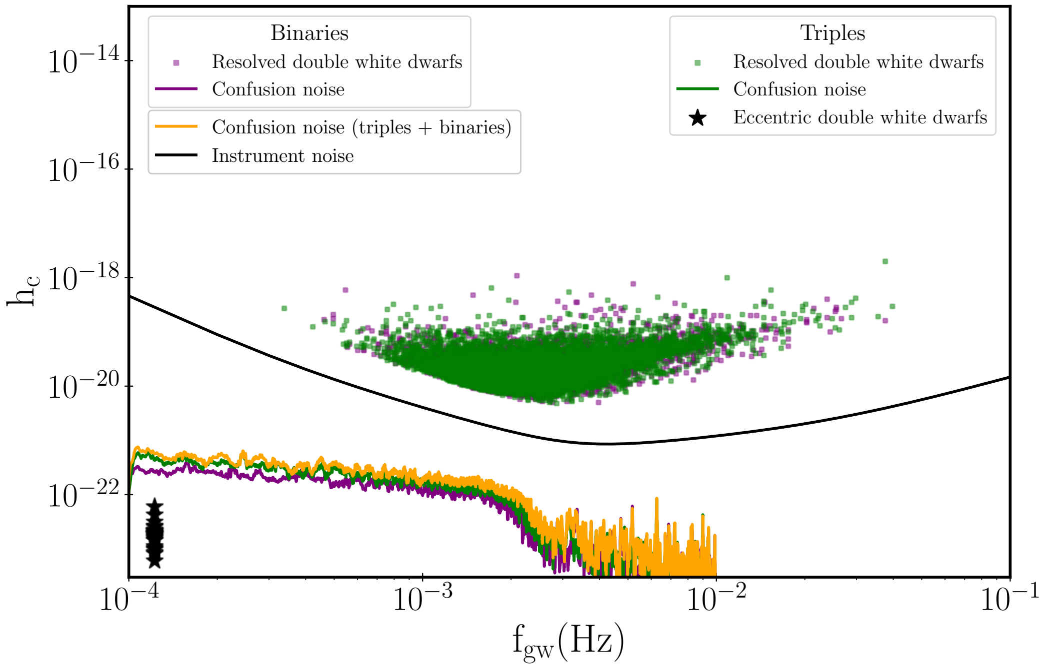

Figure 4.9: Characteristic strain $h_c = \mathcal{A}_{\rm gw}\sqrt{f_{\rm gw}T_{\rm obs}}$ of resolved double white dwarf binaries in our mock simulation for a mission duration of $T_{\rm obs} = 4\,yr$: triples in green points and isolated binary channel in purple points. This is compared to the LISA instrumental noise (black solid line). Triples with highly eccentric orbits ($e > 0.9$) and other low signal-to-noise sources are marked in black and dark gray markers, respectively. The confusion background from the Galactic double white dwarf population is represented by green, purple, and orange lines for triples, binaries, and their combined contribution, respectively. All the eccentric systems (black markers) tend to have narrow periapsis time (10^4 s) and hence they occupy a narrow frequency range. The astrophysical noise from these backgrounds remains significantly lower than the instrumental noise.

As the next step, I estimate the confusion noise produced by these gravitational-wave sources in our mock Milky Way using the pipeline[2] described in Karnesis et al. (2021, see also Timpano et al. 2006; Crowder & Cornish 2007; Nissanke et al. 2012). The pipeline approximates the so-called "global fit" analysis, which is the currently adopted approach to handling LISA's complex data analysis (Colpi et al., 2024, see also Littenberg & Cornish 2023; Katz et al. 2024; Deng et al. 2025). The pipeline employs a signal-to-noise (ρ) evaluation to iteratively estimate the strain amplitude spectral density resulting from the combined signals of the unresolved (i.e., low ρ) part of the input population. As a result,

---

[2] `https://gitlab.in2p3.fr/Nikos/gwg`.

I also obtain a catalog of individually resolved (i.e., high ρ) binaries. For our analysis, I adopt LISA's instrumental noise requirements as defined in the technical note by LISA Science Study Team (2018). I assume a mission duration of 4 yr and use an ρ threshold of 7 to distinguish between individually resolvable LISA sources and unresolved ones, a choice commonly adopted in detailed simulations (e.g., Crowder & Cornish, 2007; Cornish & Littenberg, 2007; Finch et al., 2023)

I estimate a confusion foreground from our mock population containing double white dwarf binaries from both isolated binary and triple channels to be at the level of the LISA instrument noise. I also obtain $\sim 1.7 \times 10^4$ sources above the ρ threshold, of which $\sim 6.5 \times 10^3$ come from the isolated binaries and $\sim 1.1 \times 10^4$ come from the triples. I illustrate these in Figure 4.9 (see Section 4.5.1 for comparison to previous works). Our estimate of the confusion noise is lower than those presented in the LISA mission proposal (Amaro-Seoane et al., 2017) and the more recent LISA Definition Study Report (Colpi et al., 2024), which used a different population synthesis study (Nelemans et al., 2004; Korol et al., 2017). This discrepancy arises from multiple aspects of population modeling, including variations in binary evolution prescriptions, Milky Way modeling, and, importantly, the inclusion of the triple formation channel in our simulations. However, since the same systematics are applied to both our triple and isolated binary populations, their differential properties remain largely unaffected. These factors collectively influence the total number of binaries in the LISA band and their properties. Identifying a single source of the difference is challenging, as these aspects are interrelated and non-trivially correlated. The LISA Consortium's Astrophysics Working Group is currently investigating the differences and uncertainties in predicting the confusion foreground as part of the Ultra-Compact Binaries catalog comparison project (Valli et al., 2023, as well as Breivik et al. and Bobrick et al. in prep.). I refer the reader to those forthcoming results and provide a comparison using our test simulation, in which all LISA binaries were generated solely via the isolated binary channel.

Eccentric systems

Here, I focus on eccentric systems originating from the triple formation channel. These systems were excluded from the analysis above as they are estimated to be very few (and therefore do not contribute to the overall Galactic confusion signal) and because their gravitational-wave signals differ from those of circular systems.

I find that approximately 3×10^{-6} of all Galactic double white dwarfs exhibit eccentric orbits. These systems result primarily from two reasons: (1) the ZLK effect excites the eccentricity of the inner binary orbit, or (2) the system becomes dynamically unstable and eventually achieves a stable configuration with high eccentricity.

In our simulations, all eccentric systems show high eccentricities ($e > 0.9$) and wide semi-major axis ($10^1 - 10^6$ au). For such orbital configurations, gravitational-wave emission predominantly occurs near pericenter passage, lasting up to a few hours and producing burst-like gravitational-wave signals. Since the orbital periods of these systems in our simulations are significantly longer than the mission duration (> 46 yr), the double white dwarf burst signals will not repeat within LISA's observation window of 4 yr.

The probability to observe a gravitational-wave burst from an individual system at periapsis is $\sim \mathrm{T_{obs}/T_{orb}}$, where $\mathrm{T_{obs}}$ is the observational time ($\sim 4\,\mathrm{yr}$). Assuming Poisson binomial distribution, I estimate that LISA will detect at most one eccentric double white dwarf during its operational duration. Following Xuan et al. (2024), I estimate the frequency and strain amplitude of such a burst signal as

$$f_{\rm burst} \sim \frac{2}{T_{\rm orb}(r_{\rm p})}, \tag{4.7}$$

$$\mathrm{h_{burst}} = \frac{2(G\mathcal{M})^{5/3}}{c^4 d}\left[\frac{2\pi}{T_{\rm orb}(r_{\rm p})}\right]^{2/3}, \tag{4.8}$$

where $r_{\rm p}$ is the periapsis distance. I find the (dimensionless) strain amplitudes of the gravitational-wave emitted during the periapsis are between $\sim 10^{-24}$ and 10^{-22}, i.e. below the noise curve (black stars in Figure 4.9). Therefore, such a signal would not be detectable by LISA.

4.4.2 Population properties

In this section, I describe the similarities and differences in the population properties of double white dwarfs formed from triple systems and binary systems. Figure 4.10 shows the distribution of population properties such as chirp mass, primary mass, eccentricity, and gravitational-wave frequency. The green color corresponds to the properties of double white dwarfs from triple systems while the purple color shows the properties of double white dwarfs from binary star systems. The shaded green and purple regions represent the properties of resolvable double white dwarfs from triple and binary star systems, respectively. The resolved double white dwarf population traces the features of the total double white dwarf population. It is also interesting to note that all double white dwarfs in our mock Milky Way with $f_{\rm gw} > 2\times10^{-3}$ are fully resolvable by LISA. Individually resolving any double white dwarf with $f_{\rm gw} < 2\times10^{-3}$ is more difficult for LISA due to the higher degree of overlap in this frequency range.

Triple systems produce about ~ 1.5 times more LISA double white dwarf systems with primary masses greater than $0.9\,\mathrm{M_\odot}$ and ~ 3.9 times more super-Chandrasekhar mass double white dwarfs (binary white dwarfs in which total mass of both the white dwarfs combined exceeds $1.44\,\mathrm{M_\odot}$) than the isolated binary channel. In addition, triple systems produce ~ 1.6 times more extremely low-mass white dwarfs ($m < 0.25\,\mathrm{M_\odot}$) that enter the LISA frequency bandwidth than isolated binaries. Isolated binaries do not produce binaries with a chirp mass greater than $0.9\,\mathrm{M_\odot}$. In contrast, triple systems produce $\sim 10^3$ binaries whose chirp mass is greater than $0.9\ \mathrm{M_\odot}$. There are two possible ways to form massive white dwarfs: 1) The system originates from a massive main-sequence progenitor that evolves to a massive white dwarf; 2) Two less massive progenitors merge to form a massive main-sequence progenitor that subsequently forms a massive white dwarf. In our simulations, initial massive main-sequence progenitors are rare. Hence, it is difficult to

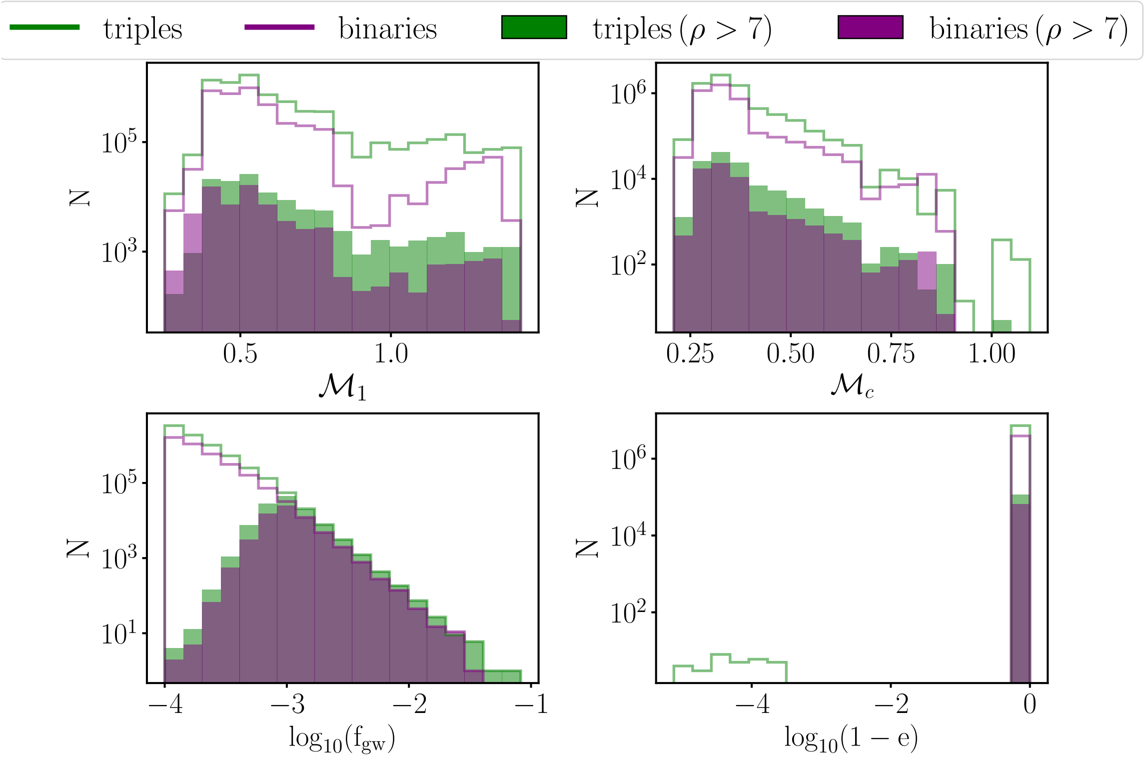

Figure 4.10: Population properties of LISA-detectable double white dwarfs from triple systems compared to isolated binaries. Overall, triple systems produce more massive white dwarfs than isolated binaries. For more details, see Section 4.4.2.

form massive white dwarfs in isolated binaries. However, in triple systems, the two less massive progenitors in the inner binary can merge to form a massive progenitor. The merged star co-evolves with the former tertiary component to form a double white dwarf with a massive component.

There is no significant difference in the frequency distribution of double white dwarf binaries formed from isolated binaries and triple systems. This is because most double white dwarfs emerge as short-period binaries after a common envelope phase, eventually emitting gravitational waves to enter the LISA band.

4.4.3 Different types of double white dwarfs

From the `MSE` single-star evolution model, Helium (He) white dwarfs originate from binary interactions where the progenitor loses its envelope before helium ignition, with typical masses of $\lesssim 0.45\,\mathrm{M}_\odot$. Carbon-Oxygen (CO) white dwarfs form from intermediate-mass stars that exhaust helium in their cores and expel their outer layers, resulting in masses between $\sim 0.45 - 1.1\,\mathrm{M}_\odot$. Oxygen-Neon (ONe) white dwarfs arise from more massive stars that undergo carbon burning before shedding their envelopes, with typical masses of

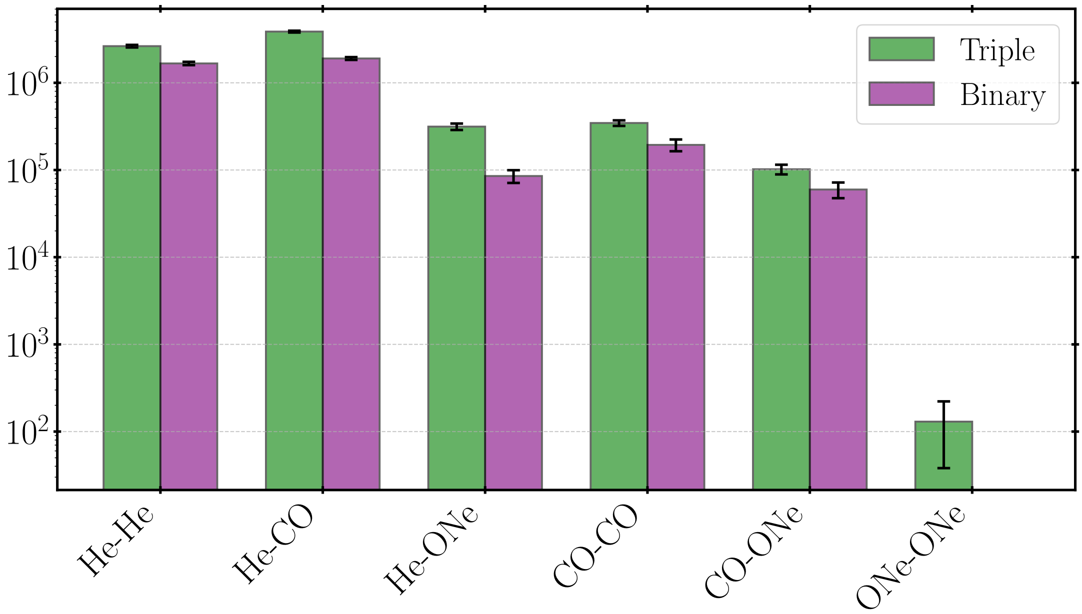

Figure 4.11: Types of LISA-detectable double white dwarfs formed from triple systems compared to isolated binaries. In our models, ONe-ONe double white dwarfs are produced exclusively in triple systems. Error bars represent the scaled-up fractional Poisson error from the intrinsic population evolved with MSE.

$\gtrsim 1.1\,\mathrm{M}_\odot$.

Figure 4.11 shows the relative numbers of different double white dwarf (core composition) types from binary and triple systems, respectively. Our simulations produce all types of double white dwarfs in the LISA frequency bandwidth from both triple and binary star systems, including He-He, He-CO, He-ONe, CO-CO, and CO-ONe systems. He-CO systems dominate the population of double white dwarfs originating from both triples and isolated binaries. Our simulations produce ONe-ONe systems only from the triple populations, but the sampling uncertainties in this mass range are too high to draw meaningful conclusions.

4.4.4 Detectability of the third star

I enfranchise again that approximately 57 % of all double white dwarfs detectable by LISA will have a bound tertiary companion. The bound tertiary star can be found in various evolutionary stages, including as a main-sequence star, a giant star, or a white dwarf. In the remaining 43 % of systems, the third star either became unbound or there was a merger of two stars, reducing the system from a triple to a binary (cf. Section 4.3.3). If the tertiary is retained, it can impart accelerations to the center of mass of the binary, leading to observable Doppler shifts in the gravitational-wave signals (e.g., Seto, 2008; Robson et al., 2018; Tamanini & Danielski, 2019).

In the context of LISA Galactic binaries in hierarchical triple systems, Robson et al. (2018) identifies three regimes, essentially governed by the ratio of the outer orbital period to the observation time: 1) When the outer period is much larger than the observation time the hierarchical orbit imparts an overall unobservable Doppler shift. 2) When the outer period is up to a factor ten larger than the observation time the influence of the companion can be detected. 3) When the outer period is shorter than or comparable to the observation time, the eccentricity and period of the hierarchical orbit can be inferred. Specifically, a tertiary companion leaves a detectable imprint in the gravitational-wave signal if the outer binary period satisfies:

$$T_2 \lesssim T_{\rm lim} = 43.2\,{\rm yr}\left(\frac{\rho}{10}\cdot\frac{m_3}{1.0M_\odot}\cdot\frac{f}{5\,{\rm mHz}}\right)^{3/4}\left(\frac{m_1+m_2}{2{\rm M}_\odot}\right)^{-1/2} \times\left(\frac{T_{\rm obs}}{4\,{\rm yr}}\right)^{3/8}\left(\frac{1+\frac{1}{2}e_2^2}{(1-e_2^2)^{5/2}}\right)^{3/8}, \tag{4.9}$$

where ρ is the signal-to-noise ratio of the binary.

In our simulations, in all systems that have retained the tertiary companion, the outer orbits are too wide to have any detectable effect within the resulting LISA gravitational-wave signal. Figure 4.12 compares the outer orbital period T_2 with the factor on the right hand side of the Eq. (4.9). The black line shows the limit where T_2 equals the factor on the right hand side. I find that none of our surviving triple systems lie within, or close to, the detectable limit. In addition, I find no systems where $T_{\rm orb} \leq T_{\rm obs}$ or $T_{\rm orb} \approx 10 \times T_{\rm obs}$. The minimum outer semi-major axis across all systems is found to be approximately 21 au, which corresponds to an orbital period of around 63 yr.

4.5 Discussion

I discuss our results in the context of previous works, present the uncertainties associated with our models, and describe the constraints imposed by electromagnetic observations.

4.5.1 Comparison to previous works

I calculated the number and population properties of LISA double white dwarfs that originated from triple systems (cf. Section 4.2). I also simulated LISA double white dwarfs from an isolated binary population (cf. Appendix C) to compare with triple populations. Our isolated binary simulation predicts $\approx 10^4$ individually resolvable double white dwarfs in the LISA frequency bandwidth, which agrees with previous works, including Nelemans et al. (2004); Ruiter et al. (2010); Yu & Jeffery (2010); Korol et al. (2017); Lamberts et al. (2019); Li et al. (2023); Thiele et al. (2023); Tang et al. (2024). In total, our models predict $\sim 1.1 \times 10^7$ double white dwarf sources that emit gravitational waves in the LISA frequency bandwidth but have too low ρ to be individually detected by LISA.

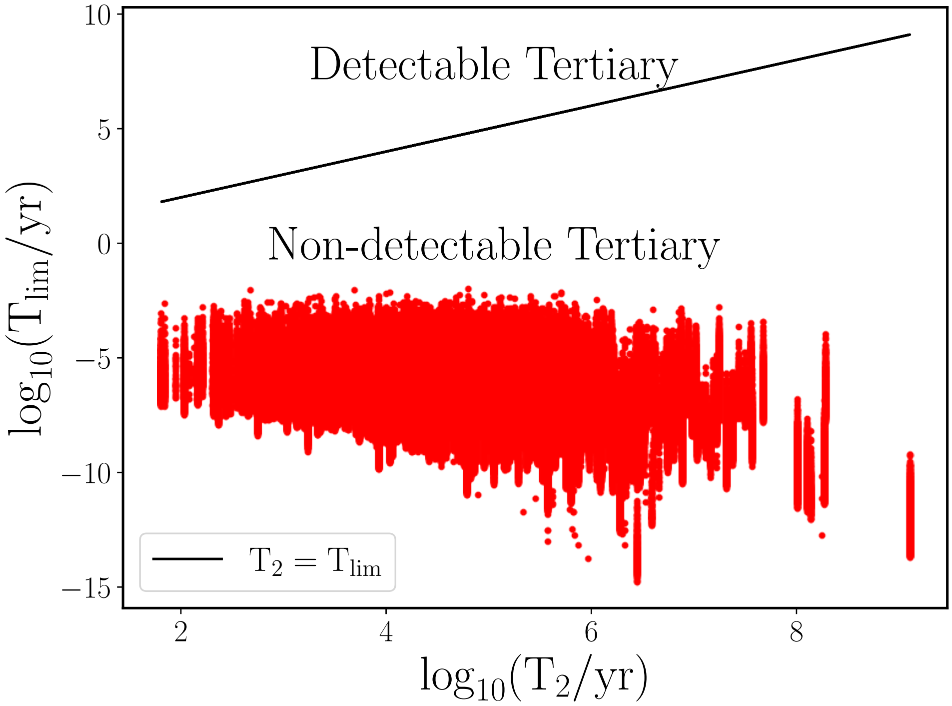

Figure 4.12: Comparison between the outer orbital period of a triple system and the factor on the right-hand side of Eq. (4.9). Red points represents $T_{\rm lim}$ vs outer orbital period T_2 for all the Galactic LISA double white dwarfs with a bound third star. The black line represents the points where $T_2 = T_{\rm lim}$. No tertiary star satisfies Eq. (4.9) for detectability within the LISA frequency bandwidth.

In particular, Korol et al. (2017) used the binary population model of Toonen et al. (2012) based on the `SeBa` binary population synthesis code (Portegies Zwart & Verbunt, 1996) and an analytic Galactic potential and star formation history to estimate the number of Galactic double white dwarfs. They predict $\sim 2.6 \times 10^7$ LISA double white dwarfs as foreground noise and $\sim 2.5 \times 10^4$ as individually resolvable LISA double dwarf sources. Korol et al. (2022) performed a data-driven analysis using existing observational double white dwarf data and also estimated a LISA double white dwarf population of $\sim 2.6 \times 10^7$ as foreground noise and $\sim 6.0 \times 10^4$ as individually resolvable LISA double dwarf sources. Using the `BSE` code (i.e. similar to our isolated binary evolution channel but with different underlying assumptions) combined with the `Fire` cosmological simulation, Lamberts et al. (2019) constructed the Galactic LISA double white dwarf population and estimated $\sim 6.2 \times 10^7$ double white dwarf sources as foreground noise and $\sim 1.2 \times 10^4$ as individually resolvable LISA double dwarf sources. Further, Li et al. (2023) also used the `BSE` code but with a mass transfer stability criterion by adopting critical mass ratios from the adiabatic mass loss model by Ge et al. (2010, 2015, 2020), and estimated a foreground LISA double white dwarf population size of $\sim 5.0 \times 10^7$ and about 4.0×10^4 individually resolvable double white dwarfs. Our results are broadly consistent with previous studies in terms of the number of resolved binaries, but I estimate comparatively fewer double white dwarf sources emitting gravitational waves in the LISA frequency band (see Section 4.4.1 for details). This discrepancy may arise from multiple factors, including the use of different population synthesis codes, varying assumptions underlying binary evolution, and different approaches to modeling the Galaxy. Most importantly, previous studies model isolated binary evolution only, ignoring triples.

When comparing our isolated binary evolution results (with triple fraction set to zero, see Table 4.1) to previous studies, several factors can contribute to differences in LISA predictions. For instance, assuming a different total stellar mass for the Milky Way would linearly scale our results (cf. Eq. 4.2). As shown by Keim et al. (2023), the underlying star formation history also plays a role (see also Yu & Jeffery, 2010). However, the most likely primary source of differences is the modeling of stellar and binary evolution. This was recently demonstrated by van Zeist et al. (2024), who investigated the gravitational-wave population of the Large and Small Magellanic Clouds as a case study using the `BPASS` (Eldridge et al., 2017) and `SeBa` codes. They specifically attributed variations in the predicted number of LISA double white dwarfs to differences in the treatment of CE evolution and the stability of mass transfer. Indeed, even studies using the same population synthesis code report significant differences in LISA predictions when these processes are modeled differently (e.g., Korol et al., 2017; Li et al., 2023). As mentioned before, quantifying the impact of all these factors on LISA predictions is a large collaborative effort within the LISA Consortium's Astrophysics Working Group. I refer the reader to those forthcoming results.

4.5.2 Uncertainties in our modelling

In our normalization calculations, I assume constant multiplicity fractions 0.2, 0.3, and 0.5 for stars in triple, binary, and single systems respectively. The multiplicity fractions play a crucial role in the mass normalization and, hence, the total number of LISA double dwarfs. All previous works assume a zero triple fraction. To compare our results with previous works, I have also calculated the number of LISA double dwarfs with a 0.5 binary fraction and zero triple fraction. I found $\sim 9 \times 10^6$ systems, showing consistency with previous studies in scale. For the same isolated binary population, assuming a 0.2 triple fraction, I only obtain $\sim 3.8 \times 10^6$ systems, half as many. This highlights the sensitivity of the results to the assumed multiplicity fraction.

I adopt the default critical mass-ratio criteria in `MSE` to model the stability of mass transfer. Studies investigating alternative stability criteria find that mass transfer tends to be more stable than I have assumed, suggesting that relatively fewer systems undergo a common envelope phase (Tauris et al., 2000; Podsiadlowski et al., 2002; Ge et al., 2010; Woods et al., 2011; Passy et al., 2012; Ge et al., 2015, 2020; Temmink et al., 2023). This affects the formation of double white dwarfs (Woods et al., 2012), particularly in the LISA band (Li et al., 2023; van Zeist et al., 2024). Additionally, I assume that the orbit circularizes following the common envelope phase. However, there is ongoing debate about

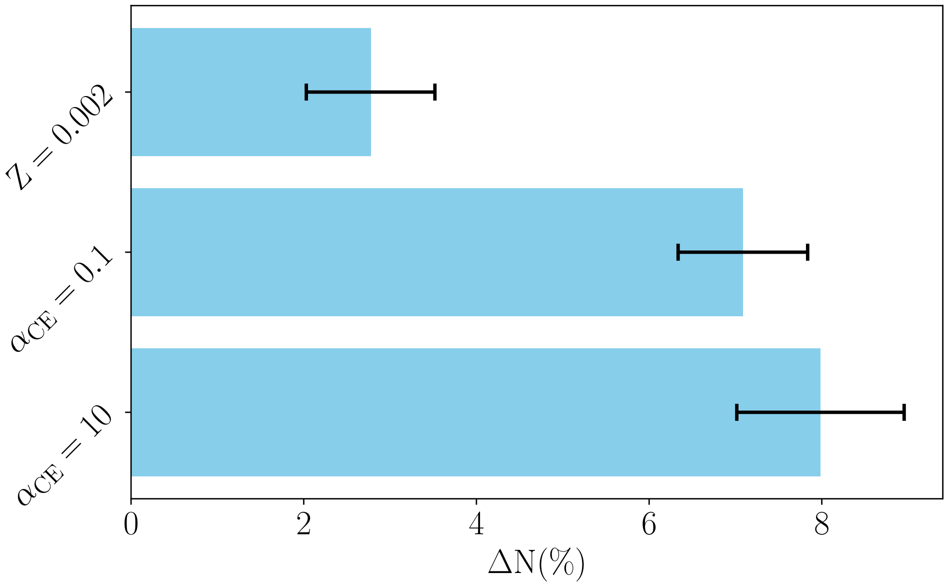

Figure 4.13: Fractional difference of LISA-detectable double white dwarfs from models with varying common envelope efficiency, α_{CE}, and sub-solar metallicity, relative to the default values ($\alpha_{\mathrm{CE}} = 1$, $Z = 0.02$). The number of double white dwarfs varies by up to 8 % when the common envelope parameters are modified. Error bars represent the scaled up fractional Poisson error from the intrinsic population evolved with MSE.

whether residual eccentricity may persist at the end of the common envelope evolution. The modeling of unstable mass transfer leading to a common envelope phase follows the approximate α-λ formalism. I investigated the effect of the common envelope efficiency parameter, α_{CE}, on our results. For lower ($\alpha_{\mathrm{CE}} = 0.1$) and higher efficiency parameters ($\alpha_{\mathrm{CE}} = 10$), our simulations yield approximately 7.5×10^6 and 7.6×10^6 LISA double white dwarfs, respectively. For a lower value of the common envelope efficiency, the common envelope phase is relatively more effective at shrinking the orbit. Consequently, these systems enter the LISA frequency bandwidth within a Hubble time. In contrast, for the default value ($\alpha_{\mathrm{CE}} = 1$), the common envelope phase results in a relatively wider orbital period. However, for a high common envelope efficiency parameter, there is an increase in the number of LISA-detectable double white dwarf binaries. This is because the more efficient common envelope phase is less likely to merge binaries that would otherwise have merged for $\alpha_{\mathrm{CE}} = 1$.

I assume that all progenitors of the Galactic LISA double white dwarfs are formed with solar metallicity. About $\sim 2\%$ of the star particles in the selected Milky Way model have subsolar metallicity. However, our Galaxy encompasses a larger range of metallicities. I also explore the impact of sub-solar metallicity by constructing the galaxy using the procedure described in Section 4.2.3 but with an initial metallicity of Z = 0.0002. It results in approximately $\sim 7.5 \times 10^6$ LISA double white dwarfs, an increase of $\sim 0.3 \times 10^6$ compared to those with solar metallicity. Stars with lower metallicity evolve relatively faster. For example, a $0.91\,\mathrm{M}_\odot$ star evolves into a white dwarf within a Hubble time at sub-solar metallicity, whereas it does not at solar metallicity. This increase in the number of low-mass stars that evolve into white dwarfs significantly contributes to the population of LISA-detectable double white dwarfs.

The ZLK effect induces eccentric oscillations in the inner binary, increasing the possibility of mass transfer at periapsis or eccentric mass transfer. The `MSE` model treats eccentric mass transfer using an approximate prescription. Furthermore, `MSE` also uses approximate prescriptions for mass transfer from the third star onto the inner binary. In our simulation, about 5.5 % of Galactic LISA double white dwarfs undergo a TCE phase before reaching the LISA frequency bandwidth. Inputs from hydrodynamical (Glanz & Perets, 2020) simulations of eccentric mass transfer and triple mass transfer are needed to improve the eccentric mass transfer and TCE prescriptions.

I highlight that simulations of triple systems are computationally expensive. I simulated 10^5 triple systems, producing $\sim 3 \times 10^3$ LISA double white dwarfs. Deriving from the mass function in Figure 4.1, there is a very low probability of producing high-mass white dwarfs. Hence, uncertainties in the statistics on the number of white dwarfs increase with mass. There is also a possibility of producing ONe white dwarfs from 8-10 $\mathrm{M}_\odot$ stars. Our models are created from progenitors in the mass range 1-8 $\mathrm{M}_\odot$. The sampling uncertainties in this mass range are too high to draw meaningful conclusions. In addition, I use random sampling to construct the initial triple population. However, more targeted sampling algorithms, such as `STROOPWAFEL` (Broekgaarden et al., 2019), could be employed to address the impact of sampling uncertainties in the initial population on rare events.

Finally, I note that `MSE` is a population synthesis code designed for statistical studies, and individual system modeling is not recommended. Due to variations in floating-point representation and rounding across different machines, the code may yield slightly different results when executed on different machines. However, these numerical difficulties average out on a large sample of the population. Given this inherent complexity, I limited the computational time to 10 hours per system. The majority of systems completed their evolution in under 2 hours. Within the ten-hour limit, 4 % of systems did not complete their evolution. Of these, around 0.4 % were dynamically unstable, while the remaining systems were undergoing stable secular evolution. Only 0.1 % of the systems did not complete their evolution within ten hours and had white dwarfs or both components massive enough to evolve into white dwarfs within a Hubble time. This 0.1 % of the systems contribute to some uncertainty in our predictions for LISA double white dwarfs, while the remaining incomplete systems were excluded without affecting the overall results.

4.5.3 Possibility of electromagnetic constraints to LISA observations

While millions of double white dwarfs will emit gravitational waves in the LISA frequency bandwidth, only a few hundred double white dwarfs are well-characterized in electromagnetic observations (e.g., Munday et al., 2023). Of these, 48 of the binaries will have a high

ρ ratio and will serve as verification binaries for the LISA mission (e.g., Stroeer & Vecchio, 2006; Kupfer et al., 2018, 2024; Finch et al., 2023). To date, it is unknown is any of these known LISA binaries are part of triple systems with wide tertiary companion.

LISA is set to be launched in 2035 (Colpi et al., 2024). However, some electromagnetic observations/surveys planned in the near future will already increase the sample of short-period double white dwarfs and offer better constraints for the modeling, data analysis, and detection techniques of LISA double white dwarfs. These include insights from Gaia's next data release (DR4), SDSS-V (Kollmeier et al., 2017), LAMOST (Zhao et al., 2012), ZTF (Bellm et al., 2019), 4MOST (de Jong et al., 2019), WEAVE (Dalton et al., 2012), the Asteroid Terrestrial-impact Last Alert System (Heinze et al., 2018; Tonry et al., 2018), the Gravitational-wave Optical Transient Observer (Steeghs et al., 2022), Euclid (Laureijs et al., 2011), the Nancy Roman Space Telescope (Akeson et al., 2019), and Vera Rubin-LSST (Collaboration et al., 2009). Similarly to the approach taken by Heintz et al. (2024), who used the age discrepancy from observational data to quantify the contribution of triple systems, applying comparable modeling techniques to forthcoming double white dwarf observations could provide further constraints on the contribution of triples to double white dwarfs in the LISA frequency bandwidth.

4.6 Conclusion

I estimated the Galactic LISA double white dwarfs from triple systems. I combined the triple population synthesis code `MSE` and the `TNG50` cosmological simulations to seed a Milky Way-like galaxy to obtain a population of LISA-detectable double white dwarfs. To compare our results with LISA double white dwarfs from isolated binaries, I also estimated the LISA double white dwarf population from isolated binaries using the same `MSE` code. The main conclusions are listed below:

1. Galactic LISA double white dwarfs have comparable contributions from both binary and triple channels. I estimate $\sim 7.2 \times 10^6$ and $\sim 3.8 \times 10^6$ LISA double white dwarfs from triple and binary star systems, respectively. Of these systems, $\sim 1.09 \times 10^4$ and $\sim 6.5 \times 10^3$ are individually resolvable double white dwarfs from triple and binary star systems, respectively. In addition, I find that the confusion foreground produced from our population (triples and isolated binaries) is below the instrument noise level.

2. I identify five different key processes that shape the evolutionary pathways of triple systems, leading to the formation of double white dwarfs that emit gravitational waves in the LISA frequency bandwidth.

    (a) Induced mass transfer: the gravitational perturbations from the third star triggers a mass transfer episode in the inner binary that leads to a shorter orbital period.

    (b) Outer binary channel: the inner binary merges to form a rejuvenated star that combines with the third star to enter the LISA frequency bandwidth.

   (c) Ejected tertiary: perturbations from the third star alter the inner binary configurations and are responsible for the short period of the inner binary, but the third star is later ejected before the inner binary enters the LISA frequency bandwidth.
   (d) Triple common envelope: Mass transfer from the tertiary star onto the inner binary that eventually brings the inner binary closer to short orbital periods.
   (e) Inner binary channel: A binary with a third star that is too distant to have any effect, enters the LISA frequency bandwidth due to effectively isolated binary interactions.

3. Our models show no major distinguishable differences in the population properties of systems originating from triples compared to those from isolated binaries.

4. Of the LISA double white dwarfs from triple systems, about $\sim 50\,\%$ of systems have a bound third star. However, the tertiary is typically too distant to have an observable imprint in the gravitational-wave signal of the inner binary.

5. Of the predicted LISA double white dwarfs from triple systems, I estimate that the majority of systems which enter the LISA frequency bandwidth have circular orbits, and only 3×10^{-6} (i.e. 31 systems in total in the Milky Way) of these systems have eccentric orbits. Meanwhile, in the estimated LISA double white dwarf population from isolated binary star systems, all systems have circular orbits. All the eccentric systems are found to have highly eccentric orbits ($e > 0.9$) and will emit gravitational bursts, with a typical periapsis period of a few hours. However, they are unlikely to be observable due to their small gravitational-wave strain amplitude.

6. In our Galactic LISA double white dwarf population, I observe all types of double white dwarfs, with those containing a He white dwarf and a CO white dwarf being the most common configuration.

Our study is the first to investigate the role of the triple evolution channel in the context of future LISA observations. I quantitatively assess the impact of including this channel on the number of observable LISA sources. While our results indicate no major distinguishable differences in the population properties of systems originating from triples compared to those formed through isolated binary evolution, they are particularly relevant for the future interpretation of LISA data on the Galactic population. Additionally, I show that the triple channel produces highly eccentric sources—although rare, these systems generate burst-like signals, in contrast to the predominantly monochromatic continuous signals emitted by the majority of the Galactic population. Thus, it is also important to consider these systems in the context of LISA data analysis.

Chapter 5

Summary and outlook

This thesis highlights the role of binary and triple-star dynamics in shaping the evolution and interactions of white dwarfs. Specifically, I investigated how these systems contribute to the thermonuclear explosion and their potential as sources of gravitational waves. In this final section, I provide a summary of the key findings of this study, reflect on their broader implications for white dwarf evolution, and suggest possible directions for future research in this area.

In Chapter 2, I conducted evolutionary population synthesis calculations to investigate the rates of SNe Ia in hierarchical triple systems. I identified five distinct formation channels: unbound tertiary, double merger, triple common envelope, eccentric collision, and dynamical instability. Our results indicate that head-on eccentric collisions of white dwarfs contribute only about 1% to the total SNe Ia, while the majority result from circular mergers driven by common envelope evolution.

I found that in about half of systems where a Type Ia supernova occurs in the inner binary, the third star remains bound. The mass distribution of the tertiary star peaks at $0.5\,\mathrm{M}_\odot$, and the outer orbital semimajor axis is broadly distributed around 10^3 au. The delay time distribution for both single and double degenerate SNe Ia was estimated, and the time-integrated SNe Ia rate from the triple evolution channel was found to slightly exceed that of the binary evolution channel, though this result is model-dependent.

Our study confirms that the combined contribution from the triple and binary channels accounts for approximately half of the observed SNe Ia rate, with triple systems surprisingly providing the largest contribution. However, a discrepancy remains between observed and theoretical rates, highlighting the need to explore additional SNe Ia progenitor scenarios. Our study outlines the prescriptions for progenitors in Section 2.2.1. Nevertheless, the progenitors of Type Ia supernovae remain largely uncertain. Unfortunately, there is no direct observational evidence for these progenitors, underscoring the need for further research to better understand the origins of these supernovae.

In Chapter 3, I simulated a grid of binary models consisting of a hot subdwarf and a white dwarf, evolving both components using MESA to track their binary evolution and stable mass transfer via Roche-lobe overflow. The orbital periods ranged from 36 minutes to 7.2 hours, covering both interacting and non-interacting systems. I identified several distinct mass transfer phases, including core helium burning, shell helium burning, and late thermal pulses. My models predict various evolutionary outcomes, such as double detonation supernovae, helium novae, and double white dwarfs, with donor stars reaching runaway velocities of up to $1000\,\mathrm{km,s^{-1}}$.

I found that systems with longer orbital periods are more likely to evolve into double white dwarfs. For our assumptions, the minimum helium shell mass required for detonation is about $0.05\,\mathrm{M_\odot}$. Additionally, double white dwarf systems that form from hot subdwarf + white dwarf binaries tend to have massive helium shells compared to those formed from single-star evolution, which could influence merger outcomes, including Type Ia supernovae. My grid of models aligns well with existing observations, providing a first-order estimate of possible outcomes for future hot subdwarf + white dwarf binary observations and serving as input for 3D merger simulations.

We presented the most up-to-date dense grid of binary parameter space that leads to He novae and double detonation supernovae. However, the criteria for distinguishing a nova from a double detonation supernova remain largely uncertain. While our stellar evolution and binary modeling remain unaffected by this criterion, a better understanding of the distinction is essential. Unfortunately, the observed parameter space is still very limited.

We identified five observed binaries with short orbital periods and sufficiently massive white dwarfs that fall within our parameter space. One crucial requirement for double detonation supernovae is a white dwarf massive enough to explode after accreting helium. However, these massive white dwarfs are faint and difficult to observe. In contrast, a sufficiently close and massive hot subdwarf is bright ($10 - 100\,\mathrm{L_\odot}$) and can be detected through its photometric brightness in the color-magnitude diagram. Furthermore, due to their short orbital periods, these systems exhibit ellipsoidal modulations caused by the tidal deformation of the hot subdwarf.

The number of observed binaries in this category is expected to increase with upcoming photometric and spectroscopic surveys. The results from these surveys will provide valuable insights that will help refine our understanding of the modeling and improve the accuracy of our predictions.

In Chapter 4, I estimated the Galactic LISA double white dwarf population originating from triple systems by combining the triple population synthesis code `MSE` with the `TNG50` cosmological simulations, comparing the results to the population from isolated binaries. This study is the first to explore the role of triple evolution in LISA double white dwarfs, revealing that both binary and triple channels contribute similarly to the overall population. I found approximately 7.2×10^6 LISA double white dwarfs from triple systems and 3.8×10^6 from binaries. Of these, around 1.09×10^4 and 6.5×10^3 systems are individually resolvable from triples and binaries, respectively, while the confusion foreground from both channels remains below the instrument's noise level.

I identified five key evolutionary pathways shaping the triple contribution to LISA double white dwarfs: induced mass transfer, the outer binary channel, ejected tertiary, triple common envelope, and the inner binary channel. The properties of systems from triples closely resemble those from binaries, with about 57% of triple-derived LISA double white dwarfs retaining a bound third star. However, the tertiary's impact on the gravitational-wave signal is typically negligible. Most LISA double white dwarfs from triple systems have circular orbits, with only a small fraction exhibiting high eccentricities that produce gravitational bursts.

While our results suggest that triple and binary channels contribute comparably to the galactic population of compact double white dwarfs, electromagnetic observations of double white dwarfs from triple systems remain scarce. LISA is scheduled for launch in 2035 (Colpi et al., 2024), but several upcoming electromagnetic surveys will expand the observed sample of short-period double white dwarfs, improving constraints on modeling, data analysis, and detection techniques. These include insights from Gaia's next data release (DR4), SDSS-V (Kollmeier et al., 2017), LAMOST (Zhao et al., 2012), ZTF (Bellm et al., 2019), 4MOST (de Jong et al., 2019), WEAVE (Dalton et al., 2012), the Asteroid Terrestrial-impact Last Alert System (Heinze et al., 2018; Tonry et al., 2018), the Gravitational-wave Optical Transient Observer (Steeghs et al., 2022), Euclid (Laureijs et al., 2011), the Nancy Roman Space Telescope (Akeson et al., 2019), and Vera Rubin-LSST (Collaboration et al., 2009). Modeling future observational data to estimate the contribution of triple systems will further refine our understanding of compact double white dwarfs.

Appendix A

Additional explanations for chapter 2

A.1 Mobile diagram

We use mobile diagrams to describe the different evolutionary stages of triple star evolution in MSE. The blue and orange boxes represent the inner and outer orbits of the triple system, respectively. Colors indicate the evolutionary stage following the stellar types defined in Hurley et al. (2000). The legend explains the colors of different stellar types, and the acronyms are described in Table A1. The red arrows pointing from one star to the other represent strong interactions such as stable mass transfer, unstable mass transfer, and collisions. The orange and red shaded regions around stars represent Roche lobe overflow and CE episodes, respectively. The star symbol in the final panel of every mobile diagram shows an SNe Ia explosion. Every SNe Ia explosion involves only two stars.

Table A1: Mobile diagram Acronyms

Acronym	Stellar type
low-mass MS	Main Sequence star ($M \lesssim 0.7$ M$_\odot$)
MS	Main Sequence star ($M \gtrsim 0.7$ M$_\odot$)
HG	Hertzsprung Gap
RGB	Red giant branch
CHeB	Core He burning
EAGB	Early Asymptotic giant branch
TPAGB	Thermally pulsating asymptotic giant branch
HeMS	He Main Sequence
HeHG	Helium Hertzsprung Gap
HeGB	Helium Giant Branch
HeWD	He WD
COWD	CO WD
ONeWD	ONe WD
NS	Neutron star
BH	Black hole

A.2 Contribution of different progenitors to Type Ia Supernovae

Table A2 shows the contribution rates of different progenitors to SNe Ia. The majority of the contribution comes from the double degenerate channel, with the dominant contributors being binaries containing a helium white dwarf and a carbon-oxygen white dwarf.

Table A2: Contribution of different progenitors to SNe Ia. The 'Binary' channel here refers to the inner binaries of the triple population, evolved without the tertiary star.

Models	Channel	DD $(10^{-4}\mathrm{M}_\odot{}^{-1})$	SD $(10^{-4}\mathrm{M}_\odot{}^{-1})$	SCM $(10^{-4}\mathrm{M}_\odot{}^{-1})$	CM $(10^{-4}\mathrm{M}_\odot{}^{-1})$	He+CO $(10^{-4}\mathrm{M}_\odot{}^{-1})$	CO+CO $(10^{-4}\mathrm{M}_\odot{}^{-1})$
Model 1	Triple	3.57 ± 0.04	0.025 ± 0.003	0.024 ± 0.004	0.0009 ± 0.0007	3.45 ± 0.04	0.122 ± 0.008
	Binary	2.88 ± 0.04	0.017 ± 0.003	0.017 ± 0.003	0.0001 ± 0.0002	2.86 ± 0.04	0.020 ± 0.003
Model 2	Triple	3.47 ± 0.04	0.031 ± 0.004	0.030 ± 0.004	0.0010 ± 0.0007	3.35 ± 0.04	0.114 ± 0.008
	Binary	2.88 ± 0.04	0.020 ± 0.003	0.020 ± 0.003	0.0001 ± 0.0003	2.86 ± 0.04	0.020 ± 0.003
Model 3	Triple	2.39 ± 0.07	0.013 ± 0.005	0.013 ± 0.005	0.0003 ± 0.0008	2.33 ± 0.071	0.054 ± 0.011
Model 4	Triple	0.90 ± 0.04	0.0	0.0	0.0	0.72 ± 0.04	0.183 ± 0.020
Model 5	Triple	3.69 ± 0.09	0.011 ± 0.005	0.010 ± 0.005	0.0003 ± 0.0008	3.59 ± 0.09	0.097 ± 0.014
Model 6	Triple	3.58 ± 0.09	0.017 ± 0.006	0.017 ± 0.006	0.0006 ± 0.0011	3.47 ± 0.09	0.114 ± 0.016

Appendix B

Interesting outliers

In this section, we present the figure explaining the evolution of properties of the two outlier systems described in section 3.4.3. Fig. B.1 shows the evolution of properties of the binary system, comprising a $0.7\,\mathrm{M}_{\odot}$ donor, a $0.7\,\mathrm{M}_{\odot}$ accretor, and an initial orbital period of ~ 1.3 hours. During evolution, the accretor undergoes two episodes of accretion to accumulate $\sim 0.18\,\mathrm{M}_{\odot}$ of He. Fore more information, see Sec. 3.4.3. Fig. B.2 shows the evolution of properties of a binary with initial donor mass of $0.7\,\mathrm{M}_{\odot}$, a $1.1\,\mathrm{M}_{\odot}$ accretor, and an initial orbital period of $\sim 1.7\,$hours. This system comes into contact during the later shell-burning phase of the donor and evolves into a double detonation supernova. For more details, see Sec. 3.4.3.

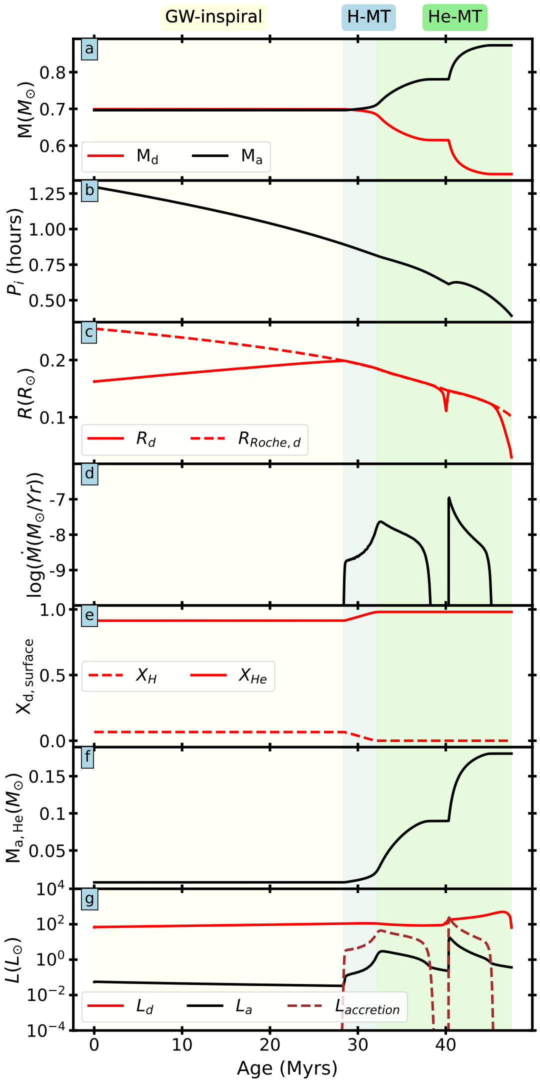

Figure B.1: WD undergoes accretion during core He burning and shell burning phases of the donor, eventually accumulating $0.18\,\mathrm{M}_\odot$ of He. The panels display the evolution of different parameters as in Fig. 3.2. The background colors yellow, blue, and green represent the gravitational-wave inspiral phase (GW-inspiral), H mass transfer phase (H-MT), and He mass transfer phase (He-MT), respectively. $0.7\,\mathrm{M}_\odot$ WD has accreted $\approx 0.18\,\mathrm{M}_\odot$ of material producing a $\approx 0.88\,\mathrm{M}_\odot$ WD. For more details, see Sec. 3.4.3. This WD has the most massive He shell in our models.

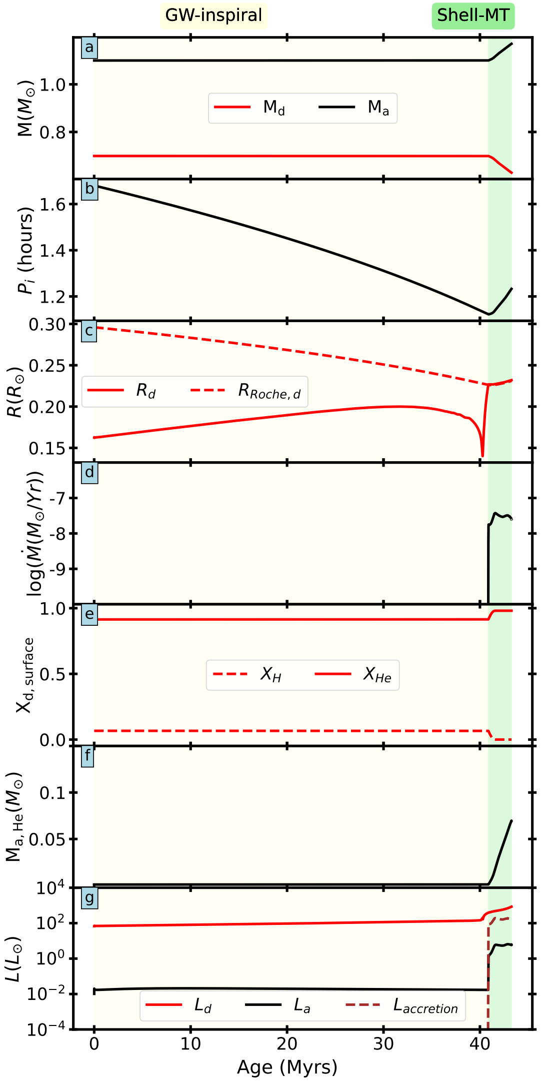

Figure B.2: An example of a system where a double detonation supernova occurs during the shell burning phase of the donor. The panels display the evolution of different parameters as in Fig. 3.2. The background colors yellow, and green represent the gravitational-wave inspiral phase (GW-inspiral), and mass transfer phase during the He shell burning phase (Shell-MT), respectively. The accretor accretes with a relatively higher accretion rate of $\sim 10^{-7}\,\mathrm{M}_\odot\,\mathrm{yr}^{-1}$, resulting in ignition in the He layers less dense than the assumed critical density for detonation ($< 10^6\,\mathrm{g\,cm^{-3}}$).

Appendix C

Galactic LISA double white dwarfs from isolated binaries

This section explains how we seed the double white dwarfs from isolated binary channels to a Milky Way-like galaxy. We do it in two steps.

In the first step, we construct a synthetic population of isolated zero-age-main-sequence binaries in the first step. The primary mass (m_1) is sampled from Kroupa's IMF (Kroupa, 2001). Following this, we sample the orbital period of these binaries following empirically derived functions from Moe & Di Stefano (2017). Using m_1 and T_1, we sample the initial mass ratio and eccentricities using functions from Moe & Di Stefano (2017). This mass ratio is then used to calculate m_2. For a fair comparison to the triple systems, all masses are restricted to be between $1 - 8\,\mathrm{M}_\odot$. Furthermore, we reject any systems that are Roche lobe filling (Eggleton, 1983). We note that this population inherently differs from the inner binaries of triple systems. The crucial, though not the only, distinction arises from the dynamical stability requirement in triples, which forces the inner binary to be more compact. As a result, the semi-major axis distribution of inner binaries in triples is significantly more compact compared to that of isolated binaries (Rajamuthukumar et al., 2023). We repeat the process described in Sec 4.2.3 to create a population of 10^5 isolated binaries. Based on Figure 4.1 we note that this isolated binary population looks distinctly different from the inner binary population of the triple systems. We evolve this synthetic population until Hubble time using `MSE` and select the double white dwarf that enters LISA frequency bandwidth.

In the second step, We use the same galaxy and a similar method as mentioned in Section 4.2.3 to seed the LISA double white dwarfs in the Galaxy. However, the total stellar mass in the simulated population is calculated after using an isolated binary population and is given by:

$$M_{\mathrm{tot,\ MSE}} = \frac{N_{b,\,\mathrm{in\,range}}}{f_{b,\,\mathrm{in\,range}} \cdot f_b} \cdot \left[f_t \cdot m_t + f_b \cdot m_b + (1 - f_t - f_b) \cdot m_s \right], \tag{C.1}$$

where $N_{b,\,\mathrm{in\,range}} = 10^5$ is the number of simulated isolated binary-star systems with `MSE`, $f_{b,\,\mathrm{in\,range}}$ is the fraction of binaries in this range relative to the full mass range, and $f_t = 0.2$, $f_b = 0.3$, and $1 - f_t - f_b = 0.5$ represent the fractions of triples, binaries, and singles in the full stellar population; $m_t = 3.5\,\mathrm{M}_\odot$, $m_b = 0.9\,\mathrm{M}_\odot$, and $m_s = 0.5\,\mathrm{M}_\odot$ denote the average masses of triple, binary, and single systems, respectively. This gives an estimate of about $\sim 3.8 \times 10^6$ LISA double white dwarfs.

To assess the impact of the triple fraction on normalization, we repeat the same procedure with zero triple fraction ($f_t = 0$). Under this assumption, the estimated number of Galactic LISA double white dwarfs originating from isolated binaries is approximately $\sim 9 \times 10^6$. All these results are presented in Table 4.1.

Glossary of abbreviations

BH	Black Hole
CO WD	Carbon-Oxygen White Dwarf
CE/CEE	Common Envelope (Evolution)
CHeB	Core-Helium Burning
EAB	Early Asymptotic Giant Branch
GW	Gravitational Wave
He	Helium
He GB	(Naked) Helium star Giant Branch
He MS	(Naked) Helium star Main-Sequence
He WD	Helium White Dwarf
HeHG	(Naked) Helium star Hertzprung Gap
HG	Hertzprung Gap
LISA	Laser Interferometer Space Antenna
MS	Main-Sequence
NS	Neutron Star
PN	Post-Newtonian
RGB	Red Giant Branch
RLOF	Roche-Lobe Overflow
SBH	Stellar(-mass) Black Hole
SNe Ia	Type Ia Supernova
SN	Supernova
TCE	Triple Common Envelope
TPAGB	Thermally Pulsing Asymptotic Giant Branch
`BSE`	Binary Star Evolution (code)
`MSE`	Multiple Stellar Evolution (code)
`SSE`	Single Star Evolution (code)
`TNG50`	The Next Generation 50 Mpc Simulation
ZLK/LK	(von Zeipel)-Lidov-Kozai
ZAMS	Zero-Age Main-Sequence

Table C.1: Table of abbreviations used in this thesis.

Bibliography

Akeson R., et al., 2019, arXiv e-prints

Amaro-Seoane P., et al., 2017, arXiv e-prints, p. arXiv:1702.00786

Amaro-Seoane P., et al., 2023, Living Reviews in Relativity, 26, 2

Antognini J. M., Shappee B. J., Thompson T. A., Amaro-Seoane P., 2014, MNRAS, 439, 1079

Antonini F., Murray N., Mikkola S., 2014, ApJ, 781, 45

Antonini F., Toonen S., Hamers A. S., 2017, ApJ, 841, 77

Bauer E. B., Kupfer T., 2021, ApJ, 922, 245

Bauer E. B., Schwab J., Bildsten L., 2017, ApJ, 845, 97

Bauer E. B., Chandra V., Shen K. J., Hermes J. J., 2021, ApJ, 923, L34

Bellm E. C., et al., 2019, PASP, 131, 018002

Blaes O., Lee M. H., Socrates A., 2002, ApJ, 578, 775

Bland-Hawthorn J., Gerhard O., 2016, ARA&A, 54, 529

Bloecker T., 1995, A&A, 299, 755

Bloemen S., et al., 2016, in Hall H. J., Gilmozzi R., Marshall H. K., eds, Society of Photo-Optical Instrumentation Engineers (SPIE) Conference Series Vol. 9906, Ground-based and Airborne Telescopes VI. p. 990664, doi:10.1117/12.2232522

Bode M. F., Evans A., 2008, Classical Novae (2nd Edition). Cambridge University Press, `https://www.cambridge.org/us/universitypress/subjects/physics/astrophysics/classical-novae-2nd-edition?format=HB&isbn=9780521843300`

Böhm-Vitense E., 1958, Z. Astrophys., 46, 108

Boos S. J., Townsley D. M., Shen K. J., Caldwell S., Miles B. J., 2021, ApJ, 919, 126

Braudo J., Soker N., 2024, The Open Journal of Astrophysics, 7, 7

Broekgaarden F. S., et al., 2019, Monthly Notices of the Royal Astronomical Society, 490, 5228–5248

Brooks J., Bildsten L., Marchant P., Paxton B., 2015, ApJ, 807, 74

Brooks J., Bildsten L., Schwab J., Paxton B., 2016, ApJ, 821, 28

Brown W. R., Anderson J., Gnedin O. Y., Bond H. E., Geller M. J., Kenyon S. J., 2015, ApJ, 804, 49

Burdge K. B., et al., 2024, Nature, 635, 316

Claeys J. S. W., Pols O. R., Izzard R. G., Vink J., Verbunt F. W. M., 2014, A&A, 563, A83

Collaboration L. S., et al., 2009, arXiv e-prints

Collins C. E., Gronow S., Sim S. A., Röpke F. K., 2022, MNRAS, 517, 5289

Colpi M., et al., 2024, arXiv e-prints, p. arXiv:2402.07571

Comerford T. A. F., Izzard R. G., 2020, MNRAS, 498, 2957

Cornish N. J., Littenberg T. B., 2007, Physical Review D, 76

Crowder J., Cornish N. J., 2007, Phys. Rev. D, 75, 043008

Dalton G., et al., 2012, in McLean I. S., Ramsay S. K., Takami H., eds, Society of Photo-Optical Instrumentation Engineers (SPIE) Conference Series Vol. 8446, Ground-based and Airborne Instrumentation for Astronomy IV. p. 84460P, doi:10.1117/12.925950

Danielski C., Korol V., Tamanini N., Rossi E. M., 2019, A&A, 632, A113

Dawson H., et al., 2024, A&A, 686, A25

De K., et al., 2019, ApJ, 873, L18

Deng S., Babak S., Jeune M. L., Marsat S., Éric Plagnol Sartirana A., 2025, Modular global-fit pipeline for LISA data analysis (`arXiv:2501.10277`), `https://arxiv.org/abs/2501.10277`

Deshmukh K., Bauer E. B., Kupfer T., Dorsch M., 2024, MNRAS, 527, 2072

Dong S., Katz B., Kushnir D., Prieto J. L., 2015, MNRAS, 454, L61

Eggleton P. P., 1983, ApJ, 268, 368

Eggleton P. P., Kiseleva-Eggleton L., 2001a, ApJ, 562, 1012

Eggleton P. P., Kiseleva-Eggleton L., 2001b, The Astrophysical Journal, 562, 1012

Eggleton P. P., Kisseleva-Eggleton L., 2006, Ap&SS, 304, 75

Eggleton P. P., Tokovinin A. A., 2008, MNRAS, 389, 869

Eggleton P. P., Kiseleva L. G., Hut P., 1998, ApJ, 499, 853

Eldridge J. J., Stanway E. R., Xiao L., McClelland L. A. S., Taylor G., Ng M., Greis S. M. L., Bray J. C., 2017, Publ. Astron. Soc. Australia, 34, e058

Ergma E., Fedorova A. V., Yungelson L. R., 2001, A&A, 376, L9

Fabrycky D., Tremaine S., 2007, ApJ, 669, 1298

Finch E., et al., 2023, MNRAS, 522, 5358

Fink M., Hillebrandt W., Röpke F. K., 2007, A&A, 476, 1133

Fink M., Röpke F. K., Hillebrandt W., Seitenzahl I. R., Sim S. A., Kromer M., 2010, A&A, 514, A53

Fuller J., Lai D., 2014, MNRAS, 444, 3488

Gaia Collaboration et al., 2016, A&A, 595, A1

Gaia Collaboration et al., 2018, A&A, 616, A1

Ge H., Hjellming M. S., Webbink R. F., Chen X., Han Z., 2010, The Astrophysical Journal, 717, 724

Ge H., Webbink R. F., Chen X., Han Z., 2015, The Astrophysical Journal, 812, 40

Ge H., Webbink R. F., Chen X., Han Z., 2020, The Astrophysical Journal, 899, 132

Geier S., Nesslinger S., Heber U., Przybilla N., Napiwotzki R., Kudritzki R. P., 2007, A&A, 464, 299

Geier S., et al., 2013, A&A, 554, A54

Geier S., et al., 2015, Science, 347, 1126

Gianninas A., Bergeron P., Dupuis J., Ruiz M. T., 2010, ApJ, 720, 581

Glanz H., Perets H. B., 2020, Monthly Notices of the Royal Astronomical Society, 500, 1921

Glanz H., Perets H. B., 2021, MNRAS, 500, 1921

Götberg Y., Korol V., Lamberts A., Kupfer T., Breivik K., Ludwig B., Drout M. R., 2020, ApJ, 904, 56

Grishin E., Perets H. B., 2022, MNRAS, 512, 4993

Gronow S., Collins C. E., Sim S. A., Röpke F. K., 2021, A&A, 649, A155

Hachisu I., Kato M., 2001, ApJ, 558, 323

Hallakoun N., Maoz D., 2019, MNRAS, 490, 657

Hamers A. S., 2018, MNRAS, 476, 4139

Hamers A. S., 2020, MNRAS, 494, 5492

Hamers A. S., Dosopoulou F., 2019, ApJ, 872, 119

Hamers A. S., Portegies Zwart S. F., 2016, MNRAS, 459, 2827

Hamers A. S., Thompson T. A., 2019, ApJ, 882, 24

Hamers A. S., Pols O. R., Claeys J. S. W., Nelemans G., 2013, MNRAS, 430, 2262

Hamers A. S., Rantala A., Neunteufel P., Preece H., Vynatheya P., 2021, MNRAS, 502, 4479

Hamers A. S., Glanz H., Neunteufel P., 2022, ApJS, 259, 25

Han Z., Podsiadlowski P., Maxted P. F. L., Marsh T. R., Ivanova N., 2002, MNRAS, 336, 449

Han Z., Podsiadlowski P., Maxted P. F. L., Marsh T. R., 2003, MNRAS, 341, 669

Hansen C. J., Kawaler S. D., Trimble V., 2004, Stellar Interiors: Physical Principles, Structure, and Evolution, 2nd edn. Springer-Verlag, New York

Heber U., 1986, A&A, 155, 33

Heber U., 2016, PASP, 128, 082001

Heber U., Edelmann H., Lisker T., Napiwotzki R., 2003, A&A, 411, L477

Heintz T. M., Hermes J. J., Tremblay P. E., Ould Rouis L. B., Reding J. S., Kaiser B. C., van Saders J. L., 2024, ApJ, 969, 68

Heinze A. N., et al., 2018, AJ, 156, 241

Hirsch H. A., Heber U., O'Toole S. J., Bresolin F., 2005, A&A, 444, L61

Hjellming M. S., Webbink R. F., 1987, ApJ, 318, 794

Hoyle F., Fowler W. A., 1960, ApJ, 132, 565

Hurley J. R., Pols O. R., Tout C. A., 2000, MNRAS, 315, 543

Hurley J. R., Tout C. A., Pols O. R., 2002, MNRAS, 329, 897

Hut P., 1981, A&A, 99, 126

Iben Jr. I., Livio M., 1993, PASP, 105, 1373

Iben I. J., Tutukov A. V., 1984, ApJS, 54, 335

Ivanova N., et al., 2013, A&ARv, 21, 59

Jermyn A. S., et al., 2023, ApJS, 265, 15

Jiang Y.-F., Tremaine S., 2010, MNRAS, 401, 977

Justham S., Wolf C., Podsiadlowski P., Han Z., 2009, A&A, 493, 1081

Kang Y., Liu C., Shao L., 2021, AJ, 162, 247

Karnesis N., Babak S., Pieroni M., Cornish N., Littenberg T., 2021, Phys. Rev. D, 104, 043019

Kato M., Hachisu I., 2004, ApJ, 613, L129

Kato T., Kanatsu K., Takamizawa K., Takao A., Stubbings R., 2000, IAU Circ., 7552, 1

Katz B., Dong S., 2012, arXiv e-prints, p. arXiv:1211.4584

Katz B., Dong S., Malhotra R., 2011, Phys. Rev. Lett., 107, 181101

Katz M. L., Danielski C., Karnesis N., Korol V., Tamanini N., Cornish N. J., Littenberg T. B., 2022, MNRAS, 517, 697

Katz M. L., Karnesis N., Korsakova N., Gair J. R., Stergioulas N., 2024, An efficient GPU-accelerated multi-source global fit pipeline for LISA data analysis (`arXiv:2405.04690`), `https://arxiv.org/abs/2405.04690`

Keim M. A., Korol V., Rossi E. M., 2023, MNRAS, 521, 1088

Kervella P., Thévenin F., Lovis C., 2017, A&A, 598, L7

Kiseleva L. G., Eggleton P. P., Mikkola S., 1998a, MNRAS, 300, 292

Kiseleva L. G., Eggleton P. P., Mikkola S., 1998b, Monthly Notices of the Royal Astronomical Society, 300, 292

Kolb U., Ritter H., 1990, A&A, 236, 385

Kollmeier J. A., et al., 2017, arXiv e-prints, p. arXiv:1711.03234

Korol V., Rossi E. M., Groot P. J., Nelemans G., Toonen S., Brown A. G. A., 2017, MNRAS, 470, 1894

Korol V., Hallakoun N., Toonen S., Karnesis N., 2022, MNRAS, 511, 5936

Korol V., Buscicchio R., Pakmor R., Morán-Fraile J., Moore C. J., de Mink S. E., 2024, A&A, 691, A44

Kozai Y., 1962, AJ, 67, 591

Kromer M., Sim S. A., Fink M., Röpke F. K., Seitenzahl I. R., Hillebrandt W., 2010, ApJ, 719, 1067

Kroupa P., 2001, MNRAS, 322, 231

Krtička J., Kubát J., Krtičková I., 2016, A&A, 593, A101

Kuhfuss R., 1986, A&A, 160, 116

Kupfer T., et al., 2018, MNRAS, 480, 302

Kupfer T., et al., 2020a, ApJ, 891, 45

Kupfer T., et al., 2020b, ApJ, 898, L25

Kupfer T., et al., 2022, ApJ, 925, L12

Kupfer T., et al., 2024, ApJ, 963, 100

LISA Consortium Waveform Working Group et al., 2023, arXiv e-prints, p. arXiv:2311.01300

LISA Science Study Team 2018, Technical Report ESA-L3-EST-SCI-RS-001, LISA Science Requirements Document, `www.cosmos.esa.int/web/lisa/lisa-documents/`. ESA, `www.cosmos.esa.int/web/lisa/lisa-documents/`

Lamberts A., Blunt S., Littenberg T. B., Garrison-Kimmel S., Kupfer T., Sanderson R. E., 2019, MNRAS, 490, 5888

Langer N., 1991, A&A, 252, 669

Laureijs R., Amiaux J., Arduini S., et al., 2011, arXiv e-prints

Li Z., Chen X., Ge H., Chen H.-L., Han Z., 2023, A&A, 669, A82

Lidov M. L., 1962, Planet. Space Sci., 9, 719

Lillo-Box J., et al., 2021, A&A, 653, A40

Littenberg T. B., Cornish N. J., 2023, Physical Review D, 107

Liu Z.-W., Röpke F. K., Han Z., 2023, Research in Astronomy and Astrophysics, 23, 082001

Livio M., Mazzali P., 2018, Phys. Rep., 736, 1

Livio M., Soker N., 1988, ApJ, 329, 764

Livne E., 1990, ApJ, 354, L53

Livne E., Glasner A. S., 1990, ApJ, 361, 244

Livne E., Glasner A. S., 1991, ApJ, 370, 272

Luo L., Katz B., Dong S., 2016, MNRAS, 458, 3060

Maoz D., Graur O., 2017, ApJ, 848, 25

Maoz D., Mannucci F., Brandt T. D., 2012, MNRAS, 426, 3282

Maoz D., Mannucci F., Nelemans G., 2014, ARA&A, 52, 107

Maoz D., Hallakoun N., Badenes C., 2018, MNRAS, 476, 2584

Mardling R. A., Aarseth S. J., 2001, MNRAS, 321, 398

Maxted P. F. L., Marsh T. R., 1999, MNRAS, 307, 122

Maxted P. F. L., Marsh T. R., Moran C. K. J., Han Z., 2000a, Monthly Notices of the Royal Astronomical Society, 314, 334

Maxted P. F. L., Marsh T. R., North R. C., 2000b, MNRAS, 317, L41

Mazeh T., Shaham J., 1979, A&A, 77, 145

Michaely E., 2021, MNRAS, 500, 5543

Michaely E., Perets H. B., 2014, ApJ, 794, 122

Moe M., Di Stefano R., 2017, ApJS, 230, 15

Munday J., et al., 2023, MNRAS, 518, 5123

Naoz S., 2016, ARA&A, 54, 441

Napiwotzki R., Karl C. A., Lisker T., Heber U., Christlieb N., Reimers D., Nelemans G., Homeier D., 2004, Ap&SS, 291, 321

Napiwotzki R., et al., 2020, A&A, 638, A131

Nelemans G., 2010, Ap&SS, 329, 25

Nelemans G., Yungelson L. R., Portegies Zwart S. F., 2004, MNRAS, 349, 181

Nelson D., et al., 2019, MNRAS, 490, 3234

Neunteufel P., 2020, A&A, 641, A52

Neunteufel P., Yoon S. C., Langer N., 2016, A&A, 589, A43

Neunteufel P., Yoon S. C., Langer N., 2017, A&A, 602, A55

Neunteufel P., Yoon S. C., Langer N., 2019, A&A, 627, A14

Neunteufel P., Preece H., Kruckow M., Geier S., Hamers A. S., Justham S., Podsiadlowski P., 2022, A&A, 663, A91

Nissanke S., Vallisneri M., Nelemans G., Prince T. A., 2012, ApJ, 758, 131

Nomoto K., 1980, Space Sci. Rev., 27, 563

Nomoto K., 1982a, ApJ, 253, 798

Nomoto K., 1982b, ApJ, 257, 780

Offner S. S. R., Moe M., Kratter K. M., Sadavoy S. I., Jensen E. L. N., Tobin J. J., 2023, in Inutsuka S., Aikawa Y., Muto T., Tomida K., Tamura M., eds, Astronomical Society of the Pacific Conference Series Vol. 534, Protostars and Planets VII. p. 275 (`arXiv:2203.10066`), doi:10.48550/arXiv.2203.10066

Ostrowski J., Baran A. S., Sanjayan S., Sahoo S. K., 2021, MNRAS, 503, 4646

Paczyński B., 1971, Acta Astron., 21, 1

Paczynski B., 1976, in Eggleton P., Mitton S., Whelan J., eds, IAU Symposium Vol. 73, Structure and Evolution of Close Binary Systems. p. 75

Pagel B. E. J., 1997, Nucleosynthesis and Chemical Evolution of Galaxies

Pakmor R., Kromer M., Röpke F. K., Sim S. A., Ruiter A. J., Hillebrandt W., 2010, Nature, 463, 61

Pakmor R., Kromer M., Taubenberger S., Springel V., 2013, ApJ, 770, L8

Pakmor R., Zenati Y., Perets H. B., Toonen S., 2021, MNRAS, 503, 4734

Pakmor R., Seitenzahl I. R., Ruiter A. J., Sim S. A., Röpke F. K., Taubenberger S., Bieri R., Blondin S., 2024, A&A, 686, A227

Passy J.-C., Herwig F., Paxton B., 2012, The Astrophysical Journal, 760, 90

Paxton B., Bildsten L., Dotter A., Herwig F., Lesaffre P., Timmes F., 2011, ApJS, 192, 3

Paxton B., et al., 2013, ApJS, 208, 4

Paxton B., et al., 2015, ApJS, 220, 15

Paxton B., et al., 2018, ApJS, 234, 34

Paxton B., et al., 2019, ApJS, 243, 10

Pelisoli I., Vos J., Geier S., Schaffenroth V., Baran A. S., 2020, A&A, 642, A180

Pelisoli I., et al., 2021, Nature Astronomy, 5, 1052

Perets H. B., Kratter K. M., 2012, ApJ, 760, 99

Perpinyà-Vallès M., Rebassa-Mansergas A., Gänsicke B. T., Toonen S., Hermes J. J., Gentile Fusillo N. P., Tremblay P. E., 2019, MNRAS, 483, 901

Peters P. C., 1964, Physical Review, 136, 1224

Piersanti L., Tornambé A., Yungelson L. R., 2014, MNRAS, 445, 3239

Piersanti L., Yungelson L. R., Bravo E., 2024, arXiv e-prints, p. arXiv:2405.17896

Pillepich A., et al., 2019, MNRAS, 490, 3196

Podsiadlowski P., Rappaport S., Pfahl E. D., 2002, The Astrophysical Journal, 565, 1107

Polin A., Nugent P., Kasen D., 2019, ApJ, 873, 84

Pols O. R., Schröder K.-P., Hurley J. R., Tout C. A., Eggleton P. P., 1998, MNRAS, 298, 525

Portegies Zwart S. F., Verbunt F., 1996, A&A, 309, 179

Postnov K. A., Yungelson L. R., 2014, Living Reviews in Relativity, 17, 3

Raghavan D., et al., 2010, ApJS, 190, 1

Rajamuthukumar A. S., Hamers A. S., Neunteufel P., Pakmor R., de Mink S. E., 2023, ApJ, 950, 9

Ransom S. M., et al., 2014, Nature, 505, 520

Rantala A., Pihajoki P., Mannerkoski M., Johansson P. H., Naab T., 2020, MNRAS, 492, 4131

Rebassa-Mansergas A., Xu S., Raddi R., Pala A. F., Solano E., Torres S., Jiménez-Esteban F., Cruz P., 2022, ApJ, 927, L31

Reimers D., 1975, Memoires of the Societe Royale des Sciences de Liege, 8, 369

Ritter H., 1988, A&A, 202, 93

Robson T., Cornish N. J., Tamanini N., Toonen S., 2018, Phys. Rev. D, 98, 064012

Ruiter A. J., 2020, IAU Symposium, 357, 1

Ruiter A. J., Belczynski K., Benacquista M., Larson S. L., Williams G., 2010, ApJ, 717, 1006

Ruiter A. J., Belczynski K., Sim S. A., Hillebrandt W., Fryer C. L., Fink M., Kromer M., 2011, MNRAS, 417, 408

Schaffenroth V., Pelisoli I., Barlow B. N., Geier S., Kupfer T., 2022, A&A, 666, A182

Seto N., 2008, ApJ, 677, L55

Shappee B. J., Thompson T. A., 2013, ApJ, 766, 64

Shariat C., Naoz S., El-Badry K., Rodriguez A. C., Hansen B. M. S., Angelo I., Stephan A. P., 2024, arXiv e-prints, p. arXiv:2407.06257

Shen K. J., Boos S. J., Townsley D. M., Kasen D., 2021, ApJ, 922, 68

Sim S. A., Röpke F. K., Hillebrandt W., Kromer M., Pakmor R., Fink M., Ruiter A. J., Seitenzahl I. R., 2010, ApJ, 714, L52

Sim S. A., Fink M., Kromer M., Röpke F. K., Ruiter A. J., Hillebrandt W., 2012, MNRAS, 420, 3003

Solheim J. E., 2010, PASP, 122, 1133

Steeghs D., et al., 2022, MNRAS, 511, 2405

Stegmann J., Antonini F., Schneider F. R. N., Tiwari V., Chattopadhyay D., 2022a, Phys. Rev. D, 106, 023014

Stegmann J., Antonini F., Moe M., 2022b, MNRAS, 516, 1406

Stegmann J., et al., 2024, Astrophys. J. Lett., 972, L19

Stroeer A., Vecchio A., 2006, Classical and Quantum Gravity, 23, S809

Sullivan M., et al., 2006, ApJ, 648, 868

Taam R. E., 1980a, ApJ, 237, 142

Taam R. E., 1980b, ApJ, 242, 749

Tamanini N., Danielski C., 2019, Nature Astronomy, 3, 858

Tang P., Eldridge J., Meyer R., Lamberts A., Boileau G., van Zeist W., 2024, arXiv e-prints, p. arXiv:2405.20484

Tauris T. M., den Heuvel E. P. J. v., Savonije G. J., 2000, Astrophys. J. Lett., 530, L93

Temmink K. D., Pols O. R., Justham S., Istrate A. G., Toonen S., 2023, Astronomy and; Astrophysics, 669, A45

Thiele S., Breivik K., Sanderson R. E., Luger R., 2023, ApJ, 945, 162

Thompson T. A., 2011, ApJ, 741, 82

Timpano S. E., Rubbo L. J., Cornish N. J., 2006, Phys. Rev. D, 73, 122001

Tokovinin A., 2008, MNRAS, 389, 925

Tokovinin A., 2014, AJ, 147, 87

Tokovinin A., 2016, ApJ, 831, 151

Tokovinin A., 2018, ApJS, 235, 6

Tonry J. L., et al., 2018, PASP, 130, 064505

Toonen S., Nelemans G., Portegies Zwart S., 2012, A&A, 546, A70

Toonen S., Claeys J. S. W., Mennekens N., Ruiter A. J., 2014, A&A, 562, A14

Toonen S., Perets H. B., Hamers A. S., 2018, A&A, 610, A22

Toonen S., Portegies Zwart S., Hamers A. S., Bandopadhyay D., 2020, A&A, 640, A16

Tout C. A., Pols O. R., Eggleton P. P., Han Z., 1996, MNRAS, 281, 257

Townsley D. M., Bildsten L., 2004, ApJ, 600, 390

Townsley D. M., Miles B. J., Shen K. J., Kasen D., 2019, ApJ, 878, L38

Triaud A. H. M. J., et al., 2020, Nature Astronomy, 4, 650

Udalski A., Szymański M. K., Szymański G., 2015, Acta Astron., 65, 1

Usher P. D., Mattson D., Warnock A. I., 1982, ApJS, 48, 51

Valli R., Graziani L., the LISA Synthetic UCB Catalogue Group 2023, arXiv e-prints, p. arXiv:2311.03431

Vennes S., Kawka A., O'Toole S. J., Németh P., Burton D., 2012, ApJ, 759, L25

Vynatheya P., Hamers A. S., Mardling R. A., Bellinger E. P., 2022, MNRAS, 516, 4146

Wang B., Han Z., 2009, A&A, 508, L27

Wang B., Han Z., 2012, New Astron. Rev., 56, 122

Wang B., Meng X., Chen X., Han Z., 2009, MNRAS, 395, 847

Wang B., Justham S., Han Z., 2013, A&A, 559, A94

Warner B., 1995, Cataclysmic Variables and Related Objects. Cambridge University Press

Webbink R. F., 1984, ApJ, 277, 355

Wen L., 2003, ApJ, 598, 419

Whelan J., Iben Icko J., 1973, ApJ, 186, 1007

Wilhelm M. J. C., Korol V., Rossi E. M., D'Onghia E., 2021, MNRAS, 500, 4958

Woods T. E., Ivanova N., van der Sluys M. V., Chaichenets S., 2011, The Astrophysical Journal, 744, 12

Woods T. E., Ivanova N., van der Sluys M. V., Chaichenets S., 2012, ApJ, 744, 12

Woosley S. E., Kasen D., 2011, ApJ, 734, 38

Woosley S. E., Weaver T. A., 1994, ApJ, 423, 371

Xuan Z., Naoz S., Kocsis B., Michaely E., 2024, ApJ, 965, 148

Yoon S. C., Langer N., 2003, A&A, 412, L53

Yoon S. C., Langer N., 2004a, A&A, 419, 623

Yoon S. C., Langer N., 2004b, A&A, 419, 645

Yoon S. C., Langer N., 2005, A&A, 435, 967

Yoon S. C., Langer N., Scheithauer S., 2004, A&A, 425, 217

Yu S., Jeffery C. S., 2010, A&A, 521, A85

Yungelson L. R., 2008, Astronomy Letters, 34, 620

Zahn J. P., 1977, A&A, 57, 383

Zhao G., Zhao Y., Chu Y., Jing Y., Deng L., 2012, arXiv e-prints, p. arXiv:1206.3569

Ziegerer E., Heber U., Geier S., Irrgang A., Kupfer T., Fürst F., Schaffenroth J., 2017, A&A, 601, A58 de Jong R. S., et al., 2014, in Ramsay S. K., McLean I. S., Takami H., eds, Society of Photo-Optical Instrumentation Engineers (SPIE) Conference Series Vol. 9147, Ground-based and Airborne Instrumentation for Astronomy V. p. 91470M, doi:10.1117/12.2055826

de Jong R. S., et al., 2019, The Messenger, 175, 3

van Zeist W. G. J., Nelemans G., Zwart S. F. P., Eldridge J. J., 2024, Astronomy and Astrophysics, 691, A316

van den Heuvel E. P. J., 1976, in Eggleton P., Mitton S., Whelan J., eds, IAU Symposium Vol. 73, Structure and Evolution of Close Binary Systems. p. 35

von Zeipel H. V., 1909, Astronomische Nachrichten, 183, 345

von Zeipel H., 1910, Astronomische Nachrichten, 183, 345

Acknowledgements

I would like to express my deepest gratitude to all those who have supported me throughout my research journey and contributed to the completion of this thesis.

First and foremost, I would like to thank my supervisors, Adrian Hamers, Rüdiger Pakmor, Stephen Justham, and Selma E. de Mink. Their guidance, expertise, and constant support have been invaluable throughout this work. I am truly grateful for their insightful feedback, their encouragement to explore new ideas, and their patience in helping me develop as a researcher. Each of them has played a crucial role in shaping the direction of my research, and I am fortunate to have had the opportunity to work with such distinguished mentors.

A special thanks go to my collaborators, Evan Bauer, Valeriya Korol, Jakob Stegmann, Patrick Neunteufel, Holly Preece, Silvia Toonen, and Alejandro Vigna-Gomez, for their collaboration, contributions, and insightful discussions. Their expertise and guidance have enriched my research and been essential in shaping the outcomes of this thesis.

I am grateful to all my colleagues at the Stellar Department for fostering a collaborative and supportive research environment. The daily interactions from everyone have made this journey both enjoyable and enriching.

I would like to thank the MPA secretaries Maria, Gabi, Sonja, Cornelia, Solvejg, Isabel, and Ana, for their assistance and support throughout my time at the department. Your help with administrative tasks and your kindness have been greatly appreciated.

I would also like to express my heartfelt thanks to my family for their unwavering encouragement and love. To my dad, Rajamuthukumar, my mom, Muthu Krishnaveni, and my sister, Ashtothra Rubini, you have been great pillars of support throughout this entire journey. Your belief in me has kept me going through difficult moments, and I am truly thankful for everything you have done.

A special thanks to my best friend, Gautam, for always being there through thick and thin. Your support, understanding, and encouragement have been a source of strength and comfort, and I am beyond grateful to have you by my side.

To my friends in Munich, Pavan, Anshuman, Hitesh, Arghyadeep, Silvia, Geza, Vyoma, Joane, Akash, Katyayani, Nikita, and my stellar department friends, Jing-Ze, Teresa, Ruggero, Taeho, Chen, Alexandra, thank you all for the wonderful memories, the support, and the many stimulating discussions. You made this journey both enjoyable and meaningful, and I couldn't have done it without your friendship and encouragement.